CHAPITRE IV :

Mesure de la réactivité atmosphérique totale avec les radicaux hydroxyles à Paris pendant la campagne MEGAPOLI hiver 2010

Ce quatrième chapitre propose une étude de caractérisation de la réactivité atmosphérique totale avec les radicaux hydroxyles conduite à Paris, au Laboratoire d'Hygiène de la Ville de Paris (LHVP), pendant la campagne de mesure d'hiver (Janvier-Février 2010) réalisée dans le cadre du projet européen MEGAPOLI.

Le projet MEGAPOLI, acronyme de ***M***egacities: ***E***missions, urban, regional and ***G***lobal ***A***tmospheric ***POL***lution and climate effects, and ***I***ntegrated tools for assessment and mitigation, est un projet européen qui a débuté en 2008 et qui a eu une durée de 4 ans (2008 – 2011), comprenant 23 partenaires européens et dont la coordination française était assurée par M. Matthias Beekmann, directeur de recherche au Laboratoire Interuniversitaire des Systèmes Atmosphériques (LISA) de l'Université Paris VII et de l'Université XII. Dans le contexte actuel de fort développement de la population urbaine avec une augmentation des nombres de mégacités (villes avec un nombre supérieur de 10 millions habitants) à travers le monde, des études pour mieux comprendre l'effet de ces mégapoles sur la qualité de l'air sont devenus indispensables et ce projet a eu pour but d'étudier les liens entre les mégapoles, la qualité de l'air et le climat. Les objectifs directs de ce projet étaient ainsi de :

1. Déterminer les impacts des mégacités sur la qualité de l'air à l'échelle locale, régionale et globale
2. Quantifier les rétroactions qualité de l'air – climat
3. Développer les outils intégrés de prédiction de la pollution de l'air dans les mégacités

Afin de mieux répondre à ces objectifs, des groupes de travails ont été formés. Pour atteindre le premier objectif, le groupe de travail WP3 avait été chargé de réaliser des mesures expérimentales dans une mégacité européenne. Entre les zones hautement peuplées en Europe (Londres, Paris, la région Rhine-Rhur, la Valée de Po, Moscow et Istanbul) Paris a été choisie comme étude de cas à cause de sa position géographique. En effet, Paris avec ses régions limitrophes (appelées 'Ile de France') constitue une des seules mégacités européennes avec une population d'environ 12 millions d'habitants. De plus, l'Ile de France est entourée par des zones rurales, permettant donc une analyse directe du panache de pollution issu directement de la mégacité et de ne pas avoir des influences des autres zones urbaines voisines. Dans le cadre de cette étude de cas, 2 campagnes intensives de mesures avaient été prévues : en Juillet 2009 et en Janvier – Février 2010. Ses objectifs étaient de quantifier les sources des aérosols organiques primaire et secondaire et de leurs précurseurs gazeux et d'étudier le panache de pollution de l'agglomération parisienne. Quatre taches majeures avaient été identifiées :

- Documenter la variabilité de la composition chimique de l'aérosol en région source
- Evaluer la contribution des sources (par des modèles de 'source apportionment')
- Suivre l'évolution de l'aérosol primaire et secondaire dans le panache, et

- Intégrer le jeu de données pour évaluer et améliorer les modèles

Mon étude de réactivité atmosphérique avec les radicaux hydroxyles s'inscrivait donc dans cet objectif de caractérisation des sources (locales/continentales) des précurseurs gazeux et permettaient de compléter la palette des résultats expérimentaux obtenus pendant cette campagne.

Cette campagne a permis de mettre en œuvre le montage CRM mis au point pendant la 1ère année de thèse et dont les travaux ont été décrits dans le chapitre 2. Les résultats de cette étude sont présentés dans l'article intitulé « Total OH reactivity measurements in Paris during the 2010 MEGAPOLI winter campaign » et soumis à la revue « Atmospheric Chemistry and Physics ».

L'article est structuré en deux parties distinctes. Une première partie présente la mise en œuvre de la mesure de réactivité OH par CRM. La série des tests nécessaires à la caractérisation et la qualification de la méthode, tests réalisés en début de la campagne, est ainsi présentée. Ces tests comprennent des tests d'évaluation du système avec du propane, de correction de la différence d'humidité entre l'air synthétique de l'air ambiant et l'étude de quantification de l'artefact de recyclage des radicaux hydroxyles par des molécules de NO. Cette dernière étude nous a permis de corriger les valeurs de réactivité brute de cet artefact.

La seconde partie de l'article présente les résultats obtenus lors des mesures atmosphériques de réactivité avec OH. L'analyse de ce jeu de données original a permis dans un premier temps d'apporter des informations concernant les niveaux de réactivité enregistrés dans une mégacité européenne et de comparer ces valeurs avec celles trouvées dans d'autres mégacités du monde. De plus, la position géographique favorable de Paris (entourée par des régions rurales) a permis de distinguer entre une réactivité atmosphérique avec les OH directement caractéristique (propre) de Paris, quand les masses d'air étaient originaires de l'Océan, et celle impliquant aussi une réactivité importée, quand les masses d'air étaient originaires de la partie nord - est du continent. De même, la large gamme d'instruments déployés sur le site de LHVP dans le cadre de ce projet, a permis l'obtention de mesures de nombreux composés gazeux (composés usuels caractérisant les niveaux de pollution : le CO, les NOx, et l'O_3 ; des hydrocarbures non méthaniques ; et des composés oxygénés (OCOVs)) et particulaires (des aérosols de diverses tailles : PM1, PM2.5, PM10 ; des fractions ioniques…). Tous ces composés nous ont permis de quantifier la réactivité manquante avec les radicaux hydroxyles et de conclure sur sa potentielle nature oxydée. Toutes ces discussions ont été présentées dans la deuxième partie de l'article. Des comparaisons avec des études dans d'autres mégacités ont été de même présentées.

Total OH reactivity measurements in Paris during the 2010 MEGAPOLI winter campaign

C. Dolgorouky[1], V. Gros[1], R. Sarda-Esteve[1], V. Sinha[2], J. Williams[3], N. Marchand[4], S. Sauvage[5,6], L. Poulain[7] J. Sciare[1], and B. Bonsang[1]

[1] {Laboratoire des Sciences du Climat et de l'Environnement (LSCE), Unité Mixte CEA-CNRS-UVSQ (Commissariat à l'Energie Atomique, Centre National de la Recherche Scientifique, Université de Versailles Saint-Quentin-en-Yvelines), F-91198 Gif-sur-Yvette, France}

[2] {Indian Institute of Science Education and Research (IISER) Mohali, Sector 81 SAS Nagar, Manauli PO Punjab 140306, India}

[3] {Max Planck Institute for Chemistry, Air Chemistry Department, D-55128 Mainz, Germany}

[4] {Aix Marseille Université, Laboratoire Chimie Environnement, 3 place Victor, F-13331 Marseille, France}

[5] {Université de Lille Nord de France, F-59000 Lille, France}

[6] {Ecole de Mines Douai, Departement Chimie environnement, F-59508 Douai, France}

[7] {Leibniz – Institut für Troposphärenforschung (IFT), Leipzig, Germany}

Corresponding author: V. Gros (valerie.gros@lsce.ipsl.fr)

Abstract:

Hydroxyl radicals play a central role in the troposphere as they control the lifetime of many trace gases. Measurement of OH reactivity (OH loss rate) is important to better constrain the OH budget and also to evaluate the completeness of measured VOC budget. Total atmospheric OH reactivity was measured for the first time in an European Megacity: Paris and its surrounding areas with 12 million inhabitants, during the MEGAPOLI winter campaign 2010. The method deployed was the Comparative Reactivity Method (CRM). The measured dataset contains both measured and calculated OH reactivity from CO, NO_x and VOCs measured via PTR-MS, GC-FID and GC-MS instruments. The reactivities observed in Paris covered a range from $10s^{-1}$ to $130s^{-1}$, indicating a large loading of chemical reactants. The present study showed that, when clean marine air masses influenced Paris, the purely local OH reactivity ($20s^{-1}$) is well explained by the measured species. Nevertheless, when there is a continental import of air masses, high levels of OH reactivity were obtained (120 – 130 s^{-1}) and the missing OH reactivity measured in this case jumped to 75%. Using covariations of the missing OH reactivity to secondary inorganic species in fine aerosols, we suggest that the missing OH reactants were most likely highly oxidized compounds issued from photochemically processed air masses of anthropogenic origin.

1. Introduction

The hydroxyl radical (OH) represents the most important oxidant in the troposphere. It governs the atmospheric lifetime of most reactive trace species of anthropogenic and biogenic origin and contributes to the self-cleansing capacity of the atmosphere.

Generally, the production processes for OH are relatively well understood. However, the loss processes or the sink term of the OH radicals is still poorly constrained. In most cases the overall sink term of OH radicals is estimated by the sum of the products of concentration and the rate coefficient of all individually measured species reactive to the OH radical. This method has proved to be rather limited due to the large number of "OH reactive" volatile organic compounds (VOCs) in urban air (Lewis et al., 2000 and Xu et al., 2003). Recently, Goldstein and Galablly (2007) postulated that 10^5 different VOCs have been detected in the Earth's atmosphere. Moreover, recent studies showed that there are unknown reactive species that contribute to the total OH reactivity (Di Carlo et al., 2004; Sinha et al., 2010; Kato et al., 2011). The necessity of measuring the total sink of OH radicals, also called the OH reactivity (s^{-1}), has therefore become evident. Presently three different types of instruments exist for the direct measurement of the total OH reactivity. The LIF community has two versions depending on how they produce OH in their reactor. The first method is based on the Laser Induced Fluorescence (LIF) technique which records the decay (loss rate) of the OH radicals. Two versions of instruments using LIF technique exist: one that measures the OH reactivity as the inverse of the atmospheric OH lifetime in a reaction flow tube with a movable OH injector (Kovacs and Brune, 2001; Mao et al., 2010; Ingham et al., 2009) the other one uses a laser pump and probe technique (Sadanaga et al., 2005). The second method is called the Comparative Reactivity Method (CRM) and is based on comparative OH reactivity measurement in a flow reactor against the known OH reactivity of an added reagent (e.g. pyrrole, C_4H_5N). CRM has been developed and described in detail by Sinha et al. (2008).

Total OH reactivity has been measured in different environments for the last decade. Lou et al. (2010) reported 18 studies conducted in urban, rural and forested areas. The urban areas investigated included studies over New York City (summer 2001 and winter 2004), Mexico City Metropolitan area (spring 2003), Tokyo (summer 2003, winter 2004), Houston (autumn 2000, autumn 2006), Nashville (summer 1999) and Mainz (summer 2008). The ranges of the OH reactivity registered in these urban areas went from $6s^{-1}$, for the clean atmosphere of the small city of Mainz, Germany (Sinha et al., 2008) to $200s^{-1}$, for the extremely polluted air of Mexico City (Shirley et al., 2006). More recently, Sinha et al. (2012) (paper submitted to ACPD) report measurements from El Arenosillo in Spain, where OH reactivity ranged from below detection limit in marine air masses up to $70s^{-1}$ in continental air masses.

Studies from forested areas have identified high percentages of missing OH reactivities, obtained from the comparison between the measured and the calculated reactivity, (70% in the tropical forest of Surinam, Sinha et al., 2008 and 50% in boreal forest in Finlande, Sinha et al., 2010), but also in rural areas (50% in

a subtropical rural area in PRD of China, Lou et al., 2010). In contrast, missing OH reactivity studies in megacities reported relatively low levels of missing OH reactivity: maximums of 30% for New York 2004 and Tokyo 2003. If the studies showed that in the case of the forested areas, the "responsible compounds" of the missing OH reactivity were non-measured biogenic compounds, the question is still open for the origin of the missing OH reactivity in an urban area.

This paper presents the OH reactivity measurements by CRM method conducted in January – February 2010 within the framework of the EU project MEGAPOLI (http://megapoli.dmi.dk), in the city of Paris and its surrounding region (called "Ile de France") with almost 12 million inhabitants, and which constitutes one of the few megacities in Europe.

The employed method (CRM) was previously described in only four other studies: Sinha et al. (2008), Sinha et al. (2010), Kim and al. (2011) (but this is a modified version and not strictly our method) and Sinha et al. (2012). All of these measurements were made in environments poor in NO emissions, as interferences dues to OH recycling via NO + HO_2 reactions at NO > 5 ppbv in the setup were reported. This is for the first time that the CRM method has been used to measure OH reactivity measurements in an urban area characterized by high levels of NO emissions, as Paris was identified as a city mainly impacted by traffic emissions (Vardulakis et al., 2002). Therefore, the initial part of the article presents the experimental setup and the quantification of interferences in the system used for the MEGAPOLI winter campaign 2010.

The geographical location of Paris – a relatively small-area basin surrounded by rural areas – makes it a favourable place to study purely local OH reactivity levels emitted by a megacity when air masses come from the clean marine western sector, and to characterize the impact of the European contribution when air masses come from the eastern sector.

Within the MEGAPOLI framework a large number of compounds has been simultaneously measured during this campaign: NOx (sum of NO and NO_2), carbon monoxide (CO), ozone (O_3), non-methane hydrocarbons (NMHCs) and oxygenated VOCs (OVOCs). We could therefore compare the observed OH reactivity with the calculated values, which were derived using the observed concentrations of the trace species.

2. Experimental:

2.1. Experimental setup and field deployment

2.1.1. Experimental setup:

The comparative reactivity method for measuring the total OH reactivity is described in detail by Sinha et al. (2008). A brief overview of the principle of the measurement is nevertheless presented here:

Firstly, a mixture of pyrrole (C_4H_5N) and synthetic dry air is injected into the reactor. The concentration C_1 of the pyrrole is monitored in the flow exiting the reactor by a Proton Transfer Reaction – Mass Spectrometer (PTR-MS). Secondly, the UV rays emitted by a mercury lamp produce OH radicals ([OH] < [pyrrole]) to react with pyrrole (k_{Py+OH} = 1.2 x 10^{-10} $cm^3 molecules^{-1} s^{-1}$). The pyrrole concentration registered now is C_2. Next, the synthetic air is replaced with ambient air. The OH reactive species contained in the ambient air compete with pyrrole for the available OH radicals. This causes an increase in the pyrrole monitored concentration from C_2 to C_3. The three measured concentrations, C_1, C_2 and C_3, allow the calculation of the total OH reactivity via the following equation based on competitive kinetics, which has been derived by Sinha et al. (2008).

$$R_{air} = \frac{(C_3 - C_2)}{(C_1 - C_2)} \cdot k_{Py+OH} \cdot C_1 \qquad (1)$$

The schematic diagram of the CRM measurement system deployed for the MEGAPOLI campaign is shown in Fig. 1. The glass reactor used for the MEGAPOLI winter campaign is identical in shape and dimension with the one described in Sinha et al. (2008).

To measure C_1, C_2 and C_3, three different instrumental modules were used: the "synthetic air" module, the "nitrogen" module and the "ambient air" module (see Fig 1). The "nitrogen" module is used to produce the OH radical via the UV photolysis of the water molecules imported by the humidified nitrogen bubbled through a pure water bottle. The same method to produce OH radicals has largely been used in the techniques of OH radical measurements (LIF measurements: Kovacs et al. 2003; Mao et al., 2009).

While switching from C_1 to C_2, the synthetic air entering the reactor is humidified via the "synthetic air" module. Two mass flow controllers (MFC A and MFC B on the Fig. 1) are used and two flows of a 100% humidified and dry zero air are mixed together. Their mixing proportion determines the humidity of the final zero air flow. The relative humidity of C_2 baseline signal during MEGAPOLI was maintained constant at 50%, for a temperature of 24°C. For more details concerning the correction applied to the data set because of the difference in the humidity of the synthetic air and ambient air, the reader is referred to Sect. 2.2.2, OH reactivity quantifying tests.

When switching from C_2 to C_3, the "synthetic air" module is switched OFF and the "atmospheric air" module is then connected, via a 3 way valve. This module consists of a Teflon VOC pump (KNF), a Teflon micro valve and ¼ and 1/16 inch flow reducing Teflon tubing (see Fig. 1).

The used detector located in the exit of the reactor is a high sensitivity PTR-MS, from Ionicon Analytik, Austria. The PTR-MS technology has been firstly introduced in studies of atmospheric

chemistry by Lindinger et al. (1998). For this campaign the main monitored compound is pyrrole which is detected at the mass m/z=68a.m.u. Other studies showed that this detector is ideal for measuring pyrrole, as the protonated ion does not fragment (Sinha et al., 2008 and 2009). Also this mass is known to be free of interferences. The explored calibration range of pyrrole concentrations that are measured is from 0.5 to 250ppbv, but on field measurements were always higher than 10ppbv. The instrumental precision is of 6% for 2 standard deviations (2σ). The humidity inside the reaction cell is important for accurate determination of the OH reactivity. To track the humidity into the reactor, the masses of the first two water clusters are also monitored: m/z 37 (cluster $H_3O^+H_2O$) and m/z 55 (cluster $H_3O^+(H_2O)_2$), an approach described by Amman et al. (2006) and Sinha et al. (2008).
Besides the water cluster measurements that were used as proxies for the humidity into the reactor, an extra sensor for relative humidity and temperature was also installed in the exhaust line of the reactor (see Fig. 1). In contrast to the reactivity setup of Sinha et al. (2008) for the CRM used during the MEGAPOLI winter campaign, no other extra pump has been used at the exhaust line, the reactor being therefore maintained at ambient pressure with no over pressure inside the reactor.

2.1.2. Field deployment:

The CRM system was deployed at the Laboratoire d'Hygiène de la Ville de Paris (LHVP) during the MEGAPOLI winter campaign 2010. The site is located in the heart of Paris (the 13th district) and therefore considered to be representative of the background pollution of central Paris.
The OH reactivity system was installed in a room where the temperature was maintained at 24°C. The ambient air was sampled through a Teflon line of ¼ inch of diameter and a length of about 10 meters. The inlet was situated on the roof of LHVP, at a height of around 14 meters above the ground level. In order to avoid any particulate contamination, a 0.45 µm Teflon filter was used at the entrance of the sampling line. OH reactivity studies showed that the OH reactivity measurements are not influenced by the positioning of a Teflon filter in the entrance of the inlet line (Sadanaga et al., 2006).
Ambient air was then sampled at 150 ml/min in a total flow of 245 ml/min (dilution factor of the OH reactivity into the reactor of 1.65). The residence time of the compounds in the inlet lines was kept at < 35s by using a Teflon VOC sampling pump which draws a flow of 3L/min. A 1/4inch and 1/16inch flow-reducing Teflon tubes were used downstream to stabilize the ambient air flow into the reactor at 150 ml/min (see Fig. 1).
Atmospheric OH reactivity measurements were performed between the 23rd of January and the 13th of February. The time resolution of the measurements was of 2 minutes. Gaps in the data set were due to regular check-up of the instrument.

2.2. Reactivity tests

2.2.1. Evaluation of the system

At the beginning of the campaign, a series of tests were conducted from the 8th to the 23rd of January to characterize the system and the new reaction cell.

To check the accuracy of the CRM OH reactivity quantification, two standards have been used: a propane gas standard (Westfalen A.G.; 29.8 ppm in N_2; stated uncertainty 5%) and a standard which was a mixture of 3 compounds in N_2: acetone, methanol and isoprene (Messer; 5,01ppm acetone, stated uncertainty 5%; 6,78ppm methanol, stated uncertainty 5%; 3,90ppm isoprene, stated uncertainty10%). The second standard has been analyzed in the laboratory in December 2009 prior to the MEGAPOLI campaign. Different quantities of standard have been introduced into the reactor. Using the definition of the OH reactivity, the reactivity due to the standard has been calculated via the equation:

$$R_{total} = \sum k_{compound+OH} \cdot [compound] \quad (2)$$

where the $k_{compound + OH}$ represents the constant rate of each compound (propane, acetone, methanol and isoprene) with the OH radical ($k_{OH + propane}$ = 1.1 x 10^{-12} $cm^3 molecules^{-1} s^{-1}$, $k_{OH + acetone}$ = 1.8 x 10^{-23} $cm^3 molecules^{-1} s^{-1}$, $k_{OH + methanol}$ = 7.65 x 10^{-13} $cm^3 molecules^{-1} s^{-1}$, $k_{OH +}$ isoprene = 1.0 x 10^{-10} $cm^3 molecules^{-1} s^{-1}$, Atkinson et al., 2006) and the [compound] is the concentration of the compound in molecules cm^{-3}. Figure 2 presents the measured versus the calculated reactivity. The two standards allowed us to cover a range of OH reactivity from 3 to 50 s^{-1} for the propane standard, and a dynamic range comprised from 50 up to 300 s^{-1} for the acetone, methanol and isoprene standard. Corrections using facsimile for deviations from the first order kinetics as described by Sinha et al. (2008) and for dilution of air in the reactor have already been applied.

The total uncertainty of the calculated reactivity is around 20% and comprises: uncertainty due to the rate coefficient of the standards with the OH radicals (18%), flow fluctuations (~10%) and uncertainty due to the accuracy of the standards (5%). The measured reactivity is obtained with the CRM (vertical axis). The total uncertainty for the measured reactivity is around 18% and comprises: uncertainty due to the rate coefficient of the pyrrole with the OH radicals (13%), uncertainty of the standards (5%), due to flow fluctuations (10%) and the instrument precision (2σ, ~6%).

The calibration tests show a good linearity and accountability of the measured reactivity. The estimated detection limit of the ambient OH reactivity measurements within the setup is around $3s^{-1}$.

2.2.2. OH reactivity quantifying tests

As already identified by Sinha et al. (2008), interferences are potentially present in the setup. The penray mercury lamp is used to photolyse water at 185nm. A fraction of the pyrrole is also photolyzed

at 185nm. The percentage of pyrrole photolysed in our setup is 19±2%, but this does not influence our measurement because the eq. (1) takes into consideration the real pyrrole concentration (after photolysis) available for reaction with the OH radicals (C1 base line).

Humidity difference between the zero air and the ambient air

Another potential interference is the humidity difference between the zero air and the ambient air. Different humidity conditions for the C_2 and C_3 signals correspond to different yields of OH radicals in the reactor, and therefore can lead to over or under estimation of the total OH reactivity. To avoid this, the humidity of the zero air must be kept the same as the one of the ambient air. In the experimental setup used during the winter 2010 MEGAPOLI campaign, the zero air was humidified to a constant value of 50%. As the atmospheric humidity varied over the day, corrections were applied on the C_2 base line signal so that the overall OH field stays constant. To do this, a "humidity test" was run. The zero air flowing into the reactor was humidified to different degrees by mixing varying amounts of wet and dry zero air, with the help of the "synthetic air" module presented in Fig. 1. The decrease in the pyrrole baseline (C_2) is then recorded for different relative humidities. During this test the mercury lamp is maintained ON, as the purpose is the quantification of the real OH radical production into the setup. The humidity is tracked via the sensor installed on the exhaust line of the reactor.

As the campaign took place in winter, the relative humidity of the ambient air rarely went below 50%, usually the relative humidity being between 50 and 90%. The results of this test are therefore presented for a relative humidity range between 50 and 100% (see Fig. 3).

A humidity correction has been applied based on this test on the C_2 baseline signal. Note that while this correction may seem significant (~ up to 30%), as the ambient air was more humid than zero air, it would only cause underestimation of the true OH reactivity thus leave conclusions of the paper regarding missing OH reactivity robust and intact.

The test revealed that for a relative humidity of between 60-70%, the setup is much more sensitive to a change in the pyrrole signal than for humidity comprised between 80 and 90% (the slope being smaller). Therefore, if there is no possibility of regulating the humidity of the C_2 signal to the one of the C_3 signal, as in the present work, it is advised to keep the total relative humidity of the C_2 base line signal in the ranges of 80 to 90%.

NO interference into the setup

As has been shown previously (Sinha et al, 2008), for high values of the NO into the setup, secondary production of OH radicals is observed due to the recycling of the HO_2 radicals. This interference is

non-negligible for measurements made during the MEGAPOLI winter campaign, as the NO atmospheric levels went up to 100 ppb during the morning rush hour (see top panel from Fig. 6). To overcome this potential interference, firstly, the NO effect on the OH reactivity was quantified. Afterwards, a correction factor was applied to the ambient OH reactivity.

For the quantification of the NO interference, different amounts of NO were injected into the reactor and the decrease of the pyrrole signal due to additional OH radicals, recycled via the $HO_2 + NO \rightarrow OH + NO_2$ (k_{HO2+NO} = 8.8 x 10^{-12} $cm^3 molecules^{-1} s^{-1}$, Atkinson et al., 2004) reaction, was analysed. The result of the test is presented in the Fig. 4, where the absolute change in the measured OH reactivity was plotted against the NO values in the setup.

The test was run for an initial OH reactivity of $50 s^{-1}$ (using the propane standard described previously) and showed a change in the slope at NO value of 20ppbv. A secondary NO test was made 2 weeks later with no propane injected into the reactor (OH reactivity null). This secondary test was not presented on Fig. 4, but again, the change in the slope was noted for NO of 20ppbv into the setup. Two different slopes were therefore considered for correction of the ambient OH reactivity.

The vertical axis uncertainty was 20% and corresponded to the total OH reactivity uncertainty as quantified for the calibration tests described in Sect. 2.2.1. The total horizontal uncertainty was 11%, and took into consideration NO flow fluctuations (10%) and the uncertainty of the NO standard (5%).

For the MEGAPOLI winter campaign, the OH reactivity data set was corrected for the NO interference as follows: for NO values into the setup smaller than 20ppbv (equivalent to ambient NO concentration of 33ppbv, for a dilution factor into the reactor of 1.65), the measured OH reactivity was increased with a value equivalent of the product between the 1st slope determined (1.13 $s^{-1}ppbv^{-1}$) and the measured NO value into the setup. For NO values higher than 20ppbv, the measured OH reactivity was increased with the 0.46*NOconcentration+12.51 s^{-1}. 99% of the OH reactivity dataset corresponds to the first regime (NO<20ppbv) and only 1% to the second regime (NO > 20ppbv).

Frequency of the C0, C1 and C2 signal measurements

No C_1 measurements were completed between the 23rd and the 30th of January, being replaced by C_0 measurements. These measurements correspond to measurements made in the same conditions as C_1 with the UV lamp turned OFF. The photolytic loss of pyrrole described by the difference between C_0 and C_1 signals is an indicator of the stability of the emission rays of the lamp, and therefore of the constant OH field production into the reactor. The photolytic loss for different C0s was quantified at the beginning and during the campaign as follows: from the 8th to the 23rd of January and after the 31st of January. The results indicated a constant photolytic loss of 19±2% over the entire period. The missing C_1 levels were therefore confidently quantified based on the correspondent C_0 levels.

The CRM method is based on the comparison between the C_2 and C_3 signals and therefore frequent measurements of the C_2 signal are required. During the MEGAPOLI winter campaign, the C_2 baseline signal was determined 2 to 3 times per day. Although not very frequently measured, the variability of the C_2 showed a daily variation of maximum 15% over the entire campaign. An additional error of 15% due to extrapolating successive baselines was therefore considered to the total uncertainty of the measured OH reactivity. A total uncertainty of 24% was finally considered for the measured OH reactivity values during the MEGAPOLI campaign. This result comprises: uncertainty due to the rate coefficient of the pyrrole with the OH radicals (13%), uncertainty of the standard (5%), due to flow fluctuations (6%), the instrument precision (2σ, ~6%) and the uncertainty due to low frequency C_2 measurements (15%).

2.3. Ancillary measurements at LHVP site during MEGAPOLI winter campaign

Within the MEGAPOLI framework, additional measurements of CO, NOx, non-methane hydrocarbons (NMHCs) and oxygenated volatile organic compounds (OVOCs), as well as aerosol chemical composition were also performed.

Ozone was measured with an analyzer based on UV absorption (41M, Environnement SA) and nitrogen oxides were measured by chemiluminescence with an AC31M analyzer (Environnement SA). CO was measured by an analyzer based on IR absorption (48i-TL instrument, Thermo Electron Corporation, Waltham, MA, USA). More details for these instruments are given in Gros et al. (2011).

2.3.1. Non-methane hydrocarbon on-line measurements by gas chromatography

Two portable gas chromatographs equipped with a flame ionization detector (GCFID, Chromatotec, Saint Antoin, France) were used to measure non-methane hydrocarbons (NMHC) in ambient air. The instruments were located on the roof of the LHVP (~14m above ground level). The first analyser, ChromaTrap, allowed the measurement of C_2 – C_6 hydrocarbons and the second, AirmoBTX, the measurement of C_6 – C_{10} hydrocarbons. As the same instruments were used for atmospheric measurements during the spring 2007 Paris campaign, their technical information (type of columns, sampling flows, preconcentration, desorption-heating temperatures and times, etc) was already described in details by Gros et al. (2011).

For both GC instruments, the sampling time was 10min and analysis time was 20min, and therefore measurements were performed with a time resolution of 30min.

2.3.2. VOC measurements by PTR-MS:

HS-PTRMS (High Sensitivity Proton Transfer Reaction Mass Spectrometer, Ionicon Analytic, Lindinger et al., 1998) was deployed during the intensive field campaign in order to quantify VOCs and oxygenated

VOCs. The sampling line was installed on the roof of the LHVP building and consists of 10m Teflon tubing. A primary flow of 10L/min was maintained in the sampling line. During the campaign 39 m/z were monitored in the SIM mode with a temporal resolution of 2.5 min. These ions include m/z = 25, 32, 37, 39, 55, 80 used to control the PTRMS performances (fragmentation, ionization) and the 33 remaining m/z correspond to individual VOC's or sum of isomers. Within this study 5 VOC's measured by PTRMS were considered: benzene (m/z=79), toluene (m/z=93), acetonitrile (m/z=42), methanol (m/z=33) and acetaldehyde (m/z=45). Transmission of the PTR-MS quadrupole were adjusted by the mean of 18 individual VOCs with certified concentration overlapping the mass range of the VOCs monitored within the field campaign. The 5 selected VOCs were also individually calibrated in the range 0.2-8 ppb at 50% HR.

2.3.3. Oxygenated compounds measurements by GC - MS:

For OVOC measurements, air sampling was performed at 15mL.min−1 flow during 30min by Air server-Unity I (Markes International, Llantrisant, UK). After sampling, the compounds were then thermally desorbed and injected through a transfer line into a high polar column and analyzed by GC (Agilent, Massy, France) equipped with a FID and a Mass Spectrometer. This device allowed the identification and the quantification of 19 OVOC and 11 NMHC from C2 to C9 with a time resolution of 1.5 hour. Technical precisions are given by Roukos et al. (2009).

2.3.4. Fine aerosol measurements by AMS:

A suite of instrumentation for the characterization of the physico-chemical properties of particles was deployed in the garden of the LHVP building (approx. 14 m below the sampling line of the OH-reactivity system). The instruments included a High Resolution Time-of-Flight Aerosol Mass Spectrometer (HR-ToF-AMS), here simply referred to as AMS, Aerodyne Research Inc., DeCarlo et al. (2006). A collection efficiency of 0.4 was calculated for the HR-ToF-AMS based on comparison with concurrent TDMPS and particle-into-liquid sampler (PILS) data (Healy et al., 2011 in ACPD). All instruments were connected to the same sampling system consisting of a PM10 inlet located approximately 6 m above ground level directly followed by an automatic aerosol diffusion dryer system maintaining the relative humidity in the line below 30% Tuch et al. (2009).

The AMS was operated at 5 min time resolution. Due to the 600°C surface temperature of the vaporizer, the AMS can only measure the non-refractory (NR) part of the particles (ammonium, nitrate, chloride, sulphate, and organic matter). Therefore, based on the aerodynamic lenses transmission efficiency and the detected compounds, AMS results are commonly considered to correspond to the non-refractory PM1 aerosol (NR-PM1) Canagaratna et al. (2007).

2.4. Description of the FLEXPART model

The FLEXPART model represents a quantitative dispersion model which takes into consideration turbulence, convection parameterizations, dry and wet deposition to do backwards calculations from a measurement site (receptor) for the volume mixing ratio of a generic inert tracer with infinite lifetime. The generic inert tracer consists of 40000 particles released in a small box at the measurement location and during the measurement interval (3 hours) and followed backward in time for 20 days. The model output unit is called PES, acronym from "potential emission sensitivity" distribution. The unit of the PES is in $s*kg^{-1}$ and its value in a particular grid (geographical place) is proportional to the particle residence time in that cell. It is a measure for the simulated mixing ratio at the receptor that a source of unit (1 kg s^{-1}) in the respective grid cell would produce. For more details on the way that the model works, the reader is sent to the FLEXPART descriptive paper of Stohl et al. (2005), available at http://zardoz.nilu.no/˜andreas/publications/web based tool.pdf.

3. Results and Discussion

In order to understand the OH reactivity results, a short description of the air masses impacting the site and a brief discussion on the pollution levels registered in Paris during the MEGAPOLI winter campaign are presented as follows.

3.1. Air mass origins during MEGAPOLI

OH reactivity measurements were made from the 23rd of January until the 13th of February. During this time, a wide variety of air masses passed over Paris and its surroundings. In the supplementary information of the article, all of these air masses are synthesized along with their origins (see Appendix A), as represented by the 20 days back trajectories calculated with the FLEXPART model.

We have chosen for discussion in this paper three contrasting periods characterising different regimes in the OH reactivity measurements. The corresponding backward trajectories are given in Fig. 5. The first period (hereafter called "period I") starts with the 26th of January, 03:00, and ends on the 27th of January, 21:00. This period corresponded to air masses originating from the eastern part of Europe, passing firstly over the Benelux area and in the second part of this period over Germany.

The second period (hereafter called "period II") started on the 2nd of February, 09:00, and ended on the 4th of February, 03:00. In this period, clean air masses originating from the Atlantic Ocean arrived over Paris.

The third period (hereafter called "period III") started with the 9th of January, 18:00, and lasted until the end of the campaign, the 13th of February, 16:00. The air masses originated again from the northern part of the continent, passing over Germany before joining Paris.

In conclusion, periods I and III were therefore characterized as "continental air masses", while period II was characterized as "oceanic air masses".

3.2. Air quality in Paris during MEGAPOLI

3.2.1. Ambient levels of VOCs in Paris – comparison to levels observed in other urban environments

The median values of the main gas tracers recorded in Paris over the entire MEGAPOLI winter campaign were: 300±98ppbv for CO, 27±11ppbv for NO_2 and 13±8ppbv for ozone (O_3). NO presented a high variability during this period: a mean value of 10ppbv and a median of 5.5ppbv. Previously a campaign has been conducted in Paris during spring 2007 (Gros et al., 2007) and a brief comparison with the pollutant levels is given on the same site as the MEGAPOLI winter campaign 2010. The median values corresponding to CO, NO, NO_2 and O_3 measured during spring 2007 were 248±80ppbv for CO, 4.4±1.6ppbv for NO, 11.2±7.4ppbv for NO_2 and 26±13ppbv for O_3. It can be seen that higher levels of CO, NO and NO_2 were registered during MEGAPOLI 2010 than for the 2007 campaign, and this is likely because of the higher anthropogenic emissions expected during the cold season. Because of a lower photochemical activity during winter, the O_3 level measured during MEGAPOLI 2010 campaign was lower than in spring 2007.

A brief comparison between the pollution levels reported from several cities where OH reactivity measurements are available is presented in Table 1. These cities were: Houston, New York, Mexico City, Tokyo and Paris. The background and the maximum registered levels of CO, NO_x, O_3 and the sum of non-methane hydrocarbons (NMHC) are summarized. The periods of the year when the measurements were done and the total population of the Metropolitan Areas were also presented. The most populated city was Tokyo with 36 million inhabitants, followed by New York and Mexico City, each of 22 million inhabitants. Paris and its surrounding area, called Ile de France, counted for 12 million inhabitants, representing one of the few megacities in Europe. Among the studied cases, Tokyo (36°N, 140°E) presented measurements in winter, in the same period when the measurements of Paris were realized. As Tokyo is at about 35°N one may expect the winter effect of more emissions to be less pronounced.

The measured levels of the compounds presented in the Table 1 correspond to median daily values. The background values correspond to midnight median levels, while the maximums represent the maximum registered of the median daily values. For more details on the measured data for Houston, New York and

Mexico City, the reader is sent to Shirley et al. (2006) and Mao et al. (2009) and references therein. For Tokyo measurements, see Yoshino et al. (2006).

In terms of carbon monoxide, the background levels measured in Paris are similar to values measured in the other cities, though slightly lower. In winter, Tokyo registered a maximum of CO 3 to 4 times higher than the Paris maximum, but 2 times lower than the maximum observed for Mexico-City. Nevertheless, the maximum level of CO in Paris measured in the cold season remains comparable to maximums observed in New York City and Houston, though smaller and for different periods.

In terms of NOx, the Paris background is slightly higher than the background levels measured in the other cities. Nevertheless, the maximum value remains comparable to the values measured in New York City and Tokyo (in summer and in autumn), but still almost two times lower than the maximum registered for the Mexico City in spring season and Tokyo in winter season. This is a comparison only on levels and does not consider inter annual variation of this pollutant concentration.

Generally, the Paris background level of NMHC sum was two times lower than in New York and Houston, 2000. The maximum is being 30% to 50% lower than those of New York and Houston, 2000 respectively. The high values in the sum of the NMHC measured for Houston in 2006 were mainly due to spikes at night correlated to emission events from plants in the Houston Ship Channel (Day et al., 2010). Greater discrepancies were nevertheless noted with respect to Mexico City when both the background and the maximum levels were 10 times higher than in Paris.

This quick comparative analysis allowed us to conclude that Paris presents intermediate levels of gaseous pollutants (CO, NOx, NMHC), between medium size cities (Houston) and megacities like Tokyo, New York and Mexico City. This is explained by its smaller population and its less industrialized character.

Examining now the speciated VOCs measured during the MEGAPOLI winter campaign, Table 2 gives their mean and range over the measurement period. Their corresponding OH reactivity, calculated as the product between the concentration and the equivalent reaction rate constant (Kovacs and Brune, 2001; Kovacs et al., 2003; Sadanaga et al., 2005; Mao et al., 2009, 2010) is also given and will be discussed in Sect. 3.4.

Alkanes, alkenes-alkynes (and isoprene, though usually under the detection limits, because of the cold season), aromatics and the oxygenated compounds accounted for 26, 19, 7 and 48% respectively of the total volume mixing ratio of the measured VOCs. The oxygenated VOCs contribute a large part to the total concentration of the compounds measured during the campaign. Among the oxygenated species, ethanol by itself accounted for more than half (56%) to the total OVOC concentration, followed by the sum of methanol and acetaldehyde 30%, and acetone with 8%.

VOC Source apportionment analysis was conducted by Gaimoz et al. (2011) for the spring 2007 campaign, allowing the characterization of the local pollution in Paris. The term “local pollution”

means pollution from Paris and "Ile de France". The main source identified for VOC was traffic emission (fuel exhaust and evaporation) contributing to 50%. Other contributing sources included natural gas emissions, background input and biogenic emissions.

3.2.2. VOC variability: influence of local sources versus long-range transport

To characterize the air quality of Paris during the MEGAPOLI winter campaign, the variability of specific compounds showing different sources and atmospheric lifetimes were analyzed. The four panels of the Fig. 6 present selected compounds and a discussion on their variability, sources and their relation to the air mass origin is given afterwards.

In the upper panel of Fig. 6, nitrogen oxide and the sum of o, m and p xylenes are presented. The baseline levels of these two anthropogenic and short life-time (a few hours) compounds do not seem to be significantly influenced by the different origins of the air masses. Secondly, as previously presented, the NO represents a typical marker of the traffic exhaust emissions. The covariation of the xylenes with the NO suggests that the xylenes' variability (but also that of other aromatic compounds, like toluene) in Paris was mainly controlled by the traffic source. This finding is in agreement with the conclusions from Gaimoz et al. (2011) (see Sect. 3.2.1).

The second panel presents two anthropogenic compounds with longer lifetimes: CO and benzene. CO represents a combustion tracer, having fossil fuel and biomass burning as primary sources. Its atmospheric life-time is relatively long, ~2month (Crutzen, 1994). Benzene has a lifetime of 12 days (for an OH concentration of $1.5x10^6$molecules cm^{-3}, Seinfeld and Pandis, 2006) and its emissions in Paris are, like other aromatic compounds, linked to traffic activities. Both compounds show higher baseline levels during periods I and III. As the life-time of these two compounds exceeds the day, additional imported sources are considered to be responsible for the higher levels registered during the periods where polluted air masses were originating from the continent.

In the third panel, two oxygenated compounds with different lifetimes are presented: acetone (66 days for an OH concentration of $1.5x10^6$molecules cm^{-3}, Seinfeld and Pandis, 2006) and acetaldehyde (11 hours for an OH concentration of $1.5x10^6$molecules cm^{-3}, Seinfeld and Pandis, 2006). These two compounds have primary sources mainly of biogenic origin and an important secondary source: the oxidation of non-methane hydrocarbons (NMHC). As shown in Fig. 6, both compounds show relatively lower baseline levels during the oceanic episode (period II) (except for the two maximums observed for the acetone) and higher baseline levels monitored during the continental air masses episodes (periods I and III). The fact that this increase is observed also for acetaldehyde, an oxygenated compound with a relatively short life-time, suggests that during the continental imported

air masses, two type of sources are responsible of the high pollution levels: the direct pollution and the imported from over the continent and already processed air masses.

In summary, the examination of the variability of the compounds that have different lifetimes and sources shows that the measurement campaign was impacted during Period II only by local and regional (Paris and its surroundings, so-called "Ile de France") emissions, whereas during the other periods (periods I and III), a significant contribution to the pollution levels in Paris was due to direct import of primary and secondary pollutants emissions that had undergone photochemical aging and mixing during transport to Paris.

The diurnal variation of the main gaseous pollutants in Paris is presented in Appendix B. We have observed that the primary species - CO, NMHC and NO - show the same daily profile related to their common source, the traffic emissions. They show a minimum value during the night, a first peak in the early morning, a slight decrease in the afternoon and a second peak formed in the evening. This double peak profile of the primary pollutants has also been remarked in Paris during spring 2007 (Gros et al., 2011) but also in other city boundaries (de Gouw et al., 2009; Velasco et al., 2007). The main primary emission source in Paris is considered to be the traffic activity.

3.3. OH reactivity in Paris

3.3.1. OH reactivity variability during the MEGAPOLI campaign

The OH reactivity measurements were made from the 23rd of January until the 13th of February. Figure 7 presents the OH reactivity levels measured: the 2min and the 30min averaged data series.

OH reactivity ranged from below the detection limit (3.5s^{-1}) up to 130s^{-1}. The median value over the entire campaign was of 33s^{-1}. Missing points in the data set correspond to periods when instrument check and calibrations were run.

Generally we observed higher OH reactivity levels measured during the night time compared to daytime levels. This variability of the OH reactivity is explained by the evolution of the height of the boundary layer, which is lower during the night, and therefore at this time the OH reactivity is less diluted. This result is in good agreement with the higher level of the OH reactivity during nighttime than during daytime (except for the double peak due to traffic emissions) measured in other megacities around the world: Nashville, USA (1999) (Kovacs et al, 2003), Houston, USA (2000 and 2006) (Mao et al, 2010), New York (2001) (Ren at al, 2003) and Mexico City (2003) (Shirley et al, 2006).

These same studies showed also that, under the influence of local pollution, the OH reactivity usually followed the diurnal cycle of the pollutants emitted by traffic emissions: a first peak more or less accentuated, in the early morning (06:30), followed by a slight decrease in the late morning (10:30)

and a second peak in the late after-noon and early evening. Nevertheless, we noticed that very few days during this campaign presented the typical diurnal (diel) cycle of a city impacted by traffic emissions. The main reason for this was that the diurnal variability was most of the time overtaken by the impact of long range transport as discussed below.
Regarding the entire MEGAPOLI winter campaign, three contrasting periods have been identified. The origins of the air masses corresponding to these OH reactivity periods have been previously described (see Sect. 3.1).

The "Period I" started with the 26th of January, mid-day, and ends on the 27th, at 2100 hours. The period is characterized by high OH reactivity levels with a maximum value of 120s^{-1} reached on the 27th of January. The air masses originated from the eastern part of the continent and passed over Germany, before reaching Paris. They were therefore charged in pollutants (see discussion from Sect. 3.2.2), and can explain the high OH reactivity levels registered during "period I".

"Period II" lasted from the 2nd to the 4th of February. During this period, low levels of OH reactivity were registered (20s^{-1}). This result is consistent with the marine origin of the air masses during this period (see Fig. 5).

"Period III" started with the 8th of February, 15:00, and lasted until the end of the campaign, the 13th of February. The OH reactivity levels reached again very high values of 110s^{-1}. As for "period I", the air masses mainly originated from the north-eastern part of the continent and the Benelux area. Therefore an additional pollutant source due to the long range transport is considered to be responsible for the higher levels of the measured OH reactivity
When considering the other time periods not-discussed here (time periods between period I, II and III), the air masses characterized intermediate regimes. The air masses originated either from the central part of France, either from intermediate regimes between the continental and oceanic (see Appendix A). These periods correspond to intermediate OH reactivity levels.
Table 3 synthetises the mean values of OH reactivity and the main gaseous pollutants for the three periods previously mentioned.

Generally all the compounds showed lower levels during the marine air mass period (II), than for the continental import periods (I and III), as already described in the previous section. The primary compounds exclusively emitted by local sources (considering their short life-time), here presented by the NO and the xylenes, show levels almost double during "period I" compared to "period III", both continental air masses periods. These high concentrations denote higher local pollution during period

I, and implicitly, higher 'local' OH reactivity. The other primary compounds presented (CO, benzene and NMHC) showed also the same difference between the two continental import periods, but because of their longer life-time, we can conclude that an additional imported source of primary compounds contributes to the total OH reactivity. Keeping in mind that the OH reactivity data are associated with an uncertainty of about 24%, some differences can still be seen between these two different periods.

Surprisingly, the sum of the oxygenated VOCs shows higher values during the oceanic air masses period. This result is due to ethanol (which represents 50% of the OVOCs) and which shows higher level during period II. Biogenic emissions are considered to be the main source of ethanol (Naik et al., 2010) and we note that Lewis et al., (2005) observed also higher OVOCs compared to other species in North Atlantic marine air too.

We conclude that the lowest OH reactivity levels corresponded to the marine period and were than only impacted by the local and regional pollution. The higher OH reactivity registered during periods I and III was mainly due to long distance transport.

3.3.2. OH reactivity levels registered over a local pollution episode

The previous section suggested that the Paris OH reactivity larger variability is mainly driven by long range transport when comes to continental air masses. A discussion concerning the diel variation of the OH reactivity can therefore be done on periods influenced by oceanic air masses, and when only the local pollution is observed. The day of the 4th of February (Thursday) was chosen because of its mainly oceanic air mass origins (pure oceanic air masses before 09:00, and oceanic and central France after 09:00; see Fig. A1). We specifically use this day as it was the only one available with marine air mass origins and enough OH reactivity data. The other days had either larger blank period in the data set due to daily instrumental check, or either didn't represent the typical diurnal cycle governed by the morning and evening pollution peaks because they were weekend days. Still, the 4th of February presented a blank of 2 hours in the data set, from 09:30 to 11:30, which was corresponding to the base line measurements.

Figure 8 presents in the top panel the variation of the OH reactivity with NO and in the bottom panel the OH reactivity plotted with acetone.

For this local pollution episode, NO showed a modified diurnal cycle. Indeed, instead of a double peak normally observed during the day and corresponding to the traffic rush hours, on the 4th of February, NO showed only the morning peak which was doubled. A small peak was observed in the early morning (06:30), followed by a larger one in the late morning, around 11:00. We note that the 4th of

February was a Thursday, when the local public transportation had a strike, probably leading to enhanced use of private vehicle and unusual rush hour time. This conclusion is also sustained by the double peak observed for the same day on other compounds related to traffic emissions: CO and xylenes.

The first maximum in the NO level corresponding to the morning rush hour is clearly seen on the OH reactivity as well as the decrease observed around 08:00 and the beginning of the increase observed at 09:00. Unfortunately the second maximum is not captured by the OH reactivity measurement because of two hours gap in the data set. The good agreement between the OH reactivity and the NO denotes that Paris local OH reactivity is well impacted by traffic related emissions. Nevertheless, in the second part of the day, an increase compared to the morning level (06:00) of the OH reactivity was observed, increase which was not showed by the NO variability. The second plot of Fig. 8 shows that acetone presents the same change in the concentration level, at the same time of the day. As acetaldehyde shows the same increase of the level measured as acetone, we concluded that for this episode, the in-situ photochemical formation of oxygenated compounds may be responsible of the increase of the OH reactivity in the afternoon.

3.4. Missing OH reactivity in Paris

The calculated OH reactivity represents the sum of the product of OH reactants and their reaction rate coefficient. As previously shown (Kovacs et al., 2003; Di Carlo et al., 2004), comparison between the measured and the calculated OH reactivity denotes the so-called "missing OH reactivity" and tests the assumption that all significant OH reactants have been measured and can be used to infer missing OH reactants.

Figure 9 presents the total measured OH reactivity plotted with the calculated OH reactivity due to the simultaneously measured OH sink compounds. The VOC species considered for these calculations are presented in Table 2. In addition, results of CO, NO and NO_2 were also taken in consideration. Because of the winter season, no biogenic emissions were identified (isoprene signal under the detection limit most of the time), and therefore no biogenic compounds were considered. No formaldehyde measurements were made at the LHVP site during the MEGAPOLI winter campaign. Nevertheless, calculations considering high values of formaldehyde were conducted but the equivalent OH reactivity was not significant (only $2s^{-1}$ for 10pbbv of formaldehyde, $k_{CH2O + OH} = 8.5 \times 10^{-12}$ cm^3 $molecule^{-1}$ s^{-1}, Atkinson et al., 2006). No formaldehyde reactivity was therefore considered. The CH_4 concentration of 1950 ppbv was assumed. Due to the temporal resolution of the instruments, calculated reactivity was performed every 1hour and 30 minutes.

When comparing the measured and the calculated OH reactivity, the calculated level is systematically smaller than the measured one, with the exception of the 5th and the 8th of February, when instrumental

interferences were noted. The median (mean) value of the calculated OH reactivity over the entire campaign is $16s^{-1}$ ($17.5s^{-1}$), while the measured OH reactivity is double, $33s^{-1}$ ($40\ s^{-1}$).

The breakdown of the total OH reactivity measured during the entire campaign is presented in Fig. 10. The mean values were taken in consideration for the calculations. The missing OH reactivity, given by the difference between the measured and the calculated reactivity, is quite high: 54%, showing that when averaged over the entire campaign, more than half of the measured OH reactivity is not explained. Pie chart b) presents the contribution of the different compounds to the calculated OH reactivity. The main compounds explaining the calculated part of the OH reactivity are NO_2 (55%), followed by the sum of NMHCs (15%), NO and CO (accounting each for 10%) and finally the sum of OVOCs (8%).

Examining now the missing reactivity according to the air mass origins, we note significant difference if the air mass was of oceanic or of continental origin. Figure 11 presents the enclosed piecharts of the breakdown total OH reactivity for periods II and III. During the period associated with oceanic air masses and therefore characteristic of the local pollution in Paris, the measured and the calculated OH reactivity agreed within 12% (see piechart a)), which is within the uncertainty range (±24%) of the measured and calculated reactivity. This good agreement points out that during period II, all the main OH reactive species were measured. As Paris is impacted by traffic emissions, high levels of NOx are emitted into the atmosphere. NO_2 and NO explain about 60% of the total measured OH reactivity. This large contribution is expected as in urban atmosphere, the main sink of OH being the formation of the nitric acid (HNO_3) (Delmas et al., 2005). The OH reactivity due to the NMHC accounts for ~14%, while the OVOC and the CO contribute with 7 and respectively 8% to the total OH reactivity. When considering only the measured VOCs presented in Table 2, among the NMHC, the species that contributed the most to the OH reactivity were ethene with13 % and propene with 7.5%. Among the oxygenated VOCs, the acetaldehyde and ethanol contributed with 16% and respectively 14% to the OH reactivity.

We note a very good agreement between the contribution of the different compounds to the total OH reactivity on the entire campaign (see piechart of Fig. 10) and during the local pollution period (pie chart a) from Fig. 11). This clearly points out that when not under continental pollution plumes, the species which were measured during the MEGAPOLI campaign (CO, NOx and list of VOCs from Table 2) characterize correctly the Paris OH reactivity levels.

Part b) of Fig. 11 indicates that during continental import, the measured OH reactivity was much higher than the calculated value. The missing OH reactivity was now of 75%. This is a huge value compared to missing OH reactivities registered in other urban areas (for more details, see Sect. 3.5.3). Calculations indicate that the reactions of OH with NO_2 are the greatest contributors to the total OH reactivity, and followed by NMHC, CO, OVOCs and NO.

For a better understanding of the variability of the not-measured OH reactivity nature, Fig. 12 presents on the top panel the missing OH reactivity series.

As already predicted, the highest values were registered during the continental air mass imports, while the lowest level was registered under the marine air mass influence. We can conclude that during the local pollution period all of the main OH reactive species were measured and therefore the OH reactivity budget can be closed simply by using the already measured compounds. On the contrary, during continental import periods, the non-measured OH reactive species are considered to be at the origin of the high level of the missing OH reactivity. Therefore these non-measured species could be: a) either primary OH reactive compounds, or b) secondary species, characteristic of reprocessed air masses. The first suggestion is less probable, if we consider that the most important classes of OH reactive species, already measured in other studies, were also measured during the MEGAPOLI winter campaign. Furthermore, the good agreement between the measured and calculated OH reactivity found for "period II" reinforces this conclusion.

The temporal variability of submicron secondary inorganic salts (ammonium nitrate and ammonium sulphate) measured by AMS is reported in Fig. 12 (second panel). At many locations ammonium nitrate has shown to be correlated with freshly (less-) photochemically aged organic aerosols (OA) whereas ammonium sulphate was more related to regional heavily aged OA (Lanz et al., 2007; Jimenez et al., 2009; Ulbrich et al., 2009). The sum of these two secondary ion components may be then used to infer the role of photochemical processes involved in the formation of secondary OA from ambient VOC. Low concentrations of these ions were observed during periods with oceanic air masses whereas significantly higher concentrations were observed during periods I and III which are influenced by continental air masses. These observations are consistent with those reported in Paris during springtime by Sciare et al. (2010) and clearly point to the major influence of photochemically processed continental EU anthropogenic emissions. The good agreement observed in Fig. 12 between the temporal variability of these ions and the missing OH reactivity strengthens the previous idea that during continental import, the OH reactivity in Paris is impacted by the non-measured oxidized compounds issues of the reprocessing of the air masses (products issued from multi-oxidation of primary compounds).

3.5. Comparison with OH reactivity in other urban areas

3.5.1. Comparison of OH reactivity levels with levels measured in other cities around the world

Table 4 synthetises the median and the maximum OH reactivity levels previously measured in other urban areas around the world.

As expected, the lowest median values were noticed in small cities. The median values registered in Nashville (United States), Houston (United States) and Mainz (Germany) hardly exceeded $10s^{-1}$. The highest OH reactivity value registered corresponded to summer measurements in Tokyo ($40s^{-1}$), followed by Mexico City with $33s^{-1}$. Intermediate values were observed for New York City, when for both the winter and the summer campaign, the OH reactivity was about $20s^{-1}$. When considering the median value of the entire winter campaign, the Paris OH reactivity was pretty high, of about the same order as for Mexico City, $33s^{-1}$. Nevertheless, this discussion must take into consideration the two contrasting periods identified for the MEGAPOLI winter campaign and which were correlated with different air mass origins (see Sect. 3.3.1). During the local pollution period characterized by the oceanic air masses, the OH reactivity levels registered were quite low, about $20s^{-1}$, value comparable with values registered in New York for the same period of the year, but also comparable to the values registered in Tokyo during winter. When considering the continental long range transport, the median of the OH reactivity levels was much higher: $60s^{-1}$.

The maximum OH reactivity observed during the MEGAPOLI winter campaign was of the same order of magnitude as the maximum measured in Tokyo and New York, but lower than the maximum OH reactivity measured in Mexico City.

3.5.2. Analysis of the contributions of different atmospheric constituents to OH reactivity in different megacities

Figure 13 presents the contributions from different atmospheric constituents to the calculated OH reactivity for 5 different urban atmospheres and different periods of the year. For Tokyo values, the data was estimated from Fig. 9 (page 7879) of the Yoshino et al. (2006) reference. The Mexico City, New York and Houston data were obtained from Mao et al. (2010).

All of the studies presented in Fig. 13 take into consideration measurements of inorganic compounds (CO, NOx), hydrocarbons (including isoprene), formaldehyde, oxygenated VOCs, but also biogenic emissions, with the exception of Paris, where no formaldehyde and biogenics (because of the winter season) were available. For more details see column “measured species” from Table 2. We can therefore conclude on the pertinence of the further discussion.

The main classes of the compounds actually identified as the main OH reactivity sinks were taken into consideration in Fig. 13. These are: CO, NO_x (sum of NO and NO_2), the sum of non-methane hydrocarbons (NMHC), sum of oxygenated VOCs (OVOCs) and the sum of biogenic VOC (BVOCs). Function of the season, the BVOC can be negligible. That is the reason why in Paris, the BVOCs contribution was not quantified. For the same reason, the BVOC contribution in Tokyo was small (<1%).

As the New York study was performed during summer (see Table 4), the contribution from the BVOC counted for 4%.

The contribution from CO is very much alike in the five studies (12 – 15%), although different seasons are considered. The contribution from the NOx exceeds 50% for Paris, Tokyo and New York cities, showing the large influence of the traffic-related emissions to the calculated OH reactivity. Still, the Paris NOx contribution is the highest registered among the five studies (65%), strengthening the idea that the local pollution in Paris is mainly impacted by traffic emissions. Mexico City and Houston showed low values of NOx (only 23% and respectively 15%), but the contribution from the NMHCs reaches 50% in both cases. Although Mexico City and New York (comprising their Metropolitan Areas) are comparable in terms of population and size, the NMHC level registered in New York City is rather low because of the more advanced pollution abatement efforts deployed here. Previous study (de Gouw et al., 2006) showed that in Mexico City the high NMHC is due to higher biomass fuel being burnt and therefore explaining the high contribution from the NMHC to the OH reactivity. In the case of Houston, Leuchner and Rappenglük (2010) announced high industrial solvent emissions. Higher contributions from aromatics (15%) were therefore reported for Houston, compared to only 3.6% in Paris, 4% in New York City and 7% in Mexico City. The contribution to the total OH reactivity from behalf of the oxygenated VOCs is respectively low, comprised between 4%, for Tokyo, 8% for Paris and 14% announced for New York and Houston.

3.5.3. Missing OH reactivity in other urban areas

Table 4 synthetises the percentages of the missing OH reactivity as previously measured and reported into the literature. Paris results present the highest missing OH reactivity determined in urban areas (up to 75%). This is followed by New York and Tokyo with the values of the missing OH reactivity of about 30%. A high missing OH reactivity has been registered also in Nashville, but in this case, the greater measured-than-calculated OH reactivity was due to the presence of the non-measured species (no biogenics were measured, although measurements were realized in summer time) during this campaign (Lewis et al., 2000; Kovacs et al., 2003).

OH reactivity measurements were performed for New York during summer time but also during winter and the results showed that the missing OH reactivity was higher in winter time that in summer. Opposite results have been obtained in Tokyo, when there was almost no missing OH reactivity during winter. As the suite of simultaneous VOC measurements was inadequate, no missing OH reactivity levels are available for the Mexico City (Shirley et al., 2006).

The value of the missing OH reactivity registered in Paris during period II was in good agreement with the winter results in Tokyo and autumn in Houston.

4. Summary and Conclusions

OH reactivity measurements using the CRM method were realized in Paris between the 23rd of January and until the 13th of February, during the MEGAPOLI winter campaign 2010. As the measurements have been realized in strong NO field (10 to 160 ppbv), correction factors were applied to the data set to overcome the NO interference into the setup.

OH reactivity ranged from below the detection limit ($3.5s^{-1}$) up to $130s^{-1}$. The median value registered for the entire campaign was of $33s^{-1}$. As Paris and its surrounding region (Ile de France) are surrounded by a rural area, it was possible to separate continental background influence from oceanic background influence, when discussing the OH reactivity levels. Considering these two main influences, we could conclude that during the marine air mass origins, the pollution in Paris was mainly due to traffic-related emissions and the measured OH reactivity level was of $20s^{-1}$, value comparable to values measured in other urban areas (New York and Tokyo). When considering the contribution of different atmospheric constituents to the OH reactivity in different megacities, two main profiles of urban areas have been identified: one related to traffic emissions, the other one to industrial emissions. Therefore, Paris has the same traffic-related emission profile as Tokyo and New York, the main compounds that contribute to the calculated OH reactivity being the NOx, with more than 50%, followed by NMHCs (15 to 28%), CO (around 14%) and OVOCs (less than 14%). Mexico City and Houston were identified as cities with industrial profiles, the main contributor to the calculated OH reactivity being the NMHCs (around 50%), followed by NOx (15 to 28%), OVOCs (11 to 14%) and CO (14%).

During the continental import air masses, an additional imported pollution added to the local one and very high OH reactivity levels were announced ($120s^{-1}$).

Additional measurements and analysis of the variability of a large panel of compounds simultaneously measured within the MEGAPOLI framework (NOx, CO, O_3, NMHCs and OVOCs) pointed out a large part of the missing OH reactivity. When considering the entire MEGAPOLI campaign, the total missing OH reactivity was of 54%, showing that when averaged over the entire campaign, more than half of the measured OH reactivity is not explained. The found value is higher than the values reported in other urban areas and when the maximum missing OH reactivity was of 33% (Sadanaga et al., 2004; Ren et al., 2006). Nevertheless, during the marine air mass influences, the missing OH reactivity is of only 12%, value comprised within the measurement uncertainties and which has shown that during the local pollution periods, the OH reactivity budget can be closed only by using the already measured compounds. Still, surprisingly, during the continental imported air masses, 75% of the measured OH reactivity could not be explained by the measured species. This percentage was higher than the missing OH reactivity values registered in other urban areas. The missing OH reactivity showed a similar variation as longer life-time compounds and photochemically produced aerosol species suggesting that air masses

corresponding to continental import were probably loaded in highly oxidized products, probably of anthropogenic origin.

We therefore concluded that levels of missing OH reactivity of the same magnitude as in forested areas were registered for the first time in an urban area. Still, if for the forested area, previous studies (Di Carlo et al., 2004; Sinha et al., 2010; Kim et al., 2011) identified the biogenic VOCs as mainly responsible of these high levels, in the case of Paris, the non-measured compounds were likely (multi)oxidized compounds issued from processed anthropogenic emissions.

Recently, Kato et al. (2011) proposed a relative rate method using GC-FID detectors to estimate the contribution of the OH reactivity of unidentified VOCs in the atmosphere of Tokyo (study conducted in spring 2004). They found that the contribution of the unidentified species was about 22% of that for all the VOCs, and that when taken into consideration they improve the percentage of the missing OH reactivity that can be explained. Still, the contribution to the total OH reactivity of the unidentified species using this method is underestimated because species with high polarity or heavy species are being lost during the concentration process.

Considering the vast complexity that the identification and quantification of the unknown OH reactive species in an urban environment pose for air quality, further studies involving more measurements of secondary compounds are required.

Appendix A. Air mass origins during MEGAPOLI

OH reactivity measurements were made from the 23rd of January until the 13th of February. During this

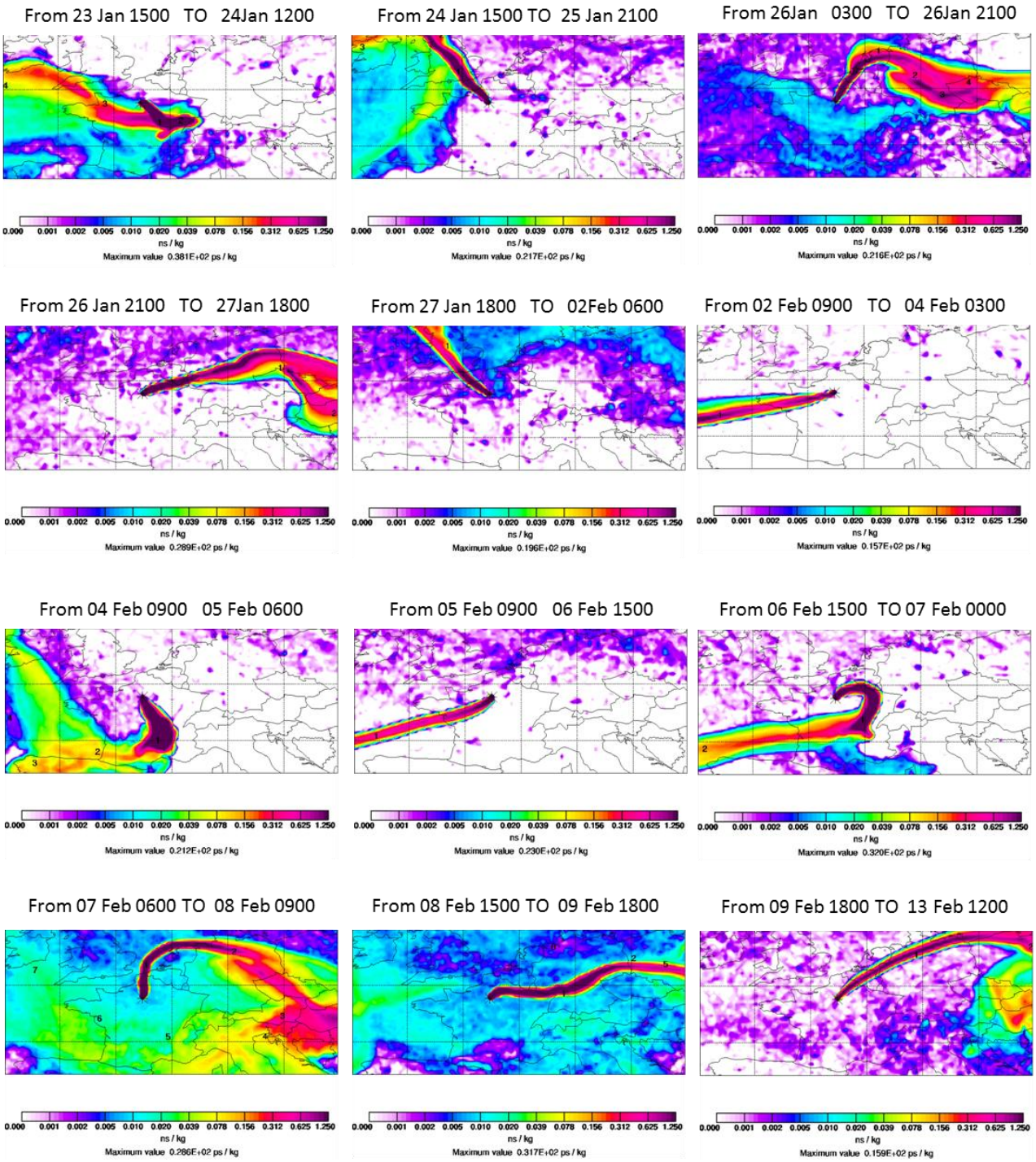

Figure A1: The 20 days backward trajectories of the air masses reaching Paris as calculated by Flexpart. The plots represent one example characterising the announced interval above each

time, a variety of air masses passed over Paris and its surroundings. Figure A1 synthesises all these air

masses, their origins in the order in which they succeeded, as represented by the 20 days backtrajectories calculated with the FLEXPART model. Above each plot, the interval on which the air mass was observed is given. 12 different types of air masses have been observed, originating from different parts of the continent or the Atlantic Ocean. At the beginning of the campaign, from the 23rd of January and for one day, the air masses originated from the central and eastern part of France. The next day they came from the northwest side of France passing first over Great Britain. From the 26th until the 27th in the evening, the air masses arriving over Paris has crossed the northern part of the European continent, thereafter switching again for air masses passing over Great Britain. These later air masses persisted from the 27th of January until the 2nd of February. From this moment and for two days, fresh and clean air masses coming from over the Atlantic Ocean area were experienced in Paris. The same conditions have been noted again for one day, from the early morning on the 5th of February until 12:00 next day. Air masses coming from central France were also noted on two other occasions: from the 4th of February, 09:00, to the 5th of February, 06:00, and from the 6th (15:00) to the 7th of February (mid-night). Finally, air masses originating from the northern part of France that have previously passed over the northern or north-eastern part of the continent. These were observed from the 7th of February and until the end of the campaign, the 13th of February (see the last 3 plots of Fig. A1).

Appendix B. Diurnal variation of gaseous pollutants in Paris

Figure B1 presents the mean daily profiles of the selected gaseous pollutants (CO, NO, NO_2, O_3, the sum of NMHC and the sum of OVOCs) characterizing the Paris atmosphere during the whole campaign.

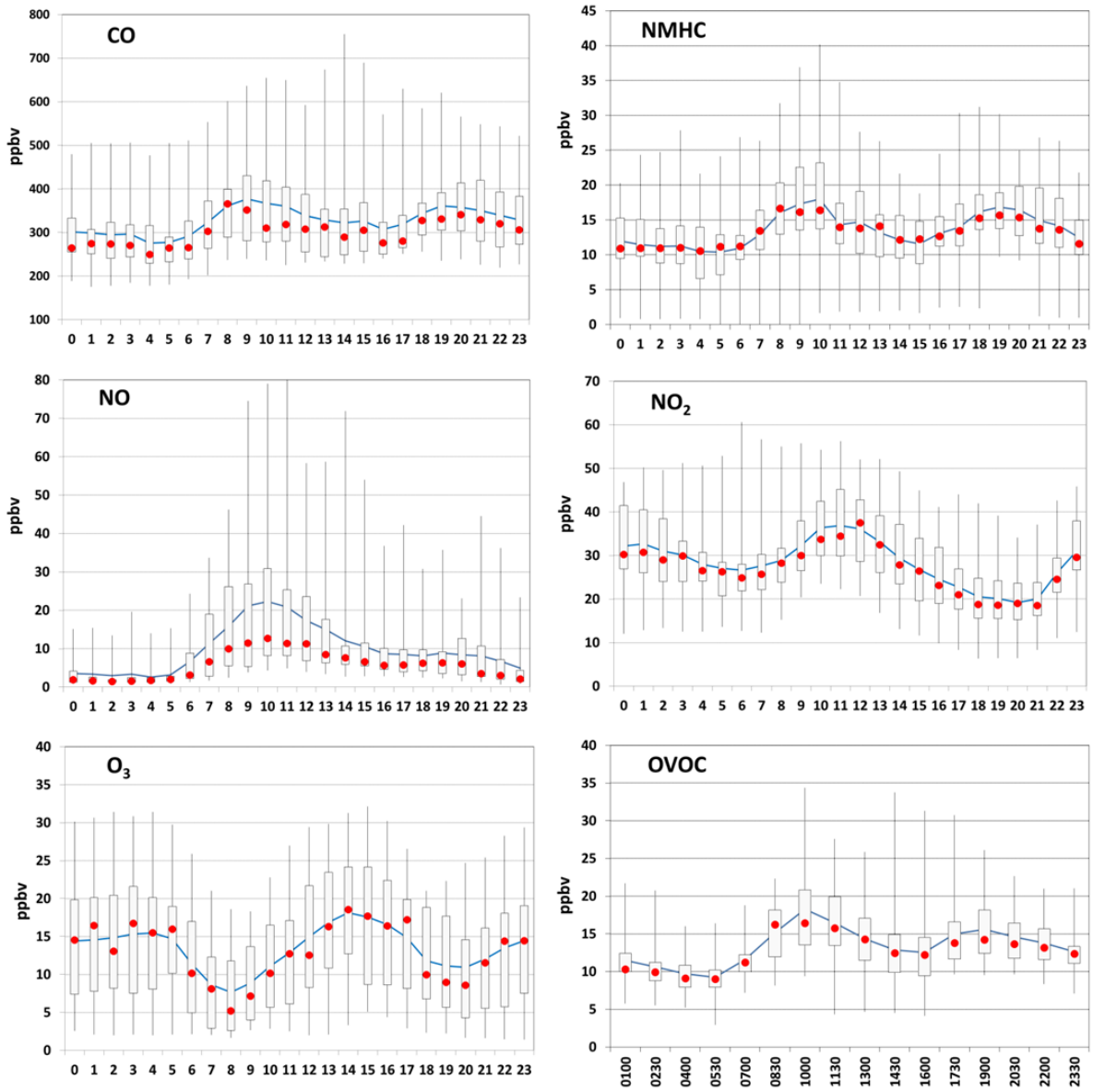

Figure B1. Hourly box plots for CO, O_3,NO, NO_2, NMHC and OVOC for the MEGAPOLI campaign. Red dots represent the median; the blue line represents the mean. The bottom and top of the box are the 25th (Q_1) and the 75th (Q_3) percentile and the ends of the whiskers represent the highest and the lowest data points.

Primary species (CO, NMHC and NO) show the same daily profile, related to their common source, the traffic related emissions (Vardulakis et al, 2002). They show a minimum value during the night, a first peak in the early morning (~0700 hours), a slight decrease in the afternoon and a second peak

starting to form in the late afternoon-early evening (16:00). The first peak corresponds to traffic emissions in a shallow boundary layer, while the second peak corresponds also to traffic emissions but this time in a well-developed boundary layer, so more diluted. The same profile of these primary pollutants was noticed in Paris during spring 2007 by Gros et al. (2011) and similar diurnal variations for primary hydrocarbons have also been reported for several sites inside the city boundaries (de Gouw et al., 2009; Velasco et al., 2007).

NO_2 is mainly of secondary origin and shows maxima in the morning, though slightly later than the primary species (about 10:00). The OVOCs, which have both primary and secondary sources, present the same diurnal cycle as the one of the primary sources. We can therefore conclude that in Paris, the oxygenated species are driven mainly by the primary emission sources.

Ozone was typically titrated by NO in the early morning. The first increase of ozone is observed at about 09:00 and it is due to mixing with free tropospheric air, when the boundary layer develops. It reaches its maximum in the afternoon, when the photochemical production is maximum. Still the maxima registered during MEGAPOLI is relatively low (only 17ppbv) compared to the ozone values registered in other cities around the world (see Table 1). The high volume mixing ratios of NOx, the smaller photochemical activity during the winter season and a high developed boundary layer during the day can explain this low value.

The analysis of the mean diurnal cycles confirms that the main primary emission source in Paris is represented by the traffic source.

Acknowledgements

We would like to thank T. Leonardis and N. Locoge (EMD) for support with GC-MS measurements, B. Temime (LCP) for the PTR-MS measurements and C. Gaimoz (LSCE and now at LISA) for the GC-FID measurements. We would like to thank also the MEGAPOLI field campaign participants and especially A. Stohl (NILU) for providing Flexpart results. The research leading to these results has received funding from the European Union's Seventh Framework Programme FP/ 2007 – 2011 within the project MEGAPOLI grant agreement n° 212520. Support from CEA, CNRS, ADEME, ANR-MEGAPOLI are acknowledged.

References:

Ammann, C., Brunner, A., Spirig, C., and Neftel, A.: Technical note: Water vapour concentration and flux measurements with ptr-ms, Atmospheric Chemistry and Physics, 6, 4643-4651, 2006.

Atkinson, R., Baulch, D. L., Cox, R. A., Crowley, J. N., Hampson, R. F., Hynes, R. G., Jenkin, M. E., Rossi, M. J., and Troe, J.: Evaluated kinetic and photochemical data for atmospheric chemistry: Volume i - gas phase reactions of o(x), ho(x), no(x) and so(x) species, Atmospheric Chemistry and Physics, 4, 1461-1738, 2004.

Atkinson, R., Baulch, D. L., Cox, R. A., Crowley, J. N., Hampson, R. F., Hynes, R. G., Jenkin, M. E., Rossi, M. J., and Troe, J.: Evaluated kinetic and photochemical data for atmospheric chemistry: Volume ii - gas phase reactions of organic species, Atmospheric Chemistry and Physics, 6, 3625-4055, 2006.

Canagaratna, M. R., Jayne, J. T., Jimenez, J. L., Allan, J. D., Alfarra, M. R., Zhang, Q., Onasch, T. B., Drewnick, F., Coe, H., Middlebrook, A., Delia, A., Williams, L. R., Trimborn, A. M., Northway, M. J., DeCarlo, P. F., Kolb, C. E., Davidovits, P., and Worsnop, D. R.: Chemical and microphysical characterization of ambient aerosols with the aerodyne aerosol mass spectrometer, Mass Spectrometry Reviews, 26, 185-222, 10.1002/mas.20115, 2007.

Crutzen, P. J.: Global budgets for non-co2 greenhouse gases, Environmental Monitoring and Assessment, 31, 1-15, 10.1007/bf00547177, 1994.

Day, B. M., Rappengluck, B., Clements, C. B., Tucker, S. C., and Brewer, W. A.: Nocturnal boundary layer characteristics and land breeze development in houston, texas during texaqs ii, Atmospheric Environment, 44, 4014-4023, 10.1016/j.atmosenv.2009.01.031, 2010.

de Gouw, J. A., Warneke, C., Stohl, A., Wollny, A. G., Brock, C. A., Cooper, O. R., Holloway, J. S., Trainer, M., Fehsenfeld, F. C., Atlas, E. L., Donnelly, S. G., Stroud, V., and Lueb, A.: Volatile organic compounds composition of merged and aged forest fire plumes from alaska and western canada, Journal of Geophysical Research-Atmospheres, 111, D10303 10.1029/2005jd006175, 2006.

de Gouw, J. A., Welsh-Bon, D., Warneke, C., Kuster, W. C., Alexander, L., Baker, A. K., Beyersdorf, A. J., Blake, D. R., Canagaratna, M., Celada, A. T., Huey, L. G., Junkermann, W., Onasch, T. B., Salcido, A., Sjostedt, S. J., Sullivan, A. P., Tanner, D. J., Vargas, O., Weber, R. J., Worsnop, D. R.,

Yu, X. Y., and Zaveri, R.: Emission and chemistry of organic carbon in the gas and aerosol phase at a sub-urban site near mexico city in march 2006 during the milagro study, Atmospheric Chemistry and Physics, 9, 3425-3442, 2009.

DeCarlo, P. F., Kimmel, J. R., Trimborn, A., Northway, M. J., Jayne, J. T., Aiken, A. C., Gonin, M., Fuhrer, K., Horvath, T., Docherty, K. S., Worsnop, D. R., and Jimenez, J. L.: Field-deployable, high-resolution, time-of-flight aerosol mass spectrometer, Analytical Chemistry, 78, 8281-8289, 10.1021/ac061249n, 2006.

Delmas, R., Mégie, G., and Peuch, V.-H.: Physique et chimie de l'atmosphère, 2005.

Di Carlo, P., Brune, W. H., Martinez, M., Harder, H., Lesher, R., Ren, X. R., Thornberry, T., Carroll, M. A., Young, V., Shepson, P. B., Riemer, D., Apel, E., and Campbell, C.: Missing oh reactivity in a forest: Evidence for unknown reactive biogenic vocs, Science, 304, 722-725, 10.1126/science.1094392, 2004.

Gaimoz, C., Sauvage, S., Gros, V., Herrmann, F., Williams, J., Locoge, N., Perrussel, O., Bonsang, B., d'Argouges, O., Sarda-Esteve, R., and Sciare, J.: Volatile organic compounds sources in paris in spring 2007. Part ii: Source apportionment using positive matrix factorisation, Environmental Chemistry, 8, 91-103, 10.1071/en10067, 2011.

Goldstein, A. H., and Galbally, I. E.: Known and unexplored organic constituents in the earth's atmosphere, Environmental Science & Technology, 41, 1514-1521, 10.1021/es072476p, 2007.

Gros, V., Sciare, J., and Yu, T.: Air-quality measurements in megacities: Focus on gaseous organic and particulate pollutants and comparison between two contrasted cities, paris and beijing, Comptes Rendus Geoscience, 339, 764-774, 2007.

Gros, V., Gaimoz, C., Herrmann, F., Custer, T., Williams, J., Bonsang, B., Sauvage, S., Locoge, N., d'Argouges, O., Sarda-Esteve, R., and Sciare, J.: Volatile organic compounds sources in paris in spring 2007. Part i: Qualitative analysis, Environmental Chemistry, 8, 74-90, 10.1071/en10068, 2011.

Ingham, T., Goddard, A., Whalley, L. K., Furneaux, K. L., Edwards, P. M., Seal, C. P., Self, D. E., Johnson, G. P., Read, K. A., Lee, J. D., and Heard, D. E.: A flow-tube based laser-induced

fluorescence instrument to measure oh reactivity in the troposphere, Atmospheric Measurement Techniques, 2, 465-477, 2009.

Jimenez, J. L., Canagaratna, M. R., and Donahue, N. M., et al., Evolution of Organic Aerosols in the Atmosphere, Science, 326, 1525–1529, doi:10.1126/science.1180353, 2009.

Kato, S., Sato, T., and Kajii, Y.: "A method to estimate the contribution of unidentified VOCs to OH reactivity", Atmospheric Environment, 45, 5531-5539, 10.1016/j.atmosenv.2011.05.074, 2011.

Kim, S., Guenther, A., Karl, T., and Greenberg, J.: Contributions of primary and secondary biogenic voc tototal oh reactivity during the cabinex (community atmosphere-biosphere interactions experiments)-09 field campaign, Atmospheric Chemistry and Physics, 11, 8613-8623, 10.5194/acp-11-8613-2011, 2011.

Kovacs, T. A., and Brune, W. H.: Total oh loss rate measurement, Journal of Atmospheric Chemistry, 39, 105-122, 10.1023/a:1010614113786, 2001.

Kovacs, T. A., Brune, W. H., Harder, H., Martinez, M., Simpas, J. B., Frost, G. J., Williams, E., Jobson, T., Stroud, C., Young, V., Fried, A., and Wert, B.: Direct measurements of urban oh reactivity during nashville sos in summer 1999, Journal of Environmental Monitoring, 5, 68-74, 10.1039/b204339d, 2003.

Lanz, V. A., Alfarra, M. R., Baltensperger, U., Buchmann, B., Hueglin, C., and Prévôt, A. S. H.: Source apportionment of submicron organic aerosols at an urban site by factor analytical modelling of aerosol mass spectra, Atmos. Chem. Phys., 7, 1503–1522, 2007.

Leuchner, M., and Rappenglueck, B.: Voc source-receptor relationships in houston during texaqs-ii, Atmospheric Environment, 44, 4056-4067, 10.1016/j.atmosenv.2009.02.029, 2010.

Lewis, A. C., Carslaw, N., Marriott, P. J., Kinghorn, R. M., Morrison, P., Lee, A. L., Bartle, K. D., and Pilling, M. J.: A larger pool of ozone-forming carbon compounds in urban atmospheres, Nature, 405, 778-781, 10.1038/35015540, 2000.

Lewis, A. C., Carslaw, N., Marriott, P. J., Kinghorn, R. M., Morrison, P., Lee, A. L., Bartle, K. D., and Pilling, M. J.: A larger pool of ozone-forming carbon compounds in urban atmospheres, Nature, 405, 778-781, 10.1038/35015540, 2000.

Lindinger, W., Hansel, A., and Jordan, A.: On-line monitoring of volatile organic compounds at pptv levels by means of proton-transfer-reaction mass spectrometry (ptr-ms) - medical applications, food control and environmental research, International Journal Of Mass Spectrometry, 173, 191-241, 1998.

Lou, S., Holland, F., Rohrer, F., Lu, K., Bohn, B., Brauers, T., Chang, C. C., Fuchs, H., Haeseler, R., Kita, K., Kondo, Y., Li, X., Shao, M., Zeng, L., Wahner, A., Zhang, Y., Wang, W., and Hofzumahaus, A.: Atmospheric oh reactivities in the pearl river delta - china in summer 2006: Measurement and model results, Atmospheric Chemistry and Physics, 10, 11243-11260, 10.5194/acp-10-11243-2010, 2010.

Mao, J., Ren, X., Brune, W. H., Olson, J. R., Crawford, J. H., Fried, A., Huey, L. G., Cohen, R. C., Heikes, B., Singh, H. B., Blake, D. R., Sachse, G. W., Diskin, G. S., Hall, S. R., and Shetter, R. E.: Airborne measurement of oh reactivity during intex-b, Atmospheric Chemistry and Physics, 9, 163-173, 2009.

Mao, J., Ren, X., Chen, S., Brune, W. H., Chen, Z., Martinez, M., Harder, H., Lefer, B., Rappenglueck, B., Flynn, J., and Leuchner, M.: Atmospheric oxidation capacity in the summer of houston 2006: Comparison with summer measurements in other metropolitan studies, Atmospheric Environment, 44, 4107-4115, 10.1016/j.atmosenv.2009.01.013, 2010.

Naik, V., Fiore, A. M., Horowitz, L. W., Singh, H. B., Wiedinmyer, C., Guenther, A., de Gouw, J. A., Millet, D. B., Goldan, P. D., Kuster, W. C., and Goldstein, A.: Observational constraints on the global atmospheric budget of ethanol, Atmospheric Chemistry and Physics, 10, 5361-5370, 10.5194/acp-10-5361-2010, 2010.

Ren, X., Brune, W. H., Mao, J., Mitchell, M. J., Lesher, R. L., Simpas, J. B., Metcalf, A. R., Schwab, J. J., Cai, C., Li, Y., Demerjian, K. L., Felton, H. D., Boynton, G., Adams, A., Perry, J., He, Y., Zhou, X., and Hou, J.: Behavior of oh and ho2 in the winter atmosphere in new york city, Atmospheric Environment, 40, S252-S263, 10.1016/j.atmosenv.2005.11.073, 2006a.

Ren, X., Brune, W. H., Oliger, A., Metcalf, A. R., Simpas, J. B., Shirley, T., Schwab, J. J., Bai, C., Roychowdhury, U., Li, Y., Cai, C., Demerjian, K. L., He, Y., Zhou, X., Gao, H., and Hou, J.: Oh, ho(2), and oh reactivity during the pmtacs-ny whiteface mountain 2002 campaign: Observations and

model comparison, Journal of Geophysical Research-Atmospheres, 111, D10s03 10.1029/2005jd006126, 2006b.

Ren, X. R., Harder, H., Martinez, M., Lesher, R. L., Oliger, A., Shirley, T., Adams, J., Simpas, J. B., and Brune, W. H.: Hox concentrations and oh reactivity observations in new york city during pmtacs-ny2001, Atmospheric Environment, 37, 3627-3637, 10.1016/s1352-2310(03)00460-6, 2003.

Roukos, J., Plaisance, H., Leonardis, T., Bates, M., and Locoge, N.: Development and validation of an automated monitoring system for oxygenated volatile organic compounds and nitrile compounds in ambient air, Journal of Chromatography A, 1216, 8642-8651, 10.1016/j.chroma.2009.10.018, 2009.

Sadanaga, Y., Yoshino, A., Kato, S., Yoshioka, A., Watanabe, K., Miyakawa, Y., Hayashi, I., Ichikawa, M., Matsumoto, J., Nishiyama, A., Akiyama, N., Kanaya, Y., and Kajii, Y.: The importance of no2 and volatile organic compounds in the urban air from the viewpoint of the oh reactivity, Geophysical Research Letters, 31, L08102 10.1029/2004gl019661, 2004.

Sadanaga, Y., Yoshino, A., Kato, S., and Kajii, Y.: Measurements of oh reactivity and photochemical ozone production in the urban atmosphere, Environmental Science & Technology, 39, 8847-8852, 10.1021/es049457p, 2005.

Sadanaga, Y., Kondo, S., Hashimoto, K., and Kajii, Y.: Measurement of the rate coefficient for the oh+no(2) reaction under the atmospheric pressure: Its humidity dependence, Chemical Physics Letters, 419, 474-478, 10.1016/j.cplett.2005.12.026, 2006.

Sciare, J., O. d'Argouges, Q. Zhang, R. Sarda-Estève, C. Gaimoz, V. Gros, M. Beekmann and O. Sanchez, Comparison between simulated and observed chemical composition of fine aerosols in Paris (France) during springtime: contribution of regional versus continental emissions, Atmos. Chem. Phys., 10, 1-18, 2010

Seinfeld, J. H., and Pandis, S. N.: Atmospheric chemistry and physics: From air pollution to climate change, 2006.

Shirley, T. R., Brune, W. H., Ren, X., Mao, J., Lesher, R., Cardenas, B., Volkamer, R., Molina, L. T., Molina, M. J., Lamb, B., Velasco, E., Jobson, T., and Alexander, M.: Atmospheric oxidation in the

mexico city metropolitan area (mcma) during april 2003, Atmospheric Chemistry and Physics, 6, 2753-2765, 2006.

Sinha, V., Williams, J., Crowley, J. N., and Lelieveld, J.: The comparative reactivity method - a new tool to measure total oh reactivity in ambient air, Atmospheric Chemistry and Physics, 8, 2213-2227, 2008.

Sinha, V., Custer, T. G., Kluepfel, T., and Williams, J.: The effect of relative humidity on the detection of pyrrole by ptr-ms for oh reactivity measurements, International Journal of Mass Spectrometry, 282, 108-111, 10.1016/j.ijms.2009.02.019, 2009.

Sinha, V., Williams, J., Lelieveld, J., Ruuskanen, T. M., Kajos, M. K., Patokoski, J., Hellen, H., Hakola, H., Mogensen, D., Boy, M., Rinne, J., and Kulmala, M.: Oh reactivity measurements within a boreal forest: Evidence for unknown reactive emissions, Environmental Science & Technology, 44, 6614-6620, 10.1021/es101780b, 2010.

Sinha, V., Williams, J., Diesch, J. M., Drewnick, F., Martinez, M., Harder, H., Regelin, E., Kubistin, D., Bozem, H., Hosaynali-Beygi, Z., Fischer, H., Andrés-Hernández, M.D., Kartal, D., Adame, J. A., and Lelieveld, J.: OH reactivity measurements in a coastal location in Southwestern Spain during DOMINO, Atmospheric Chemistry and Physics Discussions, 12, 4979-5014, 2012

Stohl, A., Forster, C., Frank, A., Seibert, P., and Wotawa, G., Technical note: The Lagragian particle dispersion model FELXPART version 6.2, Atmospheric Chemistry and Physics, 5, 2461-2474, 2005

Tuch, T. M., Haudek, A., Muller, T., Nowak, A., Wex, H., and Wiedensohler, A.: Design and performance of an automatic regenerating adsorption aerosol dryer for continuous operation at monitoring sites, Atmospheric Measurement Techniques, 2, 417-422, 2009.

Ulbrich, I. M., Canagaratna, M. R., Zhang, Q., Worsnop, D. R., and Jimenez, J. L.: Interpretation of organic components from Positive Matrix Factorization of aerosol mass spectrometric data, Atmos. Chem. Phys., 9, 2891–2918, 2009

Vardoulakis, S., Gonzalez-Flesca, N., and Fisher, B. E. A.: Assessment of traffic-related air pollution in two street canyons in paris: Implications for exposure studies, Atmospheric Environment, 36, 1025-1039, 2002.

Velasco, E., Lamb, B., Westberg, H., Allwine, E., Sosa, G., Arriaga-Colina, J. L., Jobson, B. T., Alexander, M. L., Prazeller, P., Knighton, W. B., Rogers, T. M., Grutter, M., Herndon, S. C., Kolb, C. E., Zavala, M., de Foy, B., Volkamer, R., Molina, L. T., and Molina, M. J.: Distribution, magnitudes, reactivities, ratios and diurnal patterns of volatile organic compounds in the valley of mexico during the mcma 2002 & 2003 field campaigns, Atmospheric Chemistry and Physics, 7, 329-353, 2007.

Xu, X., van Stee, L. L. P., Williams, J., Beens, J., Adahchour, M., Vreuls, R. J. J., Brinkman, U. A. T., and Lelieveld, J.: Comprehensive two-dimensional gas chromatography (gc x gc) measurements of volatile organic compounds in the atmosphere, Atmospheric Chemistry and Physics, 3, 665-682, 2003.

Yoshino, A., Sadanaga, Y., Watanabe, K., Kato, S., Miyakawa, Y., Matsumoto, J., and Kajii, Y.: Measurement of total oh reactivity by laser-induced pump and probe technique - comprehensive observations in the urban atmosphere of tokyo, Atmospheric Environment, 40, 7869-7881, 10.1016/j.atmosenv.2006.07.023, 2006.

Table 1. Gaseous pollutants levels registered in different urban atmospheres

	Population* in 2010 (10^6)	Period of the year	CO BGND level (ppbv)	CO max (ppbv)	NOx BGND levels (ppbv)	NOx max (ppbv)	Ozone BGND level (ppbv)	Ozone max (ppbv)	NMHC BGND (ppbv)	NMHC max (ppbv)
Houston	6	Aug - Sept 2000	200	250	5	22	25	70	100#	200#
New York City	22	Jun - Aug 2001	400	450	25	50	20	50	100#	150#
Mexico City	22	Apr 2003	100	3000	20	110	25	125	500#	1000#
Houston	6	Aug - Sept 2006	200	250	8	25	25	70	400#	750#
Tokyo	36**	Jan - Feb 2004	400'	1200'	25'	105'	10'	40'	NA	NA
Tokyo	36**	May 2004	300'	550'	13'	50'	50'	80'	NA	NA
Tokyo	36**	November 2004	400'	1000'	20'	65'	10'	60'	NA	NA
Paris	12	Jan - Feb 2010	250	350	30	60	15	17	12 50#	17 100#

* *Cities and Metropolitan Areas*

** *2007*

BGND corresponds to background levels measured at midnight, local time

 # Values in ppbC (ppbCarbon)

NA Non Available Data

‘ Daily mean values were taken into consideration when median diurnal cycles were not available

Table 2. Mean values of the main volatile-organic-compounds (VOC) volume mixing ratio measured during the campaign (TMB, trimethylbenzene; MVK, methyl vinyl ketone).

Compound	Measurement technique	Mean (ppbv)	Min (ppbv)	Max (ppbv)	OH reactivity (s^{-1})
Ethane	GC-FID	2.45	1.14	7.12	0.015
Ethene	GC-FID	2.61	0.33	8.36	0.547
Propane	GC-FID	2.12	0.76	5.04	0.057
Propene	GC-FID	0.44	0.07	1.67	0.323
i - Butane	GC-FID	0.91	0.15	2.84	0.052
n - Butane	GC-FID	1.54	0.34	5.03	0.087
Acetylene	GC-FID	1.77	0.62	5.04	0.044
1- Butene	GC-FID	0.09	0.02	0.26	0.093
i _Butene	GC-FID	0.19	0.02	0.55	0.306
c-2-Butene	GC-FID	0.05	0.02	0.53	0.080
trans-2- Butene	GC-FID	0.07	0.01	0.23	0.126
Isoprene	GC-FID	0.17	0.05	1.43	0.423
n - Hexane	GC-FID	0.14	0.01	1.34	0.019
n - Pentane	GC-FID	0.40	0.07	1.39	0.040
Benzene	PTR-MS	0.33	0.08	1.65	0.010
Toluene	PTR-MS	0.54	0.09	2.36	0.079
Xylenes	GC-FID	0.67	0.13	2.88	0.265
TMB	GC-FID	0.29	0.08	0.76	0.289
Acetonitrile	PTR-MS	0.55	0.09	3.69	0.000
i - Propanol	GC-MS	0.24	0.04	1.06	0.031
Ethanol	GC-MS	7.68	2.22	23.57	0.605
MVK	GC-MS	0.09	0.02	0.44	0.042
Acetone	GC-MS	1.05	0.58	2.97	0.005
2-Butanone	GC-MS	0.29	0.06	0.94	0.009
Hexanal	GC-MS	0.09	0.01	0.22	0.000
Benzaldehyde	GC-MS	0.07	0.02	0.18	0.025
i - Butanol	GC-MS	0.08	0.02	0.20	0.014
Methanol	PTR-MS	2.35	0.89	6.18	0.052
Acetaldehyde	PTR-MS	1.87	0.92	4.49	0.691

Table 3: Mean values of the main pollution compounds measured during period I, II and III

	OH reactivity (s^{-1})	CO (ppbv)	NO (ppbv)	NO2 (ppbv)	Benzene (ppbv)	Xylenes (ppbv)	Acetone (ppbv)	NMHC (ppbv)	OVOC (ppbv)	Air masses
Period I	130	536	24	39	0.7	1.0	2.1	20.6	18.7	Continental
Period II	20	249	4	28	0.2	0.5	0.7	10.1	13.1	Ocean
Period III	110	311	7	27	0.3	0.6	1.0	13.2	12.4	Continental

Table 4: Synthesis of OH reactivity levels measured in other urban atmospheres

Urban site	Season, Year	Employed technique	Average/Median^{+} (s^{-1})	Maximum (s^{-1})	Missing OH reactivity (%)	Measured species$^{£}$ (after Lou et al., 2010)	Reference
Nashville, USA	Summer 1999	**LIF-H20**	11,3±4,8	25	31	SFO	Kovacs et al.K (2003)
Houston, USA	Autumn 2000	**LIF-H2O**	10	12**	~0§	SFOB	Mao et al. (2010)
New York, USA	Summer 2001	**LIF-FAGE**	19±3	50	10	SFOB	Ren et al. (2003)
Mexico City	Spring 2003	**LIF-FAGE**	33	200	-	-	Shirley et al. (2006)
Tokyo, Japan	Summer 2003	**LIF P&P**	40	85	15 to 30	SFOB	Sadanaga et al. (2005)
New York, USA	Winter 2004	**LIF-FAGE**	20	100	33	SF	Ren et al. (2006a)
Tokyo, Japan	Winter 2004	**LIF P&P**	20*	100	5	SFOB	Yoshino et al. (2006)
Mainz, Germany	Summer 2008	**CRM**	10.4	18	-	-	Sinha et al. (2008)
Houston, USA	Autumn 2006	**LIF-H20**	15*	25	~0§	SFOB	Mao et al., (2010b)
Paris, France	Winter 2010	**CRM**	33$^{\#}$ (19.6$^{\#\#}$/60$^{\#\#\#}$)	130	12 to 75	SO	This work

LIF- H_20 Laser Induced Fluorescence Technique - OH produced by H_2O photolysis
LIF- P&P Laser Induced Fluorescence – Pump and Probe Technique
LIF-FAGE Laser Induced Fluorescence - Fluorescence Assay by Gas Expansion
+ average was used when median not available
* approximate values from graphs
** large part of missing data
# median on the entire campaign
median on the local pollution period
median on the continental import period
§ within the measurement and calculated uncertainty
£ Measured species that have used for the calculation of the OH reactivity: ***S*** = inorganic compounds (O_3, CO, NOx, etc) plus hydrocarbons (including isoprene); ***F*** = formaldehyde; ***O*** = OVOCs other than formaldehyde; ***B***= biogenic VOCs, other than isoprene

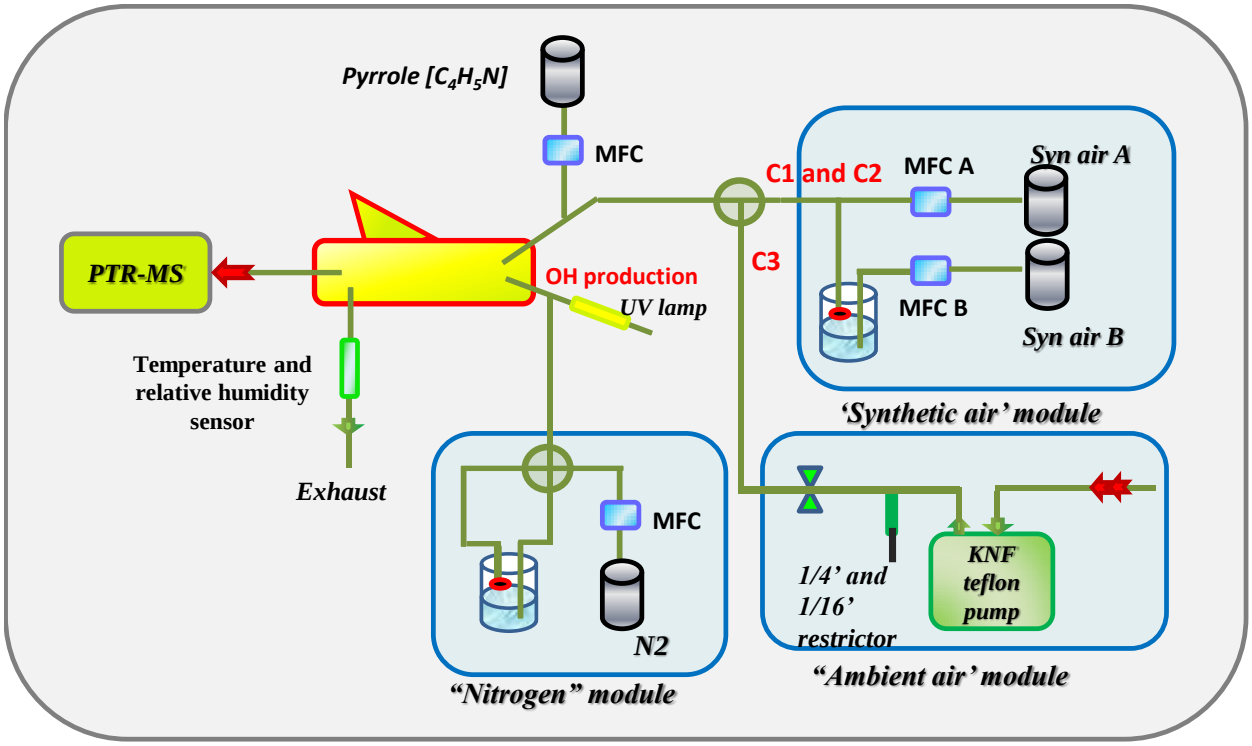

Figure 1. OH reactivity system during MEGAPOLI winter 2010

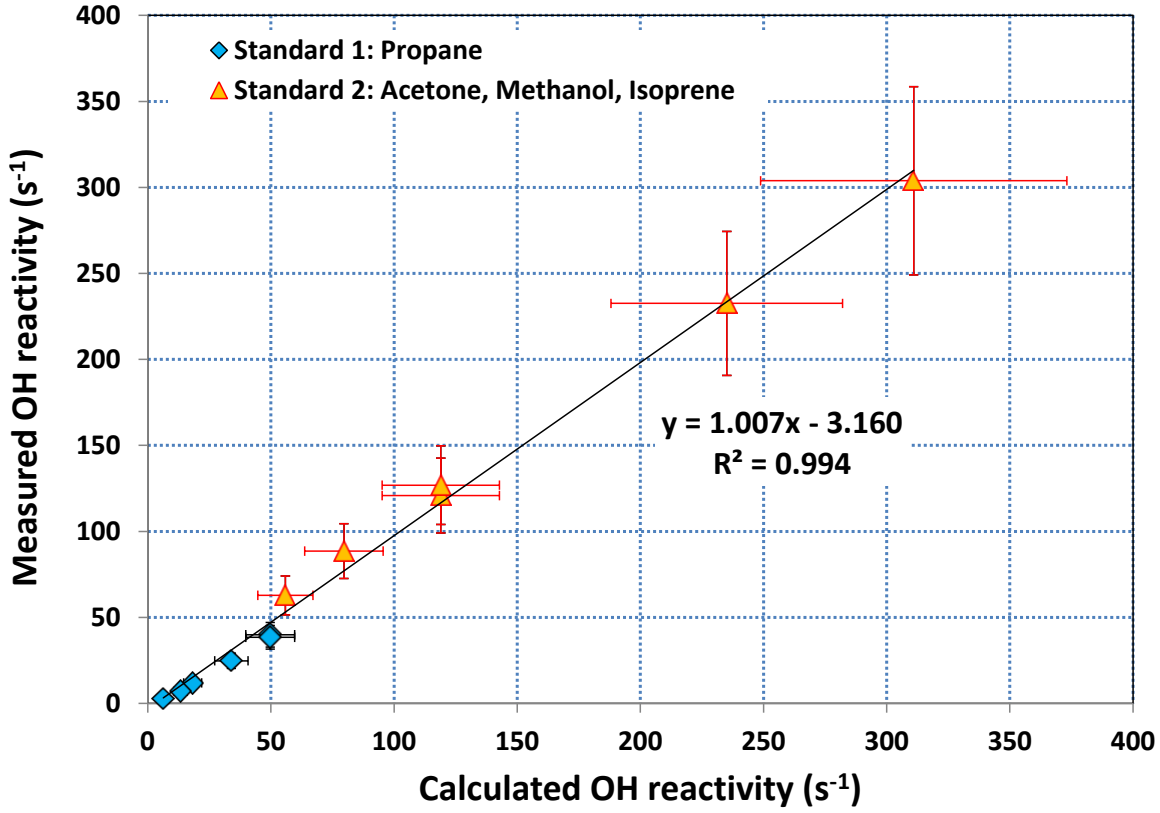

Figure 2. Calibration results using two standards bottles: propane and acetone, methanol and isoprene standard

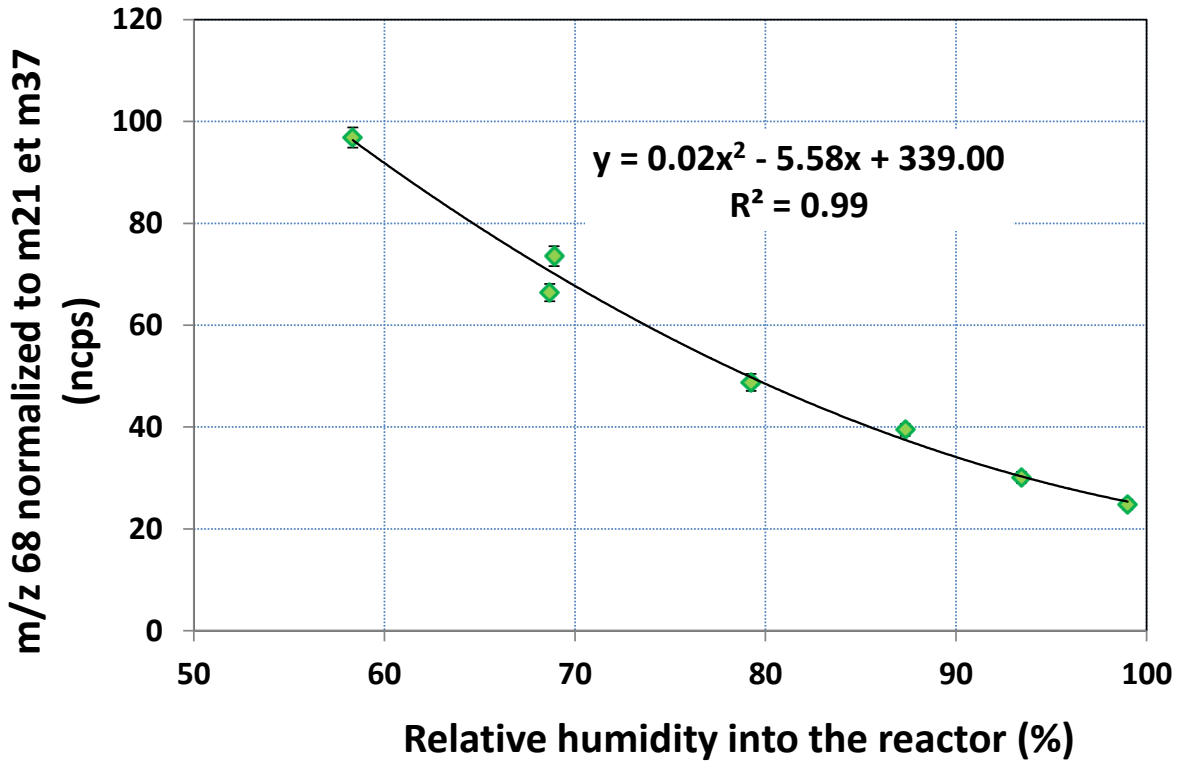

Figure 3. Change in the pyrrole signal (m/z 68) for different percentage of relative humidity into the setup. The temperature of the setup is maintained constant at 24°C

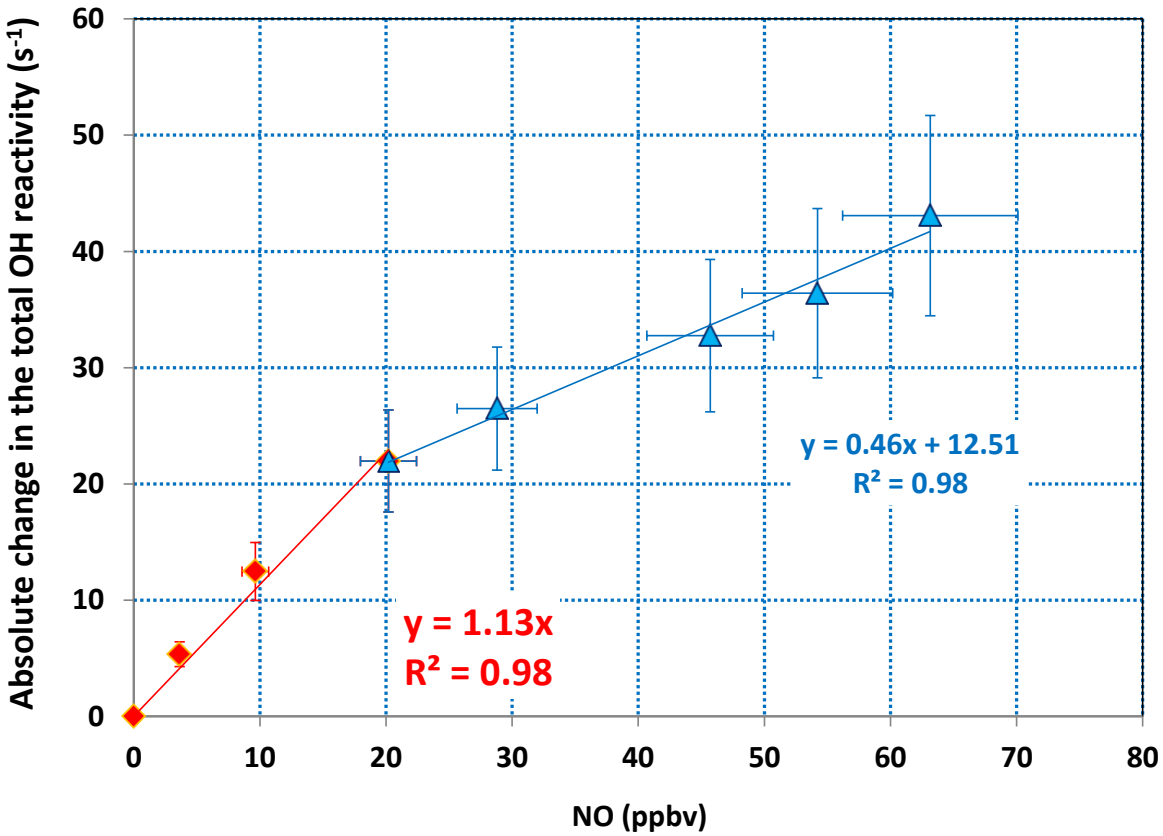

Figure 4. NO test for OH reactivity of 50s-1: the red and the blue curves represent the 2 different slopes obtained for values of NO smaller or bigger than 20ppbv

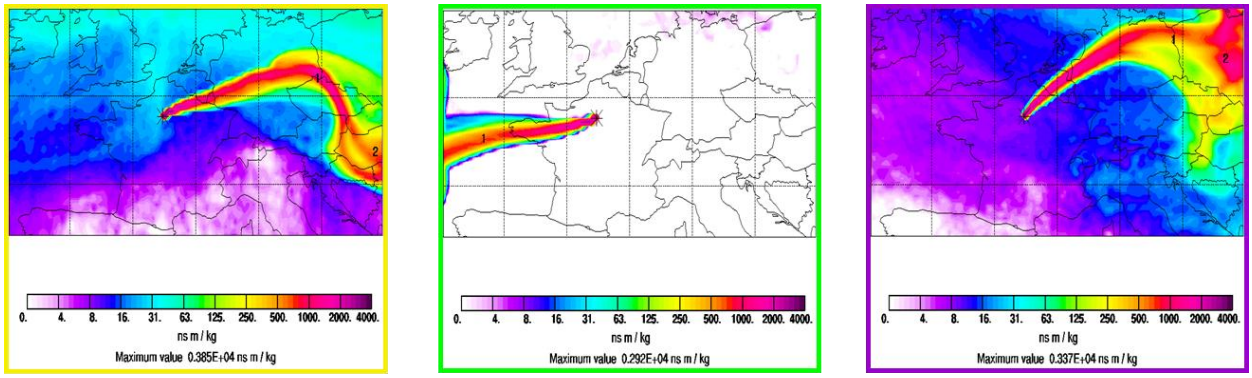

(a) Period I (b) Period II (c) Period III

Figure 5. Backward trajectories characterizing the air masses of the three contrasted OH reactivity periods (a) continental air masses on the 27th of January, (b) ocean air masses on the 3rd of February and (c) continental air masses on the 9th of February Source: FLEXPART model

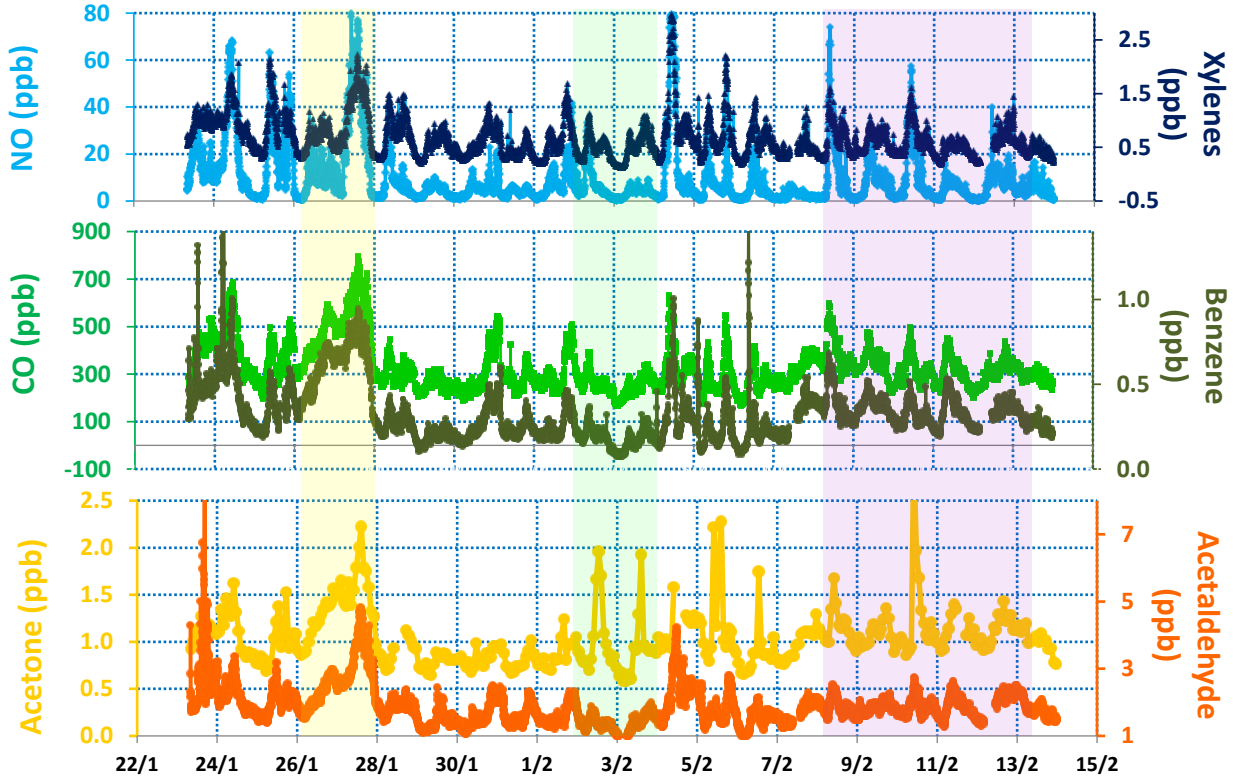

Figure 6. Campaign time series: top panel: NO in light-blue solid line and the sum of xylenes in dark-blue solid line; 2nd panel: CO in light-green solid line and benzene in dark-green solid line; 3rd panel: acetone in light-orange solid line and acetaldehyde in dark-orange solid line. The three air mass periods are colored as follows: in yellow the Period I, in green, Period II, and in violet, Period III.

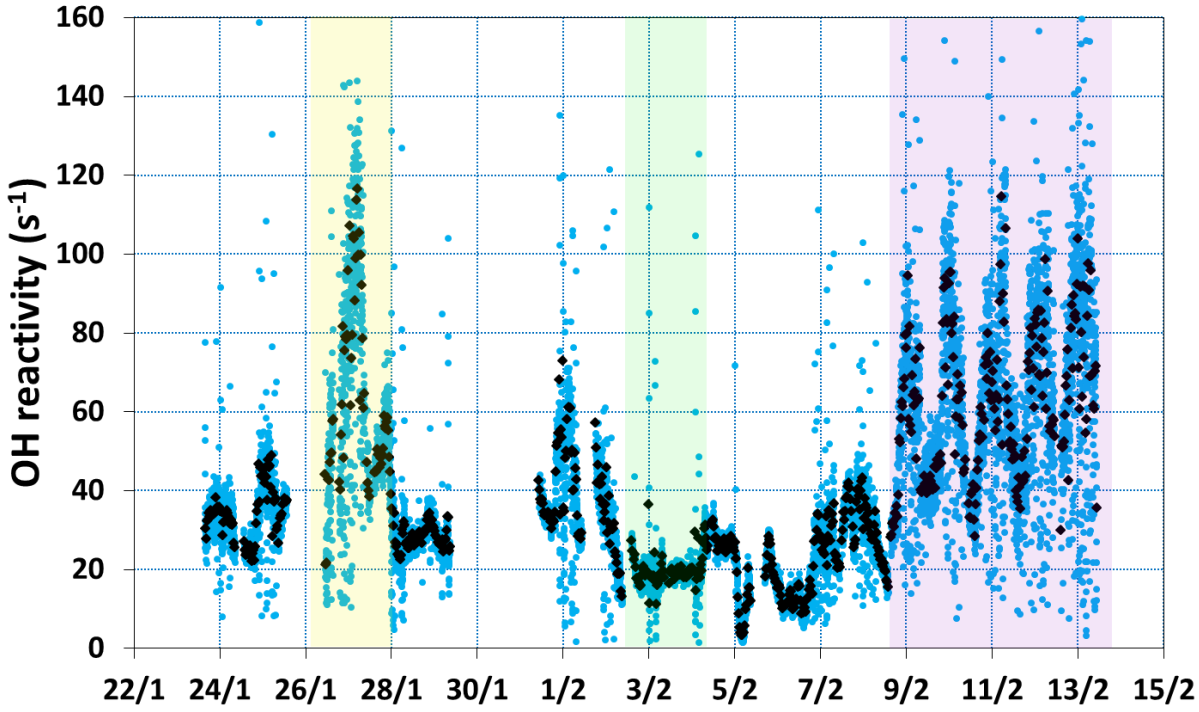

Figure 7. OH reactivity time series (2 min blue dots; 30 min black diamonds).

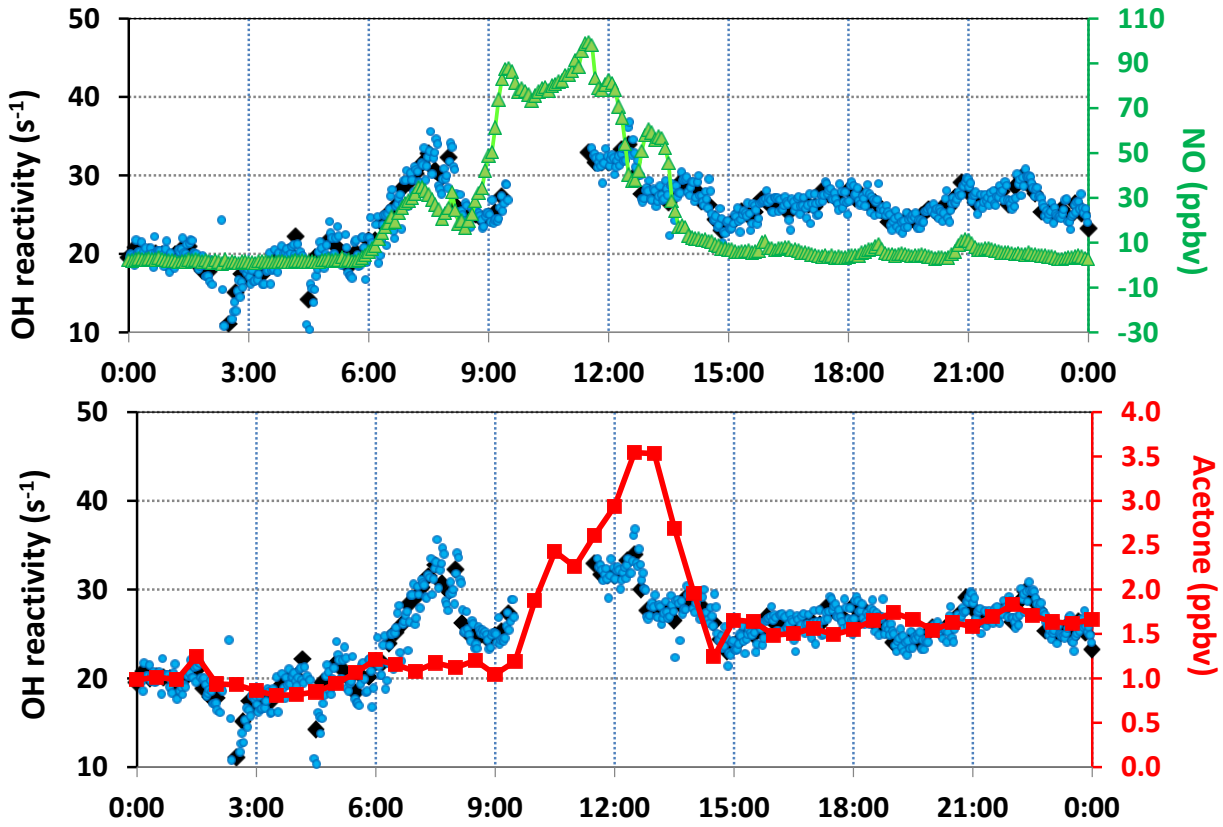

Figure 8. Daily variability of the OH reactivity during a local pollution episode: top panel: OH reactivity time series (2min blue dots and 10min black diamonds) and NO time series (5min green triangles). Bottom panel: OH reactivity time series (2 min blue dots and 10 min black diamonds); acetone time series (30 min red squares).

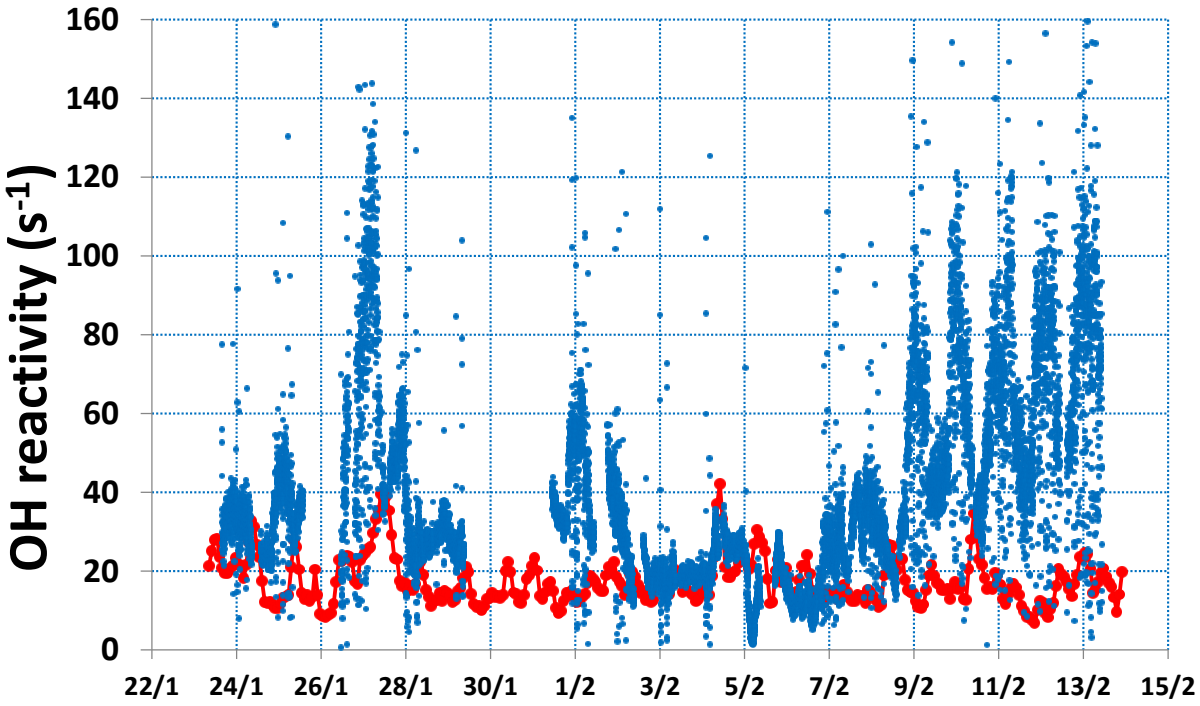

Figure 9. Calculated (90 min time resolution red curve) versus the measured OH reactivity (2 min time resolution blue dots)

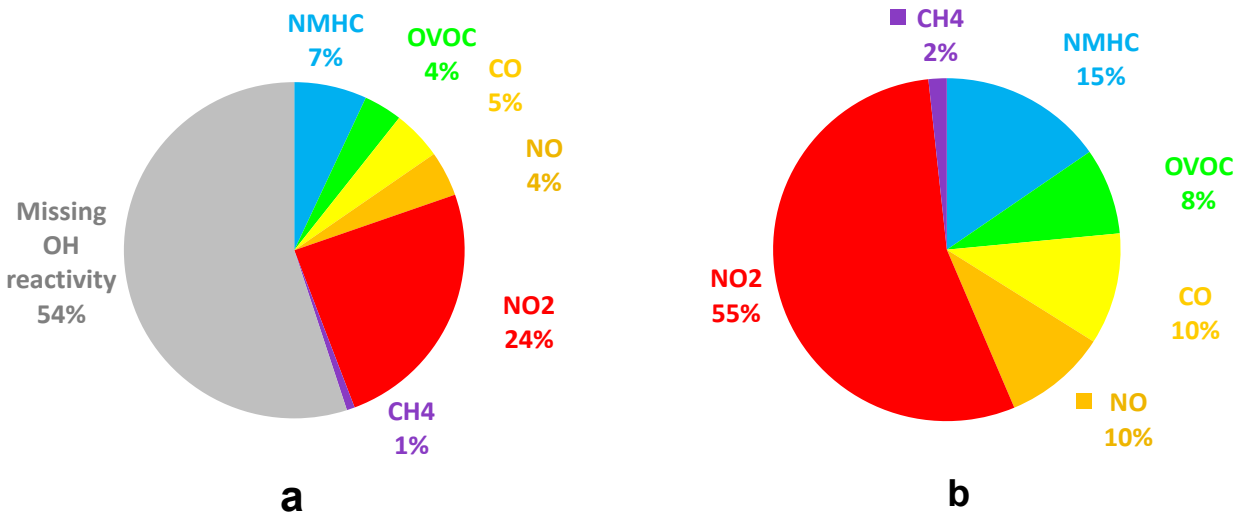

Figure 10. Breakdown of the a) total OH reactivity and b) calculated OH reactivity for the entire MEGAPOLI winter campaign

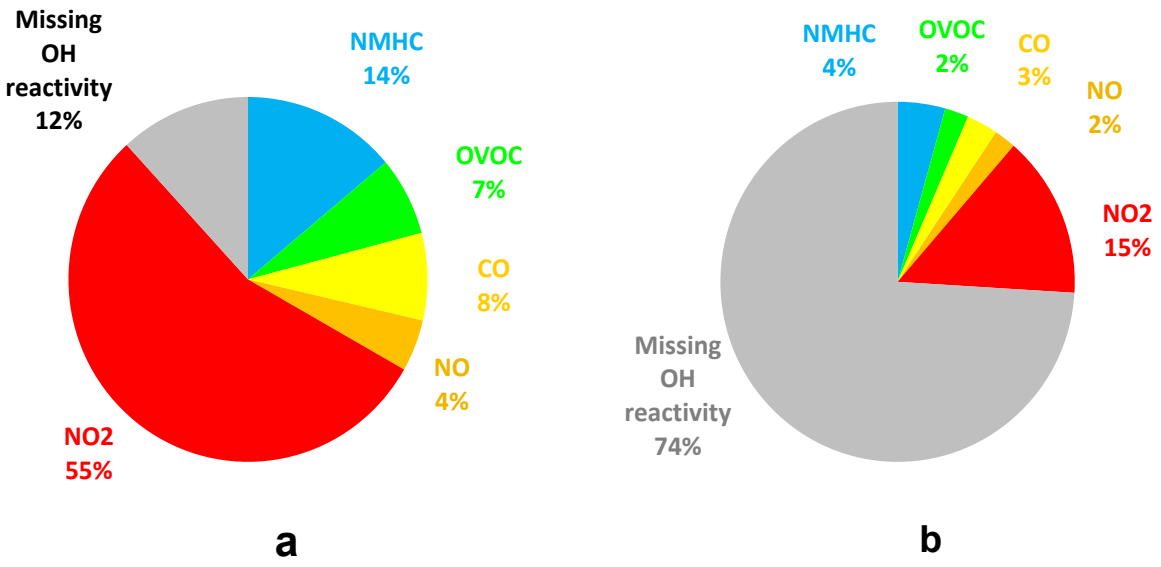

Figure 11. The Breakdown of the total OH reactivity for a) period II and b) period III

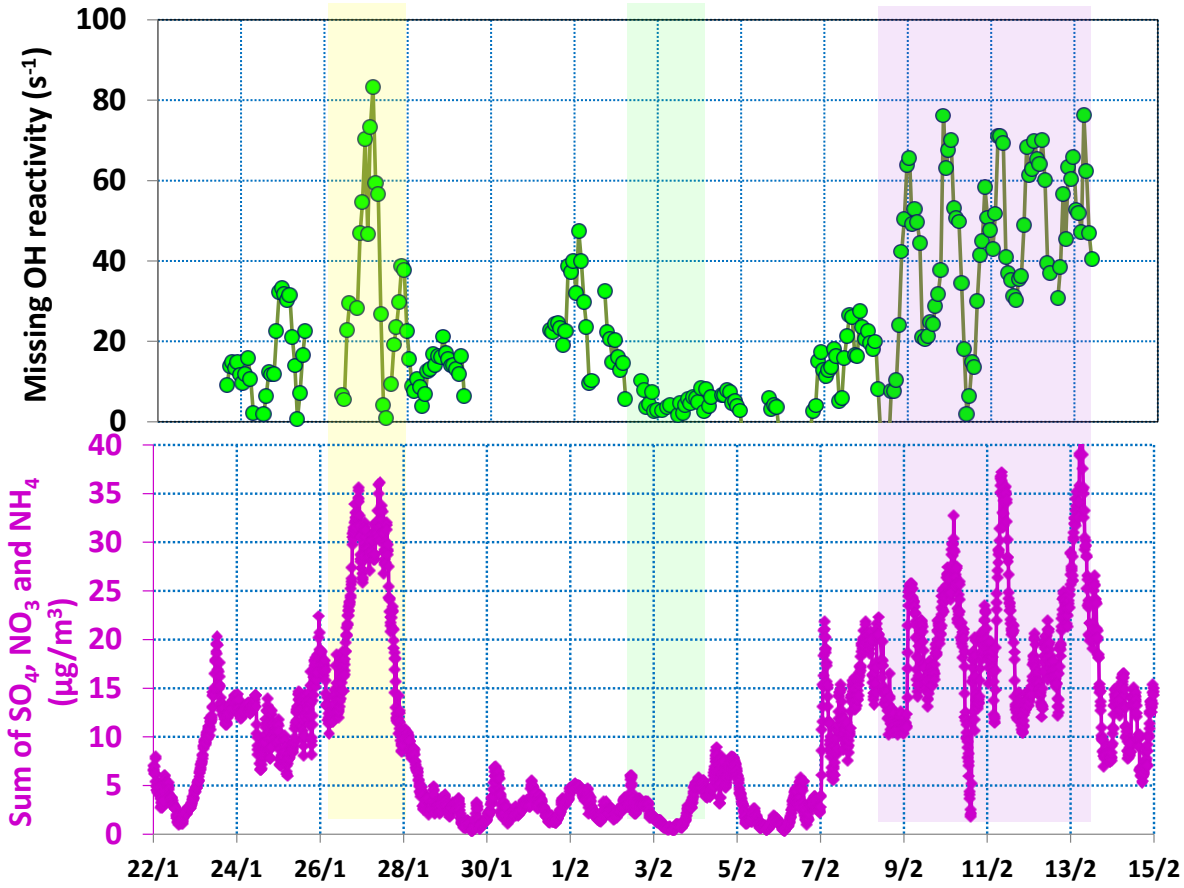

Figure 12. Top panel: Missing OH reactivity; Bottom panel: sum of SO_4, NO_3 and NH_4

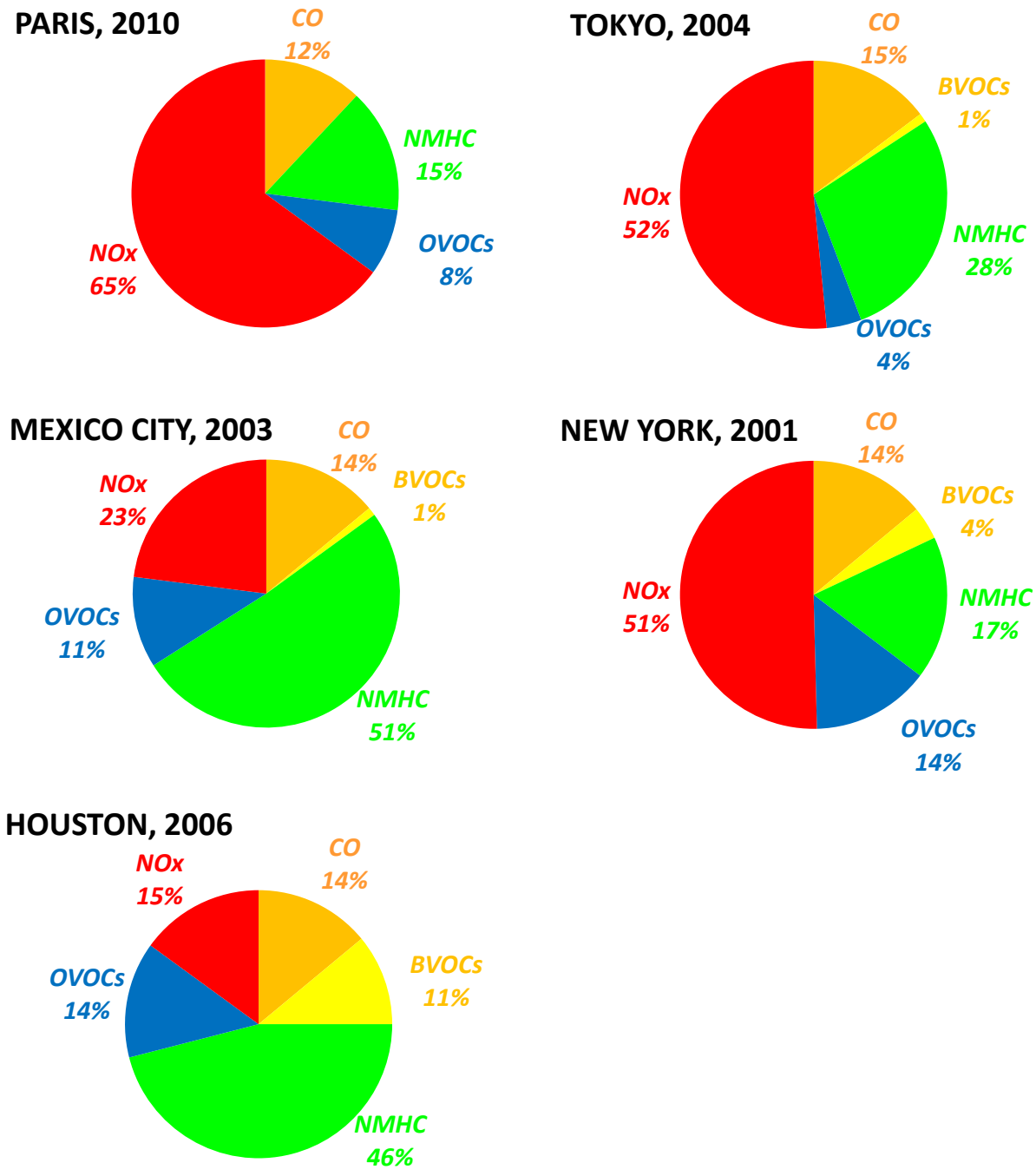

Figure 13. Contribution of different atmospheric compounds to OH reactivity in Paris (winter 2010), Tokyo (winter 2004), Mexico City (spring 2003), New York (summer 2001) and Houston (autumn 2006)

Conclusion article :

Suite à la participation à la campagne de mesure intensive MEGAPOLI hiver 2010 (Janvier – Février 2010) au Laboratoire d'Hygiène de la Ville de Paris (13ème arrondissement), un jeu de données original a été obtenu sur la mesure de réactivité atmosphérique avec les radicaux hydroxyles (OH).

La série des tests réalisée en début de campagne sur le dispositif de réactivité nous a permis, entre autres, de quantifier l'artefact principal de la méthode et caractérisant les mesures en zone riche de NO : le recyclage des radicaux hydroxyles suite à des réactions des molécules de NO avec les radicaux péroxyles (HO_2). Pour la première fois la méthode CRM avait donc été utilisée pour des mesures dans une mégacité.

Le jeu de données obtenu sur les mesures de réactivité nous ont permis de conclure que la gamme de réactivité mesurée à Paris a été comprise entre la limite de détection ($3.5s^{-1}$) et $130s^{-1}$. La valeur médiane de la réactivité OH à Paris sur toute la campagne a été de $33s^{-1}$.

Il a été possible de réaliser la distinction entre le régime 'océanique', caractérisant directement les niveaux de réactivité propres à Paris, et le régime continental, caractérisant les niveaux de réactivité de Paris et des polluants importés.

Pendant les périodes de masses d'air océanique, les niveaux de réactivité ont été d'environ $20s^{-1}$, valeurs comparables à celle obtenue dans d'autres mégacités du monde (New York et Tokyo) ayant, comme Paris, un profil de pollution impacté par des émissions trafic. L'analyse de la réactivité manquante a montré des faibles pourcentages (environ 12%), montrant que la réactivité sur Paris a été bien expliquée par la large palette des composés simultanément mesurés. Les composés qui ont contribué le plus au niveau de réactivité OH sur Paris ont été : les NOx (65%), suivi par les NMHC (15%) et le CO (10%) et finalement les OVOCs (8%).

En revanche, pendant les périodes d'import continental, les niveaux de réactivité OH mesurés ont largement dépassé le niveau local : $130s^{-1}$. La réactivité manquante pour ces périodes est de même très grande (75%), le pourcentage dépassant largement les résultats trouvés dans d'autres environnements urbains où généralement des valeurs de 30% ont été trouvées. La réactivité manquante a montré une bonne co-variation avec les aérosols fins (PM1) pour lesquels les épisodes ont été associés à des imports continentaux. Il est ainsi suggéré que la nature des espèces responsables de la partie non-expliquée de la réactivité peut être fortement oxydée, issue d'un transport longue distance.

CONCLUSIONS GENERALES

Le radical hydroxyle joue un rôle important dans la chimie atmosphérique représentant le plus important oxydant de la troposphère et le puits principal de la plus grande partie des composés organiques volatils. Malgré la précieuse information qu'il peut fournir sur la capacité oxydante de l'atmosphère, il est difficile à quantifier. Une mesure complémentaire et apportant des informations importantes sur le bilan des OH a été proposée il y a vingtaine d'années, il s'agit de la mesure de la réactivité totale avec les OH. Ce n'est que depuis une vingtaine d'années que des méthodes ont été proposées pour la mesure de la réactivité. Les instruments utilisaient la technique LIF, relativement lourde et coûteuse, et dont la grande taille pénalisait un déploiement rapide sur le terrain. Une nouvelle alternative à la mesure directe de la réactivité avait été présentée par Sinha et al., 2008 : la méthode comparative de réactivité. Celle-ci impliquait des mesures de comparaison réalisées dans un réacteur en verre, comparaison de la réactivité atmosphérique avec celle d'un traceur des radicaux hydroxyles, dont nous connaissons la constante cinétique de réaction avec les OH. Cette nouvelle méthode n'avait été utilisée auparavant que dans très peu d'études atmosphériques et seulement dans des zones où les concentrations atmosphériques étaient très faibles en oxyde d'azote, car des interférences dues aux réactions secondaires de recyclage des radicaux hydroxyles avaient été rapportés.

Ce travail de recherche a eu donc pour but deux objectifs distincts. Le premier objectif était le développement et l'optimisation de la méthode comparative de réactivité pour des mesures en zones urbaines. En particulier il fallait trouver une méthode pour s'affranchir ou corriger l'artefact dû à la forte concentration de NO. Dans un premier temps, les tests réalisés pendant diverses campagnes et au laboratoire ont permis une meilleure compréhension du montage expérimental. Deux types de tests ont été identifiés comme nécessaires pour le traitement des données brutes de réactivité. Une première classe comprend les tests de qualification du système : la calibration du système avec du pyrrole et la photolyse du pyrrole dans la cellule. Nous avons conclu que la photolyse du pyrrole dans la cellule n'intervient pas dans le calcul de la réactivité et de ses corrections, elle représentant plutôt un indicateur de la stabilité d'émission de la lampe. La deuxième catégorie de tests en revanche caractérisent des artefacts dans la cellule. Ces artefacts sont :

- L'éloignement des conditions du Pseudo premier ordre. Cet artefact intervient au moment où les conditions expérimentales concernant la concentration relative de OH par rapport à la concentration initiale de pyrrole, [pyrrole]>>[OH]. Généralement, les conditions expérimentales impliquent des rapports de [pyrrole]/[OH] proches de 2. En effectuant des simples simulations avec FACSIMILE, des facteurs correctifs sont estimés et la correction des données de réactivité a été conseillée. De manière générale, une correction due à cet effet entraine une variation de la réactivité mesure d'environ 20 à 40%. Pour diminuer cette correction, l'utilisation d'un rapport [pyrrole]/[OH] supérieur à 3 est vivement conseillée.

- La différence d'humidité relative entre le signal de base C_2 et celui atmosphérique, C_3, introduit un artefact à cause de la variation du champ des radicaux hydroxyles dans la cellule.
- Le recyclage d'OH par des réactions secondaires entre NO et les radicaux HO_2.

Les deux derniers artefacts ont été identifiés pendant la thèse comme les plus importants car directement dépendants des conditions atmosphériques de l'endroit où les mesures sont réalisées. Suite aux études caractérisant ces artefacts nous avons pu conclure sur diverses stratégies expérimentales telles que leur effet sur la mesure de réactivité soit réduit au maximum. Nous avons ainsi remarqué que :

- dans le cas de l'artefact lié à différence d'humidité entre le signal de base C_2 et le signal atmosphérique C_3, l'artefact peut être évité si l'humidité du signal de base C_2 est maintenu égal avec celui du signal atmosphérique C_3. Pour cette opération, nous recommandons l'utilisation d'un système catalytique permettant le nettoyage de l'air atmosphérique tout en préservant le taux d'humidité. Devant l'mpossibilité de réguler ce taux d'humidité, le niveau de la correction à appliquer est minimum dans le cas où l'humidité relative du signal de base est maintenue à des valeurs supérieures à 65%.
- Dans le cas du ***recyclage des radicaux hydroxyles***, la correction à appliquer sur les données brutes de réactivité est directement liée au rapport de mélange de NO existant dans le système. Ainsi, dans une première approche, deux niveaux de correction NO ont été quantifiés :
    - pour des valeurs de NO inférieures à 20 ppbv, la correction est la plus forte et égale 1.3 *[NO] ;
    - pour des valeurs de NO supérieures à 20 ppbv, le recyclage semble atteindre un effet de saturation, la correction étant de seulement 60% de la concentration du NO (0.6*[NO]).

Les études ont montré que pour réduire l'effet de recyclage de OH dans le système, le flux de l'air ambiant dans la cellule doit être réduit au maximum. De cette manière, le rapport de mélange de NO dans la cellule va être diminué. Un inconvenient à cette solution a été néanmoins identifié : la diminution du flux d'air ambiant entraine une dilution de la réactivité extérieure et donc une perte de sensibilité de la méthode en fort NO. En revanche, en milieu urbain, comme c'était le cas de la campagne MEGAPOLI hiver 2010 à Paris, la diminution du flux d'air ambiant a été vivement conseillée car à cause du fort niveau de réactivité locale, l'augmentation de la limite de détection suite à la diminution du flux n'a pas été considérée comme génante.

En considérant le recyclage des radicaux hydroxyles par le NO atmosphérique, les deux études principales portées pendant la campagne MEGAPOLI hiver 2010 et la campagne d'intercomparaison CompOH (juillet 2011) ont montré cette forte influence du NO sur le signal de réactivité enregistré. Les zones urbaines, caractérisées par des fortes concentrations de NO, sont les plus susceptibles d'être impactées par cet artefact. Les tests réalisés pendant ces deux campagnes ont permis sa quantification et

la détermination d'une stratégie pour tenir compte d'un facteur correctif nécessaire au traitement des données brutes de réactivité. De plus, le fait que le même effet de recyclage des OH a été reproduit par les deux systèmes utilisant la méthode CRM (LSCE et MPI), nous a permis de conclure que, dans une première approche, l'effet de recyclage des radicaux hydroxyles avec le NO est généralisable aux mesures par CRM.

Le système final de réactivité développé et optimisé a permis de réaliser des mesures de réactivité dans la gamme de 3 à 150 s^{-1}, avec une incertitude sur la mesure estimée à 20%.

La campagne CompOH réalisée en juillet 2011 a permis d'intercomparer notre dispositif avec celui utilisant aussi la méthode CRM de l'équipe du Max Planck Institut et avec l'instrument FAGE de l'équipe PC2A de Lille. Malgré les divers problèmes techniques, les trois instruments ont montré des comportements généralement semblables (on note toutefois que la période de comparaison était limitée). Les deux instruments CRM ont montré pour les tests avec des divers stimuli artificiels la même variabilité et des niveaux enregistrés d'environ 20%, valeur satisfaisante si nous considérons aussi que l'incertitude totale associée à la mesure CRM est d'environ 20%. L'objectif technique de la thèse concernant les travaux de développement et d'optimisation sur le système de réactivité pour en rendre le montage prêt pour des mesures en zones urbaines a été donc atteint.

Maintenant que le dispositif de réactivité est opérationnel, des travaux de compacité du montage sont néanmoins conseillés par la suite tels que le déploiement sur le terrain se fasse plus facilement. L'effet de variation du taux d'humidité dans la cellule a été identifié comme un point clé dans l'analyse des résultats. Par la suite, pour se débarrasser de cet artefact, nous proposons l'utilisation d'un catalyseur afin d'obtenir de l'air atmosphérique propre, tout en gardant le taux d'humidité de l'air. Même si cette solution a été déjà envisagée et appliquée lors des études menées pendant été 2009, l'utilisation d'un catalyseur peu sensible a rendu les résultats non-exploitables. Les artefacts identifiés précédemment sont supposés impliquer des incertitudes supplémentaires sur la valeur finale de réactivité. Il faudra mieux quantifier cette incertitude dans le futur.

Le deuxième objectif de la thèse a été la quantification et caractérisation de la réactivité atmosphérique totale avec les radicaux hydroxyles en zone urbaine. Le projet MEGAPOLI a constitué le cadre propice pour la mesure de réactivité à Paris. En effet, à cette occasion, grâce aux nombreux instruments déployés sur le site du Laboratoire d'Hygiène de la Ville de Paris, une belle série de divers composés a été disponible pour l'interprétation des résultats de réactivité. De même, la position géographique de Paris permettait d'étudier les divers régimes de masses d'air caractérisés par des influences océaniques ou continentales (Europe de nord-est). Les niveaux de réactivité enregistrés pendant cette campagne ont été compris entre la limite de détection ($3.5s^{-1}$) et $130s^{-1}$. Nous avons ainsi remarqué qu'en régime de masses

d'air océanique, la pollution de Paris et sa région est prédominante et caractérisée principalement par les émissions trafic avec des niveaux de réactivité d'environ $20s^{-1}$. Cette valeur est comparable aux valeurs enregistrées dans d'autres mégapoles ayant un même profil de pollution lié aux émissions trafic (New York et Tokyo). Dans cette période, la réactivité mesurée a été quasiment en totalité expliquée par les composés mesurés (CO, NOx, NMHC et OCOV). Les composés qui ont eu la plus forte contribution à la réactivité OH ont été les oxydes d'azotes, NOx, avec 65%, les hydrocarbures non-méthaniques avec 15%, le CO avec 10% et les composés organiques volatils avec 8%. Ce profil est comparable avec ceux des autres Mégacités impactées par des émissions trafic (New York et Tokyo).

En revanche, pendant le régime continental, une pollution supplémentaire due à l'import long distance s'est additionnée à la pollution locale et les niveaux de réactivité mesurés ont atteint des valeurs record, rivalisant avec Mexico City ($130s^{-1}$). L'étude des composés mesurés a montré que la réactivité manquante enregistrée pendant cette période a été de même très forte (75%), dépassant les valeurs enregistrées ailleurs. Les études précédentes réalisées en milieu urbain ont montré des pourcentages assez faibles de réactivité manquante (environ 30%), les niveaux plus grands étant généralement expliqués par la non-disponibilité de la mesure de certaines catégories de composés réagissant avec les OH. C'était donc la première fois qu'une étude pointe une aussi forte valeur, bien qu'en conditions particulières, d'import longue distance. Cette valeur est du même ordre de grandeur que le niveau enregistré dans diverses forêts, et où l'explication probable était l'existence des composés biogéniques non-mesurés. Dans notre cas, la covariation de la réactivité manquante avec la partie fine des aérosols (PM1) semble plutôt 'incriminer' l'import continental des masses chargées en produits fortement oxydés.

Cette conclusion constitue une nouveauté dans le domaine et cette approche discriminant entre un niveau propre, caractéristique de Paris, et un niveau influencé par un import long distance, constitue une approche unique. L'objectif scientifique cherchant à quantifier la réactivité avec OH puis à déterminer la part de la réactivité manquante a été donc atteint. Néanmoins, étant donné la complexité du sujet, des études supplémentaires pour approfondir la nature des composés actuellement non-mesurés et contribuant à la réactivité manquante sont nécessaires. Dans cette direction, les travaux de PMF (Positive Matrix Factorisation) en cours de réalisation par l'équipe allemande … vont permettre une identification et quantification des diverses fractions contribuant à la masse totale des aérosols, comme par exemple les fractions issues du combustible fossile, de la combustion de la biomasse ou la fraction organique procéssée. La confrontation de ces résultats et ceux de réactivité pourrait apporter des réponses plus précises quant à la nature des composés caractérisant la réactivité manquante enregistrée pendant la campagne MEGAPOLI hiver 2010.

Les travaux de ma thèse ont permis de mettre au point une méthode de mesure de la réactivité totale avec les radicaux hydroxyles. Par rapport aux autres techniques actuellement disponibles pour la mesure de la réactivité OH, la méthode CRM présente l'avantage d'une méthode moins couteuse et facilement de déployer sur le terrain. Les travaux effectués ont permis une meilleure compréhension du fonctionnement du système. Une méthodologie de prise en compte de tout artefact interférant sur la mesure a été proposée pour une plus précise quantification de la méthode. Néanmoins, des points faibles de la méthode ont été identifiés comme par exemple le large série de tests consommatrices du temps et nécessaires préalablement à chaque campagne de mesure. Malgré les travaux d'isolation thermique du système, celui-ci reste néanmoins très sensible aux variations extérieures de température. Des mesures en environnements régulés en température sont donc nécessaires à une bonne quantification de la méthode.

En vue d'une meilleure compréhension et identification de la nature des composés 'responsables' de la réactivité manquante, une approche utile peut s'avérer l'analyse de la réactivité de façon conjointe avec des études de modélisation. La prochaine campagne en Corse 2012 réalisée pendant le projet CHARMEX, quand des mesures des composés oxygénées conjointes aux modèles sont planifiées, permettra d'apporter des informations supplémentaires sur cette question.

REFERENCES BIBLIOGRAPHIQUES

Amedro, D.: Atmospheric and kinetic studies of oh and ho2 by fage technique, Journal of Environmental Sciences, 24, 2012.

Ammann, C., Brunner, A., Spirig, C., and Neftel, A.: Technical note: Water vapour concentration and flux measurements with ptr-ms, Atmospheric Chemistry and Physics, 6, 4643-4651, 2006.

Atkinson, R., Baulch, D. L., Cox, R. A., Crowley, J. N., Hampson, R. F., Hynes, R. G., Jenkin, M. E., Rossi, M. J., and Troe, J.: Evaluated kinetic and photochemical data for atmospheric chemistry: Volume i - gas phase reactions of o(x), ho(x), no(x) and so(x) species, Atmospheric Chemistry and Physics, 4, 1461-1738, 2004.

Atkinson, R., Baulch, D. L., Cox, R. A., Crowley, J. N., Hampson, R. F., Hynes, R. G., Jenkin, M. E., Rossi, M. J., and Troe, J.: Evaluated kinetic and photochemical data for atmospheric chemistry: Volume ii - gas phase reactions of organic species, Atmospheric Chemistry and Physics, 6, 3625-4055, 2006.

Bavia, M., Bertinelli, F., Taliani, C., and Zauli, C.: Electronic-spectrum of pyrrole in vapor and crystal, Molecular Physics, 31, 479-489, 10.1080/00268977600100361, 1976.

Calpini, B., Jeanneret, F., Bourqui, M., Clappier, A., Vajtai, R., and van den Bergh, H.: Direct measurement of the total reaction rate of oh in the atmosphere, Analusis, 27, 328-336, 10.1051/analusis:1999270328, 1999.

Canagaratna, M. R., Jayne, J. T., Jimenez, J. L., Allan, J. D., Alfarra, M. R., Zhang, Q., Onasch, T. B., Drewnick, F., Coe, H., Middlebrook, A., Delia, A., Williams, L. R., Trimborn, A. M., Northway, M. J., DeCarlo, P. F., Kolb, C. E., Davidovits, P., and Worsnop, D. R.: Chemical and microphysical characterization of ambient aerosols with the aerodyne aerosol mass spectrometer, Mass Spectrometry Reviews, 26, 185-222, 10.1002/mas.20115, 2007.

Carslaw, N., Creasey, D. J., Heard, D. E., Jacobs, P. J., Lee, J. D., Lewis, A. C., McQuaid, J. B., Pilling, M. J., Bauguitte, S., Penkett, S. A., Monks, P. S., and Salisbury, G.: Eastern atlantic spring experiment 1997 (ease97) - 2. Comparisons of model concentrations of oh, ho2, and ro2 with measurements, Journal of Geophysical Research-Atmospheres, 107, 419010.1029/2001jd001568, 2002.

Charlson, R. J., Lovelock, J. E., Andreae, M. O., and Warren, S. G.: Oceanic phytoplankton, atmospheric sulfur, cloud albedo and climate, Nature, 326, 655-661, 10.1038/326655a0, 1987.

Chatani, S., Shimo, N., Matsunaga, S., Kajii, Y., Kato, S., Nakashima, Y., Miyazaki, K., Ishii, K., and Ueno, H.: Sensitivity analyses of oh missing sinks over tokyo metropolitan area in the summer of 2007, Atmospheric Chemistry and Physics, 9, 8975-8986, 2009.

Cronin, B., Nix, M. G. D., Qadiri, R. H., and Ashfold, M. N. R.: High resolution photofragment translational spectroscopy studies of the near ultraviolet photolysis of pyrrole, Physical Chemistry Chemical Physics, 6, 5031-5041, 10.1039/b411589a, 2004.

Crutzen, P. J.: Global budgets for non-co2 greenhouse gases, Environmental Monitoring and Assessment, 31, 1-15, 10.1007/bf00547177, 1994.

Day, B. M., Rappengluck, B., Clements, C. B., Tucker, S. C., and Brewer, W. A.: Nocturnal boundary layer characteristics and land breeze development in houston, texas during texaqs ii, Atmospheric Environment, 44, 4014-4023, 10.1016/j.atmosenv.2009.01.031, 2010.

de Gouw, J., Warneke, C., Karl, T., Eerdekens, G., van der Veen, C., and Fall, R.: Sensitivity and specificity of atmospheric trace gas detection by proton-transfer-reaction mass spectrometry, International Journal of Mass Spectrometry, 223, 365-382, 10.1016/s1387-3806(02)00926-0, 2003a.

de Gouw, J., Warneke, C., Holzinger, R., Klupfel, T., and Williams, J.: Inter-comparison between airborne measurements of methanol, acetonitrile and acetone using two differently configured ptr-ms instruments, International Journal of Mass Spectrometry, 239, 129-137, 10.1016/j.ijms.2004.07.025, 2004.

de Gouw, J., and Warneke, C.: Measurements of volatile organic compounds in the earth's atmosphere using proton-transfer-reaction mass spectrometry, Mass Spectrometry Reviews, 26, 223-257, 10.1002/mas.20119, 2007.

de Gouw, J. A., Howard, C. J., Custer, T. G., and Fall, R.: Emissions of volatile organic compounds from cut grass and clover are enhanced during the drying process, Geophysical Research Letters, 26, 811-814, 10.1029/1999gl900076, 1999.

de Gouw, J. A., Goldan, P. D., Warneke, C., Kuster, W. C., Roberts, J. M., Marchewka, M., Bertman, S. B., Pszenny, A. A. P., and Keene, W. C.: Validation of proton transfer reaction-mass spectrometry (ptr-ms) measurements of gas-phase organic compounds in the atmosphere during the new england air quality study (neaqs) in 2002, Journal of Geophysical Research-Atmospheres, 108, 4682 10.1029/2003jd003863, 2003b.

de Gouw, J. A., Warneke, C., Stohl, A., Wollny, A. G., Brock, C. A., Cooper, O. R., Holloway, J. S., Trainer, M., Fehsenfeld, F. C., Atlas, E. L., Donnelly, S. G., Stroud, V., and Lueb, A.: Volatile organic compounds composition of merged and aged forest fire plumes from alaska and western canada, Journal of Geophysical Research-Atmospheres, 111, D1030310.1029/2005jd006175, 2006.

de Gouw, J. A., Welsh-Bon, D., Warneke, C., Kuster, W. C., Alexander, L., Baker, A. K., Beyersdorf, A. J., Blake, D. R., Canagaratna, M., Celada, A. T., Huey, L. G., Junkermann, W., Onasch, T. B., Salcido, A., Sjostedt, S. J., Sullivan, A. P., Tanner, D. J., Vargas, O., Weber, R. J., Worsnop, D. R., Yu, X. Y., and Zaveri, R.: Emission and chemistry of organic carbon in the gas and aerosol phase at a sub-urban site near mexico city in march 2006 during the milagro study, Atmospheric Chemistry and Physics, 9, 3425-3442, 2009.

DeCarlo, P. F., Kimmel, J. R., Trimborn, A., Northway, M. J., Jayne, J. T., Aiken, A. C., Gonin, M., Fuhrer, K., Horvath, T., Docherty, K. S., Worsnop, D. R., and Jimenez, J. L.: Field-deployable, high-resolution, time-of-flight aerosol mass spectrometer, Analytical Chemistry, 78, 8281-8289, 10.1021/ac061249n, 2006.

Delmas, R., Mégie, G., and Peuch, V.-H.: Physique et chimie de l'atmosphère, 2005.

Di Carlo, P., Brune, W. H., Martinez, M., Harder, H., Lesher, R., Ren, X. R., Thornberry, T., Carroll, M. A., Young, V., Shepson, P. B., Riemer, D., Apel, E., and Campbell, C.: Missing oh reactivity in a forest: Evidence for unknown reactive biogenic vocs, Science, 304, 722-725, 10.1126/science.1094392, 2004.

Dotan, I., Albritton, D. L., Lindinger, W., and Pahl, M.: Mobilities of co2+, n2h+, h3o+, h3o+.H2o, and h3o+.(h2o)2 ions in n-2, Journal of Chemical Physics, 65, 5028-5030, 10.1063/1.432943, 1976.

Ehhalt, D. H.: On the photochemical oxidation of natural trace gases and man-made pollutants in the troposphere, Science of the Total Environment, 143, 1-15, 10.1016/0048-9697(94)90529-0, 1994.

Ehhalt, D. H.: Photooxidation of trace gases in the troposphere, Physical Chemistry Chemical Physics, 1, 5401-5408, 10.1039/a905097c, 1999.

Gaeggeler, K., Prevot, A. S. H., Dommen, J., Legreid, G., Reimann, S., and Baltensperger, U.: Residential wood burning in an alpine valley as a source for oxygenated volatile organic compounds, hydrocarbons and organic acids, Atmospheric Environment, 42, 8278-8287, 10.1016/j.atmosenv.2008.07.038, 2008.

Gaimoz, C., Sauvage, S., Gros, V., Herrmann, F., Williams, J., Locoge, N., Perrussel, O., Bonsang, B., d'Argouges, O., Sarda-Esteve, R., and Sciare, J.: Volatile organic compounds sources in paris in spring 2007. Part ii: Source apportionment using positive matrix factorisation, Environmental Chemistry, 8, 91-103, 10.1071/en10067, 2011.

Goldstein, A. H., McKay, M., Kurpius, M. R., Schade, G. W., Lee, A., Holzinger, R., and Rasmussen, R. A.: Forest thinning experiment confirms ozone deposition to forest canopy is dominated by reaction with biogenic vocs, Geophysical Research Letters, 31, L22106 10.1029/2004gl021259, 2004.

Goldstein, A. H., and Galbally, I. E.: Known and unexplored organic constituents in the earth's atmosphere, Environmental Science & Technology, 41, 1514-1521, 10.1021/es072476p, 2007.

Gros, V., Sciare, J., and Yu, T.: Air-quality measurements in megacities: Focus on gaseous organic and particulate pollutants and comparison between two contrasted cities, paris and beijing, Comptes Rendus Geoscience, 339, 764-774, 2007.

Gros, V., Gaimoz, C., Herrmann, F., Custer, T., Williams, J., Bonsang, B., Sauvage, S., Locoge, N., d'Argouges, O., Sarda-Esteve, R., and Sciare, J.: Volatile organic compounds sources in paris in spring 2007. Part i: Qualitative analysis, Environmental Chemistry, 8, 74-90, 10.1071/en10068, 2011.

Guenther, A., Hewitt, C. N., Erickson, D., Fall, R., Geron, C., Graedel, T., Harley, P., Klinger, L., Lerdau, M., McKay, W. A., Pierce, T., Scholes, B., Steinbrecher, R., Tallamraju, R., Taylor, J., and Zimmerman, P.: A global model of natural volatile organic compound emissions, JGR, 100, No. D5, 8873-8892, 1995.

Heard, D. E., and Pilling, M. J.: Measurement of oh and ho2 in the troposphere, Chemical Reviews, 103, 5163-5198, 10.1021/cr020522s, 2003.

Hofzumahaus, A., Aschmutat, U., Hessling, M., Holland, F., and Ehhalt, D. H.: The measurement of tropospheric oh radicals by laser-induced fluorescence spectroscopy during the popcorn field campaign, Geophysical Research Letters, 23, 2541-2544, 10.1029/96gl02205, 1996.

Hofzumahaus, A., Rohrer, F., Lu, K., Bohn, B., Brauers, T., Chang, C.-C., Fuchs, H., Holland, F., Kita, K., Kondo, Y., Li, X., Lou, S., Shao, M., Zeng, L., Wahner, A., and Zhang, Y.: Amplified trace gas removal in the troposphere, Science, 324, 1702-1704, 10.1126/science.1164566, 2009.

Holland, F., Hofzumahaus, A., Schafer, R., Kraus, A., and Patz, H. W.: Measurements of oh and ho(2) radical concentrations and photolysis frequencies during berlioz, Journal of Geophysical Research-Atmospheres, 108, 8246 10.1029/2001jd001393, 2003.

Holzinger, R., Lee, A., Paw, K. T., and Goldstein, A. H.: Observations of oxidation products above a forest imply biogenic emissions of very reactive compounds, Atmospheric Chemistry and Physics, 5, 67-75, 2005.

Ingham, T., Goddard, A., Whalley, L. K., Furneaux, K. L., Edwards, P. M., Seal, C. P., Self, D. E., Johnson, G. P., Read, K. A., Lee, J. D., and Heard, D. E.: A flow-tube based laser-induced fluorescence instrument to measure oh reactivity in the troposphere, Atmospheric Measurement Techniques, 2, 465-477, 2009.

Karl, T., Fall, R., Crutzen, P. J., Jordan, A., and Lindinger, W.: High concentrations of reactive biogenic vocs at a high altitude site in late autumn, Geophysical Research Letters, 28, 507-510, 10.1029/2000gl012255, 2001.

Karl, T., Hansel, A., Mark, T., Lindinger, W., and Hoffmann, D.: Trace gas monitoring at the mauna loa baseline observatory using proton-transfer reaction mass spectrometry, International Journal of Mass Spectrometry, 223, 527-538, 10.1016/s1387-3806(02)00874-6, 2003a.

Karl, T., Jobson, T., Kuster, W. C., Williams, E., Stutz, J., Shetter, R., Hall, S. R., Goldan, P., Fehsenfeld, F., and Lindinger, W.: Use of proton-transfer-reaction mass spectrometry to characterize volatile organic compound sources at the la porte super site during the texas air quality study 2000, Journal of Geophysical Research-Atmospheres, 108, 4508 10.1029/2002jd003333, 2003b.

Kato, S., Sato, T., and Kajii, Y.: "A method to estimate the contribution of unidentified vocs to oh reactivity", Atmospheric Environment, 45, 5531-5539, 10.1016/j.atmosenv.2011.05.074, 2011.

Kim, S., Guenther, A., Karl, T., and Greenberg, J.: Contributions of primary and secondary biogenic voc tototal oh reactivity during the cabinex (community atmosphere-biosphere interactions experiments)-09 field campaign, Atmospheric Chemistry and Physics, 11, 8613-8623, 10.5194/acp-11-8613-2011, 2011.

Kirstine, W., Galbally, I., Ye, Y. R., and Hooper, M.: Emissions of volatile organic compounds (primarily oxygenated species) from pasture, Journal of Geophysical Research-Atmospheres, 103, 10605-10619, 10.1029/97jd03753, 1998.

Kovacs, T. A., and Brune, W. H.: Total oh loss rate measurement, Journal of Atmospheric Chemistry, 39, 105-122, 10.1023/a:1010614113786, 2001.

Kovacs, T. A., Brune, W. H., Harder, H., Martinez, M., Simpas, J. B., Frost, G. J., Williams, E., Jobson, T., Stroud, C., Young, V., Fried, A., and Wert, B.: Direct measurements of urban oh reactivity during nashville sos in summer 1999, Journal of Environmental Monitoring, 5, 68-74, 10.1039/b204339d, 2003.

Leuchner, M., and Rappenglueck, B.: Voc source-receptor relationships in houston during texaqs-ii, Atmospheric Environment, 44, 4056-4067, 10.1016/j.atmosenv.2009.02.029,

Lewis, A. C., Carslaw, N., Marriott, P. J., Kinghorn, R. M., Morrison, P., Lee, A. L., Bartle, K. D., and Pilling, M. J.: A larger pool of ozone-forming carbon compounds in urban atmospheres, Nature, 405, 778-781, 10.1038/35015540, 2000.

Lindinger, W., Hansel, A., and Jordan, A.: On-line monitoring of volatile organic compounds at pptv levels by means of proton-transfer-reaction mass spectrometry (ptr-ms) - medical applications, food control and environmental research, International Journal Of Mass Spectrometry, 173, 191-241, 1998.

Lou, S., Holland, F., Rohrer, F., Lu, K., Bohn, B., Brauers, T., Chang, C. C., Fuchs, H., Haeseler, R., Kita, K., Kondo, Y., Li, X., Shao, M., Zeng, L., Wahner, A., Zhang, Y., Wang, W., and Hofzumahaus, A.: Atmospheric oh reactivities in the pearl river delta - china in summer 2006: Measurement and model results, Atmospheric Chemistry and Physics, 10, 11243-11260, 10.5194/acp-10-11243-2010, 2010.

Mao, J., Ren, X., Brune, W. H., Olson, J. R., Crawford, J. H., Fried, A., Huey, L. G., Cohen, R. C., Heikes, B., Singh, H. B., Blake, D. R., Sachse, G. W., Diskin, G. S., Hall, S. R., and Shetter, R. E.: Airborne measurement of oh reactivity during intex-b, Atmospheric Chemistry and Physics, 9, 163-173, 2009.

Mao, J., Ren, X., Chen, S., Brune, W. H., Chen, Z., Martinez, M., Harder, H., Lefer, B., Rappenglueck, B., Flynn, J., and Leuchner, M.: Atmospheric oxidation capacity in the summer of houston 2006: Comparison with summer measurements in other metropolitan studies, Atmospheric Environment, 44, 4107-4115, 10.1016/j.atmosenv.2009.01.013, 2010.

Martinez, M., Harder, H., Kovacs, T. A., Simpas, J. B., Bassis, J., Lesher, R., Brune, W. H., Frost, G. J., Williams, E. J., Stroud, C. A., Jobson, B. T., Roberts, J. M., Hall, S. R., Shetter, R. E., Wert, B., Fried, A., Alicke, B., Stutz, J., Young, V. L., White, A. B., and Zamora, R. J.: Oh and ho(2) concentrations, sources, and loss rates during the southern oxidants study in nashville, tennessee, summer 1999, Journal of Geophysical Research-Atmospheres, 108, 4617 10.1029/2003jd003551, 2003.

Naik, V., Fiore, A. M., Horowitz, L. W., Singh, H. B., Wiedinmyer, C., Guenther, A., de Gouw, J. A., Millet, D. B., Goldan, P. D., Kuster, W. C., and Goldstein, A.: Observational constraints on the global atmospheric budget of ethanol, Atmospheric Chemistry and Physics, 10, 5361-5370, 10.5194/acp-10-5361-2010, 2010.

O'Dowd, C. D., Aalto, P., Hameri, K., Kulmala, M., and Hoffmann, T.: Aerosol formation - atmospheric particles from organic vapours, Nature, 416, 497-498, 10.1038/416497a, 2002a.

O'Dowd, C. D., Jimenez, J. L., Bahreini, R., Flagan, R. C., Seinfeld, J. H., Hameri, K., Pirjola, L., Kulmala, M., Jennings, S. G., and Hoffmann, T.: Marine aerosol formation from biogenic iodine emissions, Nature, 417, 632-636, 10.1038/nature00775, 2002b.

Olson, J. R., Crawford, J. H., Chen, G., Fried, A., Evans, M. J., Jordan, C. E., Sandholm, S. T., Davis, D. D., Anderson, B. E., Avery, M. A., Barrick, J. D., Blake, D. R., Brune, W. H., Eisele, F. L., Flocke, F., Harder, H., Jacob, D. J., Kondo, Y., Lefer, B. L., Martinez, M., Mauldin, R. L., Sachse, G. W., Shetter, R. E., Singh, H. B., Talbot, R. W., and Tan, D.: Testing fast photochemical theory during trace-p based on

measurements of oh, ho(2), and ch(2)o, Journal of Geophysical Research-Atmospheres, 109, D15s10 10.1029/2003jd004278, 2004.

Parker, A. E., Amedro, D., Schoemaecker, C., and Fittschen, C.: Oh radical reactivity measurements by fage, Environmental Engineering and Management Journal, 10, 107-114, 2011.

Poppe, D., Zimmermann, J., Bauer, R., Brauers, T., Bruning, D., Callies, J., Dorn, H. P., Hofzumahaus, A., Johnen, F. J., Khedim, A., Koch, H., Koppmann, R., London, H., Muller, K. P., Neuroth, R., Plassdulmer, C., Platt, U., Rohrer, F., Roth, E. P., Rudolph, J., Schmidt, U., Wallasch, M., and Ehhalt, D. H.: Comparison of measured oh concentrations with model-calculations, Journal of Geophysical Research-Atmospheres, 99, 16633-16642, 10.1029/94jd00378, 1994.

Ren, X., Brune, W. H., Mao, J., Mitchell, M. J., Lesher, R. L., Simpas, J. B., Metcalf, A. R., Schwab, J. J., Cai, C., Li, Y., Demerjian, K. L., Felton, H. D., Boynton, G., Adams, A., Perry, J., He, Y., Zhou, X., and Hou, J.: Behavior of oh and ho2 in the winter atmosphere in new york city, Atmospheric Environment, 40, S252-S263, 10.1016/j.atmosenv.2005.11.073, 2006a.

Ren, X., Brune, W. H., Oliger, A., Metcalf, A. R., Simpas, J. B., Shirley, T., Schwab, J. J., Bai, C., Roychowdhury, U., Li, Y., Cai, C., Demerjian, K. L., He, Y., Zhou, X., Gao, H., and Hou, J.: Oh, ho(2), and oh reactivity during the pmtacs-ny whiteface mountain 2002 campaign: Observations and model comparison, Journal of Geophysical Research-Atmospheres, 111, D10s03 10.1029/2005jd006126, 2006b.

Ren, X. R., Harder, H., Martinez, M., Lesher, R. L., Oliger, A., Shirley, T., Adams, J., Simpas, J. B., and Brune, W. H.: Hox concentrations and oh reactivity observations in new york city during pmtacs-ny2001, Atmospheric Environment, 37, 3627-3637, 10.1016/s1352-2310(03)00460-6, 2003.

Ren, X. R., Brune, W. H., Cantrell, C. A., Edwards, G. D., Shirley, T., Metcalf, A. R., and Lesher, R. L.: Hydroxyl and peroxy radical chemistry in a rural area of central pennsylvania: Observations and model comparisons, Journal of Atmospheric Chemistry, 52, 231-257, 10.1007/s10874-005-3651-7, 2005.

Roukos, J., Plaisance, H., Leonardis, T., Bates, M., and Locoge, N.: Development and validation of an automated monitoring system for oxygenated volatile organic compounds and nitrile compounds in ambient air, Journal of Chromatography A, 1216, 8642-8651, 10.1016/j.chroma.2009.10.018, 2009.

Sadanaga, Y., Yoshino, A., Kato, S., Yoshioka, A., Watanabe, K., Miyakawa, Y., Hayashi, I., Ichikawa, M., Matsumoto, J., Nishiyama, A., Akiyama, N., Kanaya, Y., and Kajii, Y.: The importance of no2 and volatile organic compounds in the urban air from the viewpoint of the oh reactivity, Geophysical Research Letters, 31, L08102 10.1029/2004gl019661, 2004a.

Sadanaga, Y., Yoshino, A., Watanabe, K., Yoshioka, A., Wakazono, Y., Kanaya, Y., and Kajii, Y.: Development of a measurement system of oh reactivity in the atmosphere by using a laser-induced pump and probe technique, Review of Scientific Instruments, 75, 2648-2655, 10.1063/1.1775311, 2004b.

Sadanaga, Y., Yoshino, A., Kato, S., and Kajii, Y.: Measurements of oh reactivity and photochemical ozone production in the urban atmosphere, Environmental Science & Technology, 39, 8847-8852, 10.1021/es049457p, 2005.

Sadanaga, Y., Kondo, S., Hashimoto, K., and Kajii, Y.: Measurement of the rate coefficient for the oh+no(2) reaction under the atmospheric pressure: Its humidity dependence, Chemical Physics Letters, 419, 474-478, 10.1016/j.cplett.2005.12.026, 2006.

Seinfeld, J. H., and Pandis, S. N.: Atmospheric chemistry and physics: From air pollution to climate change, 2006.

Shirley, T. R., Brune, W. H., Ren, X., Mao, J., Lesher, R., Cardenas, B., Volkamer, R., Molina, L. T., Molina, M. J., Lamb, B., Velasco, E., Jobson, T., and Alexander, M.: Atmospheric oxidation in the mexico city metropolitan area (mcma) during april 2003, Atmospheric Chemistry and Physics, 6, 2753-2765, 2006.

Singh, H. B., Viezee, W., Chen, Y., Bradshaw, J., Sandholm, S., Blake, D., Blake, N., Heikes, B., Snow, J., Talbot, R., Browell, E., Gregory, G., Sachse, G., and Vay, S.: Biomass burning influences on the composition of the remote south pacific troposphere: Analysis based on observations from pem-tropics-a, Atmospheric Environment, 34, 635-644, 10.1016/s1352-2310(99)00380-5, 2000.

Sinha, V., Williams, J., Crowley, J. N., and Lelieveld, J.: The comparative reactivity method - a new tool to measure total oh reactivity in ambient air, Atmospheric Chemistry and Physics, 8, 2213-2227, 2008.

Sinha, V., Custer, T. G., Kluepfel, T., and Williams, J.: The effect of relative humidity on the detection of pyrrole by ptr-ms for oh reactivity measurements, International Journal of Mass Spectrometry, 282, 108-111, 10.1016/j.ijms.2009.02.019, 2009.

Sinha, V., Williams, J., Lelieveld, J., Ruuskanen, T. M., Kajos, M. K., Patokoski, J., Hellen, H., Hakola, H., Mogensen, D., Boy, M., Rinne, J., and Kulmala, M.: Oh reactivity measurements within a boreal forest: Evidence for unknown reactive emissions, Environmental Science & Technology, 44, 6614-6620, 10.1021/es101780b, 2010.

Sinha, V., Williams, J., Diesch, J. M., Drewnick, F., Martinez, M., Harder, H., Regelin, E., Kubistin, D., Bozem, H., Hosaynali-Beygi, Z., Fischer, H., Andrés-Hernández, M.D., Kartal, D., Adame, J. A., and Lelieveld, J.: OH reactivity measurements in a coastal location in Southwestern Spain during DOMINO, Atmospheric Chemistry and Physics Discussions, 12, 4979-5014, 2012

Stohl, A., Forster, C., Frank, A., Seibert, P., and Wotawa, G., Technical note: The Lagragian particle dispersion model FELXPART version 6.2, Atmospheric Chemistry and Physics, 5, 2461-2474, 2005

Smith, S. C., Lee, J. D., Bloss, W. J., Johnson, G. P., Ingham, T., and Heard, D. E.: Concentrations of oh and ho2 radicals during namblex: Measurements and steady state analysis, Atmospheric Chemistry and Physics, 6, 1435-1453, 2006.

Steinbacher, M., Dommen, J., Ammann, C., Spirig, C., Neftel, A., and Prevot, A. S. H.: Performance characteristics of a proton-transfer-reaction mass spectrometer (ptr-ms) derived from laboratory and field measurements, International Journal of Mass Spectrometry, 239, 117-128, 10.1016/j.ijms.2004.07.015, 2004.

Thompson, A. M.: The oxidizing capacity of the earths atmosphere - probable past and future changes, Science, 256, 1157-1165, 10.1126/science.256.5060.1157, 1992.

Tuch, T. M., Haudek, A., Muller, T., Nowak, A., Wex, H., and Wiedensohler, A.: Design and performance of an automatic regenerating adsorption aerosol dryer for continuous operation at monitoring sites, Atmospheric Measurement Techniques, 2, 417-422, 2009.

Vardoulakis, S., Gonzalez-Flesca, N., and Fisher, B. E. A.: Assessment of traffic-related air pollution in two street canyons in paris: Implications for exposure studies, Atmospheric Environment, 36, 1025-1039, 2002.

Vardoulakis, S., Gonzalez-Flesca, N., Fisher, B. E. A., and Pericleous, K.: Spatial variability of air pollution in the vicinity of a permanent monitoring station in central paris, Atmospheric Environment, 39, 2725-2736, 10.1016/j.atmosenv.2004.05.067, 2005.

Velasco, E., Lamb, B., Westberg, H., Allwine, E., Sosa, G., Arriaga-Colina, J. L., Jobson, B. T., Alexander, M. L., Prazeller, P., Knighton, W. B., Rogers, T. M., Grutter, M., Herndon, S. C., Kolb, C. E., Zavala, M., de Foy, B., Volkamer, R., Molina, L. T., and Molina, M. J.: Distribution, magnitudes, reactivities, ratios and diurnal patterns of volatile organic compounds in the valley of mexico during the mcma 2002 & 2003 field campaigns, Atmospheric Chemistry and Physics, 7, 329-353, 2007.

Viehland, L. A., and Mason, E. A.: Transport properties of gaseous-ions over a wide energy-range .4, Atomic Data and Nuclear Data Tables, 60, 37-95, 10.1006/adnd.1995.1004, 1995.

Warneke, C., van der Veen, C., Luxembourg, S., de Gouw, J. A., and Kok, A.: Measurements of benzene and toluene in ambient air using proton-transfer-reaction mass spectrometry: Calibration, humidity dependence, and field intercomparison, International Journal of Mass Spectrometry, 207, 167-182, 10.1016/s1387-3806(01)00366-9, 2001.

A. Wisthaler, G. Tamas, D. P. Wyon, P. Strom-Tejsen, D. Space, J. Beauchamp, A. Hansel, T. D. Märk, C. J. Weschler, „Products of Ozone-Initiated Chemistry in a Simulated Aircraft Environment“, Environ. Sci. Technol., 39, 4823-4832, 2005

Williams, J., Fischer, H., Harris, G. W., Crutzen, P. J., Hoor, P., Hansel, A., Holzinger, R., Warneke, C., Lindinger, W., Scheeren, B., and Lelieveld, J.: Variability-lifetime relationship for organic trace gases: A novel aid to compound identification and estimation of ho concentrations, Journal of Geophysical Research-Atmospheres, 105, 20473-20486, 10.1029/2000jd900203, 2000.

Xu, X., van Stee, L. L. P., Williams, J., Beens, J., Adahchour, M., Vreuls, R. J. J., Brinkman, U. A. T., and Lelieveld, J.: Comprehensive two-dimensional gas chromatography (gc x gc) measurements of volatile organic compounds in the atmosphere, Atmospheric Chemistry and Physics, 3, 665-682, 2003.

Yoshino, A., Sadanaga, Y., Watanabe, K., Kato, S., Miyakawa, Y., Matsumoto, J., and Kajii, Y.: Measurement of total oh reactivity by laser-induced pump and probe technique - comprehensive observations in the urban atmosphere of tokyo, Atmospheric Environment, 40, 7869-7881, 10.1016/j.atmosenv.2006.07.023, 2006.

ANNEXES

ANNEXES :

ANNEXE 2.1. Calcul des concentrations avec le PTR-MS

L'équation de transfert de protons est décrite par l'équation 2.1.

$$H_3O^+ + COV \rightarrow [COV]H^+ + H_2O$$

La connaissance des conditions de la chambre de réaction permet le calcul des rapports de mélange volumiques sans avoir besoin de calibrer le système pour des composés spécifiques.

La densité des ions primaires H_3O^+ après avoir traversé la chambre de réaction avec le temps de réaction t_r peut être décrite par l'équation suivante :

$$[H_3O^+]_{tr} = [H_3O^+]_0 \cdot exp(-k_i \cdot [\mathrm{COV}] \cdot t_r) \qquad \text{eq. A.2.1}$$

Où :

- k_i représente la constante cinétique de réaction, en $cm^3 \cdot s^{-1}$; en manque des valeurs réelles des constantes cinétiques de réaction, une valeur moyenne de $2 \cdot 10^{-9} cm^3 s^{-1}$ est prise en considération dans les calculs réalisés par PTR-MS ;
- t_r représente le temps de réaction que les composés ont à la disposition dans la chambre de réaction, en s^{-1} ;

La densité de l'espèce [COV] est donnée par :

$$[COVH^+] = [H_3O^+]_0 \cdot \left(1 - exp(-k_i \cdot [\mathrm{COV}] \cdot t_r)\right)$$

$$\approx [H_3O^+]_0 \cdot k_i \cdot [\mathrm{COV}] \cdot t_r \qquad \text{eq. A.2.2}$$

D'où nous retrouvons la densité des molécules de COV :

$$[COV] = \frac{1}{k_i \cdot t_r} \cdot \frac{[COVH^+]}{[H_3O^+]} \qquad \text{eq. A.2.3}$$

Où :

- $[COVH^+]\ et\ [H_3O^+]$ sont données en nombre de coups/s ;

De même, la densité des neutres du gaz dans l'instrument est donnée par :

$$[air] = \frac{273.15\ [K]}{T_{Drift}\ [K]} \cdot \frac{6.02{\cdot}10^{23}[\frac{molécules}{mole}]}{22400\left[\frac{cm^3}{mole}\right]} \cdot \frac{p_{Drift}\ [mbar]}{1013\ [mbar]} \qquad \text{eq. A.2.4}$$

Où :

- T_{Drift} est la température dans la chambre de réaction (*Température du Drift tube*) ;
- p_{Drift} est la pression dans la chambre de réaction, appelée aussi « drift tube » (habituellement pour notre PTR-MS est de 2.24mbar)

Le rapport de mélange volumique du composé génériquement appelé [COV] est donné donc par :

$$(COV)_{ppbv} = \frac{[COV]}{[air]} \cdot 10^9 \qquad \text{eq. A.2.5}$$

En utilisant en eq. A.2.3 les équations A.2.1 et A.2.2., nous obtenons:

$$(COV)_{ppbv} = \frac{[COVH^+] \cdot 10^9 \cdot 22400 \cdot 1013 \cdot T_{Drift} \cdot Tr_{H_3O^+}}{k_i{\cdot}t_r{\cdot}[H_3O^+] \cdot 6.02{\cdot}10^{23}{\cdot}p_{Drift}{\cdot}273.15 \cdot Tr_{COVH^+}} \qquad \text{eq. A.2.6}$$

Où $Tr_{H_3O^+}$ et Tr_{COVH^+} représentent les coefficients de transmission des ions primaires et respectivement des molécules à analyser.

Le temps de réaction est donné par :

$$t_r = \frac{L}{v_{drift}} = \frac{L}{\mu{\cdot}E} = \frac{L}{\left(\frac{T_{drift}}{273.15}{\cdot}\frac{1013}{p_{drift}}{\cdot}\mu_o\right){\cdot}\frac{U_{drift}}{L}} = \frac{L^2}{\left(\frac{T_{drift}}{273.15}{\cdot}\frac{1013}{p_{drift}}{\cdot}\mu_o\right){\cdot}U_{drift}} \qquad \text{eq. A.2.7}$$

Où :

3. L est la longueur de la chambre de réaction (drift tube), dans notre cas 9.2cm ;
4. v_{drift} est la vitesse des ions dans la chambre de réaction ;
5. μ est la mobilité des ions dans la chambre de réaction, $\mu_o = 2.8\ cm^2/V \cdot s$ est la mobilité réduite. La mobilité réduite a été calculée pour divers ions en divers gaz, inclusivement pour les ions hydronium dans de l'azote (Viehland et al., 1995 ; Dotan et al., 1976) et généralement la mobilité réduite est reporté comme : $\mu_o = \left(\frac{p}{p_o}\right) \cdot \left(\frac{T_o}{T}\right) \cdot \mu = \left(\frac{N}{N_o}\right) \cdot \mu$, où N est la densité en nombre de gaz dans la chambre de réaction, No est la densité en nombre à une pression standard (po = 1atm) et température (T_o=273.15K) ;

6. E est le champ électrique appliqué aux parois de la chambre de réaction pour accélérer les ions = le rapport entre la tension appliquée (tension de drift $U_{drift} = 600V$) et la longueur de la chambre (9.2 cm) ;
7. T_{drift} est la température dans la chambre de réaction, en Kelvin ($T_{drift} = 273.15 + 60 = 333.15\ K$) ;
8. p_{drift} est la pression dans la chambre de réaction, où Rea, en mbar.

Donc, dans le cas de notre instrument, le temps de réaction des composés organiques volatiles dans la chambre de réaction est :

$$t_{réaction} = \frac{(9.2^2)}{\frac{333.15}{273.15}\cdot\frac{1013}{2.2}\cdot 2.8\cdot 600} = 89 \cdot 10^{-6} s \qquad \text{eq. A.2.8}$$

La valeur rencontrée dans la littérature pour le temps de réaction est de $t_{réaction} = 95.4 \cdot 10^{-6} s$.

Alors, la valeur du rapport de mélange des composés analysés peut être déduite à l'aide de l'équation suivante :

$$(COV)_{ppbv} = \frac{[COVH^+]\cdot 10^9 \cdot 22400 \cdot 1013 \cdot T_{Drift} \cdot Tr_{H_3O^+}}{2\cdot 10^{-9}\cdot 95.4\cdot 10^{-6}\cdot [H_3O^+] \cdot 6.02\cdot 10^{23}\cdot 2{,}24\cdot 273.15 \cdot Tr_{COVH^+}} \qquad \text{eq. A.2.9}$$

Et la formule finale :

$$(COV)_{ppbv} = 108498.56 \cdot \frac{[COVH^+]}{[H_3O^+]} \cdot \frac{Tr_{H_3O^+}}{Tr_{COVH^+}} \qquad \text{eq. A.2.10}$$

Où : les facteurs $Tr_{H_3O^+}$ et Tr_{COVH^+} sont connus comme des facteurs de transmission et représentent l'efficacité de détection des ions H_3O^+ et respectivement $COVH^+$. La différence de ces deux facteurs réside dans l'efficacité variable du quadrupole pour extraire les ions de diverses masses. Le rapport $\frac{Tr_{H_3O^+}}{Tr_{COVH^+}}$ doit être déterminé expérimentalement, par exemple en introduisant un seul COV et en mesurant la décroissance du signal des ions primaires (H_3O^+) simultanée avec l'augmentation du signal des ions $COVH^+$.

ANNEXE 2.2. Calcul de la sensibilité du PTR-MS

De l'équation A.2.2 nous pouvons obtenir la relation suivante :

$$\frac{[\mathrm{COV}H^+]}{[H_3O^+]_0} = [\mathrm{COV}] \cdot k_i \cdot t_r \qquad \text{eq. A.2.11}$$

Or, le temps de réaction peut être écrit comme :

$$t_r = \frac{L}{\mu_o N_o} \cdot \left(\frac{E}{N}\right)^{-1} \qquad \text{eq. A.2.12}$$

car :

- La vitesse de drift est : $v_{drift} = \mu \cdot E$ et en considérant l'équation de la mobilité réduite donnée dans l'ANNEXE 2.1, la vitesse de drift devienne :

$$v_{drift} = \mu_o N_o \cdot \left(\frac{E}{N}\right)$$

- Or le temps de réaction est donné par le rapport entre la distance parcourue, ou la longueur de la chambre de réaction, L, et la vitesse des ions dans la chambre de réaction (L/v_{drift})

Nous obtenons ainsi l'expression A.2.12.

En revenant en équation A.2.11 :

$$\frac{[\mathrm{COV}H^+]}{[H_3O^+]_0} = [\mathrm{COV}] \cdot k_i \cdot \frac{L}{\mu_o N_o} \cdot \left(\frac{E}{N}\right)^{-1}$$

$$= RMV \cdot k_i \cdot \frac{L}{\mu_o N_o} \cdot \left(\frac{E}{N}\right)^{-1} \qquad \text{eq.A.2.13}$$

Où RMV représente le rapport de mélange volumique du composé COV.

De l'équation A.2.13 nous pouvons obtenir la sensibilité comme le signal d'ions [$COVH^+$] obtenu pour un rapport de mélange volumique de 1ppbv et normalisé à 1000000 de coups/s d'ions primaires H_3O^+ :

$$Sensibilité = 10^{-3} \cdot k_i \cdot \frac{L}{\mu_o N_o} \cdot \frac{N^2}{E} \cdot \frac{Tr_{COVH^+}}{Tr_{H_3O^+}} \qquad \text{eq.A.2.14}$$

ANNEXE 2.3 Article Sciare et al., 2011

Large contribution of water-insoluble secondary organic aerosols in the region of Paris (France) during wintertime

Jean Sciare,[1] Odile d'Argouges,[1] Roland Sarda-Estève,[1] Cécile Gaimoz,[1] Cristina Dolgorouky,[1] Nicolas Bonnaire,[1] Olivier Favez,[2] Bernard Bonsang,[1] and Valérie Gros[1]

Received 1 February 2011; revised 10 August 2011; accepted 21 September 2011; published 17 November 2011.

[1] Near real-time measurements of carbonaceous aerosols were performed in fine aerosols for a 10-day period during winter at a suburban site of Paris (France). These measurements were performed using an OCEC Sunset Field instrument for elemental carbon (EC) and organic carbon (OC); a Particle-Into-Liquid-Sampler coupled with a Total Organic Carbon (PILS-TOC) instrument for water-soluble OC (WSOC); and a 7-λ aethalometer for absorption. A successful comparison was performed with filter sampling performed in parallel for EC, OC, and WSOC, providing further confidence on the results obtained by the online analyzers. A modified version of the aethalometer model was used to derive hourly concentrations of 3 organic aerosol (OA) sources: fossil fuel, wood burning, and secondary. This source apportionment was validated for primary OA (fossil fuel, wood burning) using time-resolved measurements of specific tracers (including levoglucosan, water-soluble potassium and methanol for wood burning) and showed that secondary organic aerosols (SOA) were the most abundant OA species during our study. Water-soluble properties of these different OA sources were investigated from the reconstruction of experimentally determined water-soluble/insoluble OC. About 23% of WSOC was found to be of a secondary (photochemical) origin. A large fraction of SOA was assigned as water-insoluble and could originate from semi-volatile primary OA from wood burning and/or anthropogenic emissions. These results have been obtained at a typical suburban site in France and may be then representative of a larger European area. They bring new light on the commonly accepted idea that SOA is mainly water-soluble.

Citation: Sciare, J., O. d'Argouges, R. Sarda-Estève, C. Gaimoz, C. Dolgorouky, N. Bonnaire, O. Favez, B. Bonsang, and V. Gros (2011), Large contribution of water-insoluble secondary organic aerosols in the region of Paris (France) during wintertime, *J. Geophys. Res.*, *116*, D22203, doi:10.1029/2011JD015756.

1. Introduction

[2] Fine anthropogenic aerosols (with aerodynamic diameter, A.D., below 2.5μm) have been recognized as having strong but poorly understood adverse effects on health [*Nel*, 2005]; they may also have a significant climatic role on regional scales, inducing strong radiative forcing by directly scattering the sunlight and indirectly change cloud properties though the formation of cloud condensation nuclei [*Ramanathan et al.*, 2007]. With half the world population living in cities, urban areas represent nowadays one of the major sources of fine anthropogenic aerosols on global scale, pointing out the need for a better characterization of these aerosols in the vicinity of their emission sources.

[3] Organic aerosols (OA) make up a large fraction of fine aerosols but their sources are not well understood, especially the relative contributions of primary versus secondary organic aerosol. Primary organic aerosols (POA) are directly emitted by sources; secondary organic aerosols (SOA) are formed in the atmosphere from the oxidation products of gas phase precursors. Recent ambient measurements with Aerodyne Aerosol Mass Spectrometers (AMS) have shown that oxygenated OA (OOA) is the dominant component of OA in many anthropogenically influenced environments and could significantly contribute to SOA [*Zhang et al.*, 2007]. In atmospheres which are not impacted by biomass burning, real-time measurements of water-soluble organic compounds (WSOC) performed using a Particle-Into-Liquid-Sampler coupled with a Total Organic Carbon (PILS-TOC) instrument have also shown to provide valuable information on SOA that could be mainly of biogenic origin [*Sullivan et al.*, 2004, 2006; *Heald et al.*, 2006; *Miyazaki et al.*, 2006; *Kondo et al.*, 2007; *Weber et al.*, 2007; *Hennigan et al.*, 2008a, 2008b]. Although these 2 techniques (AMS and PILS-TOC) can provide near real-time useful information on SOA, they still suffer from

[1]Laboratoire des Sciences du Climat et de l'Environnement, CNRS-CEA-UVSQ, Gif-sur-Yvette, France.
[2]Institut National de l'Environnement Industriel et des Risques, Verneuil-en-Halatte, France.

0148-0227/11/2011JD015756

several limitations regarding, for instance, the origin of SOA (see for instance *Grieshop et al.* [2009a] for discussion on biomass burning SOA).

[4] Characterization of SOA in the urban atmosphere during the winter period appears therefore to be particularly difficult to assess especially in European cities due to the large use of wood burning for domestic heating which could contribute to 50–70% of the aerosol organic mass during winter [*Gelencsér et al.*, 2007; *Puxbaum et al.*, 2007; *Lanz et al.*, 2010]. Low biogenic emissions during winter will also significantly reduce the amount of secondary water-soluble OA in the atmosphere making even more difficult the characterization of water-soluble SOA in urban atmospheres impacted by biomass burning. In this context, source apportionment of combustion and non-combustion OA sources is prerequisite for gaining more information on SOA origins and properties during winter.

[5] A source apportionment model (aethalometer model) has been developed recently by *Sandradewi et al.* [2008a] and optimized by *Favez et al.* [2010] in order to discriminate carbonaceous aerosols within 3 distinct sources; fossil fuel combustion source, biomass burning combustion source and a non-combustion source which can be assigned as SOA if we assume that primary OA sources (plants, spores, fungus) do not contribute significantly to OA levels in the fine mode. This model is based on the light absorbing properties of brown carbon which is assumed to refer to biomass burning aerosols [*Hoffer et al.*, 2006; *Lukács et al.*, 2007 and references therein]. Still very few studies have been using this model [e.g., *Favez et al.*, 2009, 2010] which still needs to be better constrained by independent estimates of these 3 OA sources. *Favez et al.* [2010] have compared this model against two commonly used source apportionment models: Chemical Mass Balance (CMB, performed with off-line filter measurements) and Positive Matrix Factorization (PMF, applied to Aerosol Mass Spectrometer measurements). Significant discrepancies were obtained in the estimation of carbonaceous material from wood burning, pointing out possible inconstancies of CMB and PMF models. The aethalometer model also requires strong hypotheses, assuming for instance that biomass burning is the only source of brown-carbon containing particles. It may not be appropriate for a small (and stable) wood burning contribution as well as large and variable SOA sources since this model is based on regression analysis which requires significant changes in concentration levels of OA sources. Consequently, efforts are still required to further validate this aethalometer model against independent (tracer-based) estimates of combustion OA sources.

[6] An hourly resolved source apportionment of OA (fossil fuel, wood burning, and SOA) in the fine mode is performed here using an improved version of the aethalometer model for a 10-day period during the winter 2009 at a suburban site of Paris (France). Fossil fuel and wood burning OA derived from this model are tested against online and filter-based measurements of tracers for these 2 sources (water-soluble potassium, levoglucosan, methanol, m,p-xylenes). Water-soluble properties of the 3 OA sources (fossil fuel, wood burning and SOA) is then investigated from independent time-resolved measurements of water-soluble/insoluble organic carbon. A focus is made on SOA which is found to be mainly composed of water-insoluble organic material during the period of the study.

2. Instrumentation

2.1. Sampling Site Description and Meteorology Overview

[7] Atmospheric measurements were performed on the terraced roof (5 m above ground level) of the Laboratoire des Sciences du Climat et de l'Environnement (LSCE; 48°42′35.47″ N, 2°08′53.40″ E). This site is located approximately 20km southwest from the city of Paris and can be considered as a suburban atmospheric station. There is no direct pollution source in the vicinity of the station and the closest city (Gif/Yvette; 20,000 inhabitants) is located at about 3km southward of the site. Results presented here were obtained for a 10-day period (12–21 February 2009). Meteorological parameters were monitored at the site every 5 min using a Campbell Scientific Weather Station. Temporal variations of air temperature (T) and relative humidity (RH) during the campaign are illustrated in Figure 1 and shows relatively cold weather (mean T of 3.7 ± 2.9°C) and very humid conditions (mean RH of 87 ± 12%).

2.2. TEOM-FDMS

[8] Reliable continuous (6-min time resolution) measurements of fine aerosol mass ($PM_{2.5}$) were performed during our study using a Tapered Element Oscillating Microbalance (TEOM) Model 1400 from Rupprecht & Pataschnik equipped with a Sample Equilibration System (SES) and a Filter Dynamic Measurement System (FDMS, 8500 model series) [*Grover et al.*, 2005; *Sciare et al.*, 2007]. This instrument delivers a surrogate for concentration of semi-volatile material (SVM), which is mainly made of ammonium nitrate for the Paris background atmosphere during winter [*Favez et al.*, 2007]. The precision limits (given by the manufacturer) for TEOM measurements are ± 5.0μg/m^3 for 10-min averaged data and ± 1.5μg/m^3 for 1-h averages. A mean $PM_{2.5}$ concentration of 24.8μg/m^3 was calculated for the period of study which is close to the yearly average of ~20μg/m^3 calculated for the Paris urban background atmosphere using $PM_{2.5}$ data from the local air quality network (AIRPARIF, http://www.airparif.asso.fr/).

2.3. PILS-IC Instrument

[9] Measurements of fine cations were performed using a Particle-into-Liquid-Sampler (PILS) [*Orsini et al.*, 2003] running at 15LPM and coupled with an Ion Chromatograph (IC). Basic and acidic annular denuders (3-channel, URG Corp., USA) were mounted upstream of the PILS instrument and downstream of a sharp cut cyclone (model SCC2.229, BGI Inc., Whaltman, MA) having a 50% cut-off diameter of 2.5μm at 16.67LPM. Ambient concentrations of ions were corrected from blanks performed every day for 1 h and achieved by placing a total filter upstream of the sampling system. Liquid flow rates of the PILS were delivered by peristaltic pumps and set to 1.5 ml/min for producing steam inside the PILS and 0.5 ml/min for rinsing the impactor.

[10] Cation measurements were performed using an IC (Dionex, model ICS1500) equipped with a 2-mm diameter Auto-Suppression, Cation Self-Regenerating Suppressor

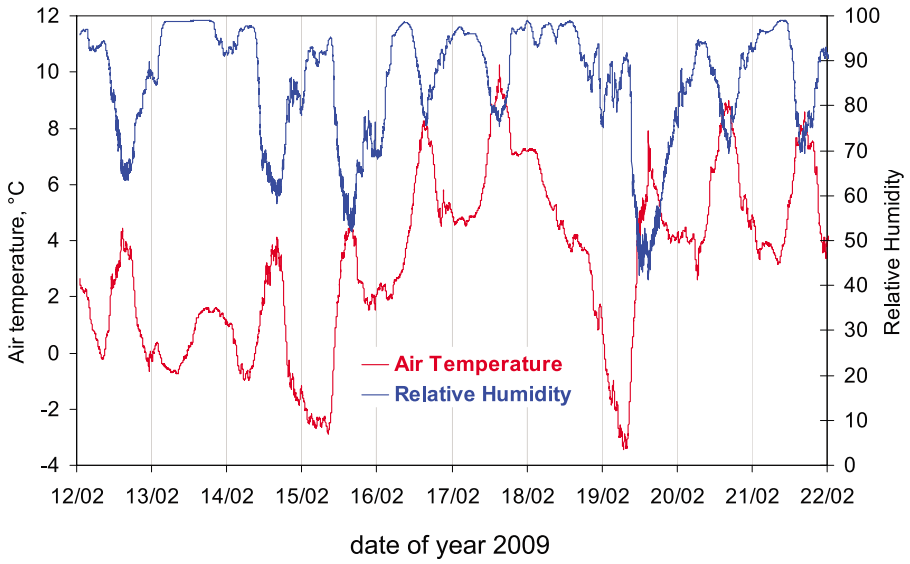

Figure 1. Air temperature and relative humidity during our study (12–22/02/2009).

(CSRS), a 2-mm diameter CS-12 pre-column and column, and a 100 μl injection loop. Analyses were performed in isocratic mode at 20 mM of Methanesulfonic Acid (MSA) at a flow rate of 0.25 ml/min, for the quantitative determination of the 5 major cations (Na^+, NH_4^+, K^+, Mg^{2+}, Ca^{2+}) every 10 min. Based on these IC settings, the detection limit (2σ) for cations was typically 0.1 ppb, which corresponds to an atmospheric concentration of ~1 ng/m^3. Calibration was performed for concentrations ranging from 1 to 100 ppb and showed a drift below 5% between the beginning and the end of the campaign.

2.4. PILS-TOC Instrument

[11] Measurements of WSOC were performed every 4 min using a modified Particle-into-Liquid-Sampler (Brechtel Manufacturing Inc., USA) [*Sorooshian et al.*, 2006] coupled with a total organic carbon analyzer (TOC, Model Sievers 900, Ionics Ltd, USA). A activated carbon parallel plate denuder [*Eatough et al.*, 1993] (similar to those operating in the OCEC Sunset field instrument and for filter sampling) was mounted upstream of the PILS instrument to minimize the influence of volatile organic compounds (VOC) on our WSOC measurements. A sharp cut cyclone (BGI Inc., Whaltman, MA) was mounted upstream of the VOC denuder in order to collected fine aerosols (50% cut-off diameter of 2.5μm at 16.67LPM). The PILS-TOC instrument was running at 15LPM and a constant dilution factor of 1.25 was taken in the instrument which is close to the one reported by *Sullivan et al.* [2006]. Liquid flow rates of the PILS were delivered by syringe pumps and set to 1.5 ml/min for producing steam inside the PILS and 0.7 ml/min for rinsing the impactor. A polyethylene filter of 0.45μm pore size diameter was set in-line in the aerosol liquid flow (downstream of the PILS collector) in order to analyze solely the water-soluble OC fraction. The collection efficiency of insoluble carbonaceous particles on the filter was checked by mounting a second in-line polyethylene filter (of 0.2μm pore size diameter) behind it. No significant variations in WSOC concentrations were observed using this set-up and a black deposit (i.e., soot particles) was only observed on the first in-line filter of 0.45μm pore size diameter. This result is consistent with the poor capability of the PILS to collect insoluble carbonaceous material [*Peltier et al.*, 2007]. Ultra-pure water (mQ grade) with trace concentrations of TOC from an ELGA Maxima Ultra Pure Water Unit was used here for the PILS-TOC instrument. Similar to the PILS-IC measurements, daily blanks for the PILS-TOC instrument were achieved by placing a total filter upstream of the sampling system for 1 h. In this configuration, approximately 15 min were necessary to reach blank values which were very stable during the campaign showing a mean concentration of 31.4 ± 2.7 ppbC. Note that most of the blank concentration refers to the TOC concentration in the ultra-pure water used in the PILS instrument (typically 25 ppbC), suggesting little contamination in the PILS instrument as well as a good efficiency of the VOC denuder placed upstream. Note also that the daily blanks for the PILS-TOC instrument were performed at different hours of the day and did not show a clear diurnal pattern that could be linked to diurnal variations of VOC. Ambient WSOC measurements were then corrected from this blank value. Limit of quantification of ambient WSOC measurements was estimated as twice the uncertainty calculated for the blank concentrations, corresponding to about 0.36μgC/m^3. A maximum uncertainty of 10% is calculated here which is comparable to the 5–10% uncertainty reported for PILS-TOC measurements [*Sullivan et al.*, 2004, 2006]. A total of 2852 valid data points were collected for the period of the study, corresponding to a mean ambient (blank corrected) WSOC concentration of 31.6 ± 21.3 ppbC (i.e., 2.10 ± 1.46μgC/m^3). Temporal variations of 4-min resolved WSOC concentrations are reported in Figure 2a. In the following, hourly data of water-insoluble organic carbon (WIOC) were obtained from the difference between OC data given by the OCEC Sunset field instrument and WSOC data given by the PILS-TOC. Conversion factors of 1.3 and 2.1 were taken to convert WIOC into WIOM (water-insoluble organic matter) and WSOC into WSOM (water-soluble

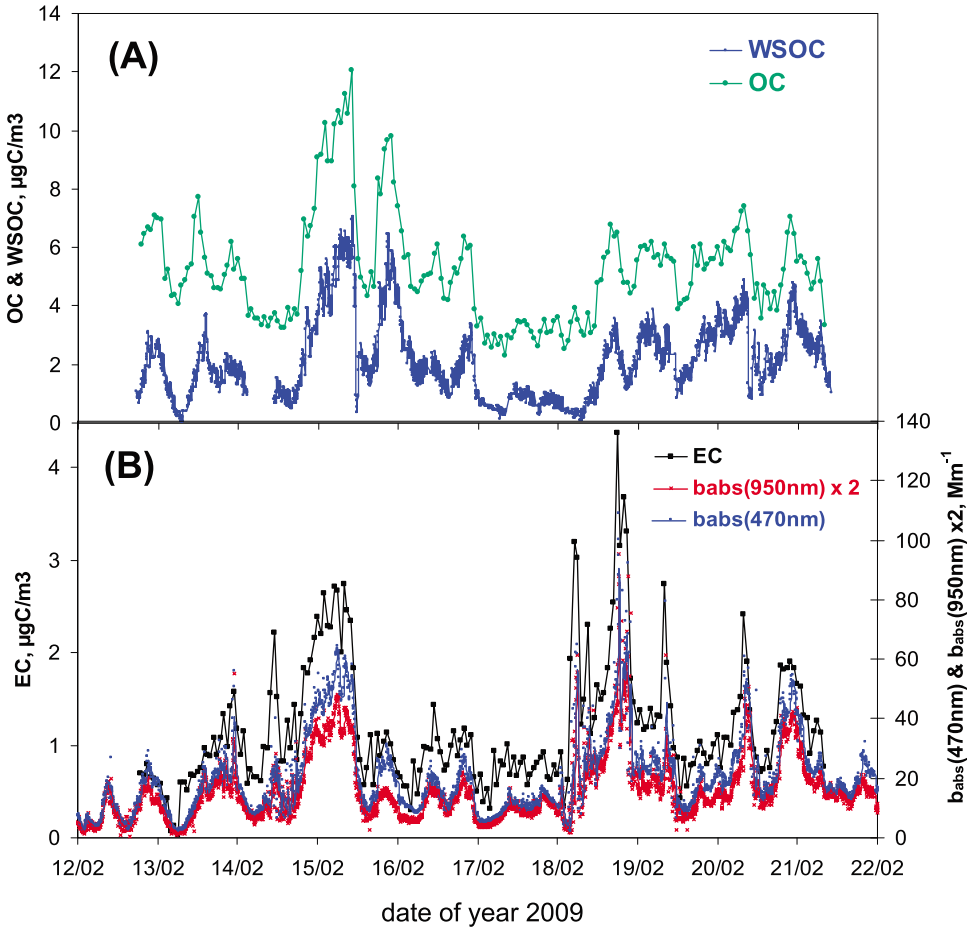

Figure 2. Temporal variations of (a) semi-continuous hourly OC concentrations (from the OCEC Sunset Lab instrument) and 4-min WSOC concentrations (from the PILS-TOC instrument). (b) Semi-continuous hourly EC concentrations (from the OCEC Sunset Lab instrument) and 5-min light absorption coefficient (b_{abs}) at 470 and 950 nm (from the 7-λ aethalometer instrument).

organic matter) [*Turpin and Lim*, 2001; *Zhang et al.*, 2005]. Note that the relative contribution of the different (primary and secondary) OA sources contributing to WSOC may be highly variable from one location to another and should also present significant temporality [*Decesari et al.*, 2001; *Sullivan and Weber*, 2006a, 2006b]. The amount of oxygenated compounds in WSOC may then change considerably, leading to quite different organic mass to organic carbon mass ratios [*Kiss et al.*, 2002]. For that reason, significant uncertainties may lie in the choice of proper and constant conversion factor for WSOC. Sensitivity studies have been performed for that purpose in order to evaluate the impact of our hypotheses on organic mass to organic carbon mass ratios on our OA source apportionment results. They are presented and discussed in section 4.3.

2.5. Filter Sampling and Chemical Analyses

[12] Fine aerosols were collected every 6 h on 47-mm diameter pre-fired quartz filters (QMA, Whatman) using a Partisol Plus sampler (model 2025, Thermo Scientific, USA) equipped with a $PM_{2.5}$ sharp cut cyclone running at 16.67LPM (model SCC2.229, BGI Inc., Whaltman, MA). A VOC denuder identical to the one used upstream of the OCEC Sunset field instrument and the PILS-TOC was set between the cyclone and the Partisol Plus sampler.

2.5.1. Determination of EC, OC, and WSOC

[13] A total of 31 continuous samples were collected for the period 13–21/02. Punches of 1.5 cm^2 were taken from each filter and analyzed for EC and OC content using a thermo-optical carbon analyzer (OCEC Sunset Lab Instrument; Sunset Laboratory, Forest Groove, OR, USA) implemented with the NIOSH thermal program [*Birch and Cary*, 1996]. The uncertainty given by the manufacturer for EC and OC measurements is 0.2μgC/cm^2 ± 5%. A total of 7 blanks were taken in the field covering the duration of the campaign and showed non-detectable amounts of EC. A mean OC value of 0.20 ± 0.10μgC/cm^2 was calculated here for blank filters and corresponded to about 5% of OC concentrations measured in the field. These blanks were then subtracted from the ambient OC values.

[14] Water-soluble organic carbon (WSOC) analyses were achieved on a second punch of 1.5 cm^2 taken on 21 consecutive quartz filters covering the period 13–19/02. WSOC measurements were performed using a total organic carbon analyzer (TOC, Model Sievers 900, Ionics Ltd, USA) in which ammonium persulphate and UV light (185 and

284 nm) are used for the chemical oxidation of WSOC into CO_2 further detected by conductivity. Information on filter extraction protocol, detection limit, and calibration for WSOC analysis is provided by *Sciare et al.* [2009]. Ambient concentrations of WSOC were ranging from 237.0 to 1403.3 ppbC (630.7 ± 275.8 ppbC on average). These concentrations were corrected using the blank filters taken in the field with blanks showing an average WSOC concentration of 83.6 ± 9.1 ppbC (corresponding to 0.46 ± 0.05μgC/m^3). An uncertainty of 10% is estimated here for the analytical determination of WSOC from the filters.

2.5.2. Determination of Levoglucosan

[15] Monosaccharides and sugar alcohols (incl. levoglucosan, mannitol, arabitol) have been determined following the technique reported by *Iinuma et al.* [2009], using an ion chromatograph (DIONEX, model ICS 3000) system equipped with an electrochemical detector and gold electrode. The separation is performed using a Dionex CarboPac MA1 4-mm diameter column. Eluant type, concentrations, and gradients are similar to those reported by *Iinuma et al.* [2009]. Punches of 1.5 cm^2 of each QMA filter sampled with the Partisol Plus sampler (see above) were placed into rinsed plastic vials containing 5 ml of mQ water, and were extracted by sonication for 40 min. Extracted liquid samples were immediately filtered (0.45μm pore size diameter polyethylene filter) and analyzed for 11 sugar alcohols, monosaccharides, and monosaccharide anhydrides (including levoglucosan, mannosan, and galactosan). Linear calibration (with r^2 better than 0.99) was obtained for all these compounds with standard concentrations ranging 10 ppb to 1 ppm allowing the quantification of levoglucosan at pbb levels. Limit of quantification for levoglucosan was about 5 pbb which is similar to the one reported by *Iinuma et al.* [2009]. Based on our sampling settings (6 h sampling at 1 m^3/h and 1.5 cm^2 of sampled filter extracted in 5 ml), this limit corresponds to an atmospheric concentration of levoglucosan of about 35 ng/m^3. Blank filters collected in the field did not show detectable amounts of levoglucosan. A total of 31 filter samples were analyzed and showed detectable amounts of levoglucosan with concentrations ranging from 10 to 127 ppb (average of 39.7 ± 30 ppb) corresponding to ambient concentrations ranging from 72 to 919 ng/m^3 (average of 285 ± 223 ng/m^3).

2.6. OCEC Sunset Field Instrument

[16] Semi-continuous hourly concentrations of elemental carbon (EC) and organic carbon (OC) in $PM_{2.5}$ were obtained in the field from an OCEC Sunset field instrument (Sunset Laboratory, Forest Grove, OR, USA; *Bae et al.* [2004]) running at 8LPM. A denuder provided by the manufacturer was set upstream in order to remove possible adsorption of VOCs onto the filter used to collect fine aerosols in the instrument. Measurement uncertainty given by the OCEC Sunset field instrument is poorly described in literature and an estimate of 20% for this uncertainty was taken here following *Peltier et al.* [2007]. A total of 206 valid EC and OC data points were collected for the period (12–21/02/2009) and reported in Figure 2.

2.7. Aethalometer

[17] Aerosol absorption coefficients (b_{abs}) were obtained every 5 min at seven different wavelengths (370, 470, 520, 590, 660, 880 and 950 nm) using a Magee Scientific aethalometer (model AE-31) equipped with a cyclone having a 50% cut-off diameter of 2.5μm (R&P, Albany, NY). This instrument was operating at a flow rate of 5LPM in an automated mode, under which the filter tape advances when the attenuation (ATN) at 370 nm reaches 100. Due to the methodology used within the aethalometer (filter-based measurements), absorption coefficients directly obtained from this instrument are affected by various sampling and analytical artifacts (mostly referred to as multiple scattering and shadowing effects) which need to be carefully corrected for [*Collaud Coen et al.*, 2010, and references therein]. In the present work, we have processed the data following the same procedures reported by *Favez et al.* [2010]. The correction procedure introduced by *Weingartner et al.* [2003] was applied to our data set as follows:

$$b_{abs,\lambda,t} = b_{aeth,\lambda,t} / \left(2.14 \times R(ATN)_{\lambda,t}\right) \quad (1)$$

Where, at a given time (t) and a given wavelength (λ), $b_{abs,\lambda,t}$ and $b_{aeth,\lambda,t}$ stand for the corrected absorption coefficient and the raw absorption coefficient, respectively. The constant (2.14) stands for multiple scattering of the light beam by the filter fibers in the unloaded filter. Finally, $R(ATN)_{\lambda,t}$ describes the decrease of the latter artifact with the gradual accumulation of soot particles on/in the filter (i.e., correction of the shadowing effect). $R(ATN)_{\lambda,t}$ was determined following the equation:

$$R(ATN)_{\lambda,t} = \left(\frac{1}{f_\lambda} - 1\right) \times \frac{\ln\left(ATN_{\lambda,t}\right) - \ln(10)}{\ln(50) - \ln(10)} + 1 \quad (2)$$

where $ATN_{\lambda,t}$ corresponds to the light attenuation measured by the aethalometer at a given time (t) and a given wavelength (λ), and f_λ allows for the correction of the instrumental error that occurs when the shadowing effect is disregarded. The latter parameter was determined here by keeping the median ratio of absorption coefficients (before and after the change of each filter spot) the closest to 1. The overall uncertainty of absorption coefficients calculated this way is on the order of 20%. Nevertheless, this uncertainty is expected to affect measurements at each wavelength in a relatively similar way, so that a higher confidence level is assumed for the spectral shape of light absorption. Note also that the b_{abs} corrections applied here [from *Weingartner et al.*, 2003] stand for the best corrections in the absence of light scattering coefficient measurements [*Collaud Coen et al.*, 2010].

[18] Temporal variations of 5-min integrated b_{abs} at 470 and 950 nm are compared in Figure 2b with the EC obtained on an hourly basis by the OCEC Sunset field instrument.

2.8. Automatic GC-FID

[19] Non-methane hydrocarbons (NMHC) in ambient air were measured using two portable gas chromatographs equipped with a flame ionization detector (GC-FID, Chromatotec, France). The first analyzer, ChromaTrap, allowed the measurement of C_2-C_6 hydrocarbons and the second, AirmoBTX, the measurement of C_6-C_{10} hydrocarbons.

[20] Briefly, for each sample, 180 mL for ChromaTrap and 660 mL for AirmoBTX of air was drawn through a 1/8 inch

diameter 6 m-long stainless steel line with a flow rate of 18 mL/min for ChromaTrap and 60 mL/min for AirmoBTX. First, for the ChromaTrap instrument, ambient air was passed through a Nafion dryer to reduce the water content. Then hydrocarbons were preconcentrated for ChromaTrap at −8°C on a glass trap containing adsorbents Carboxen 1000/ Carbopack B/Carbotrap C and for AirmoBTX at ambient temperature on a glass trap containing the adsorbent Carbotrap C. Then the trap was heated rapidly to 220°C for 3 min for ChromaTrap and to 380°C over 2 min for AirmoBTX, to desorb the preconcentrated VOC into a separating column (Plot Column Al_2O_3/Na_2SO_4, 25 m × 0.53 mm diameter for ChromaTrap and MXT30CE, 30 m × 0.28 mm diameter for AirmoBTX). For both instruments, the sampling time was 10 min and analysis time was 20 min and, therefore, measurements were performed with a time resolution of 30 min. During the campaign, a certified calibrated gas bottle (from National Physics Laboratory) containing thirty non-methane hydrocarbons at 4–5 ppb level was injected several times. These series of measurements allowed the confirmation of compound retention times and the calculation of one average response factor per instrument which was used to calibrate measurements from the campaign.

[21] Tests performed in the laboratory have shown a repeatability of the measurement better than 5% for almost all compounds and an overall uncertainty better than 15%. More technical information (including performance of this instrument) is provided by *Bonsang et al.* [2008] and *Gros et al.* [2011].

2.9. PTR-MS

[22] During the campaign, a new high sensitivity Proton Transfer Mass Spectrometer (PTR-MS from Ionicon Analytik, Austria) was used to monitor selected VOCs which were not measured by the GC-FIDs. The PTR-MS technology was first introduced in the atmospheric chemistry community by *Lindinger et al.* [1998] and has been extensively described in the literature [*Blake et al.*, 2009; *de Gouw and Warneke*, 2007, and references therein]. Briefly, compounds (R) having a proton affinity larger than water react within a flow drift tube with H_3O^+ according to the reaction ($R + H_3O^+ \rightarrow RH^+ + H_2O$), are then selected by a quadrupole mass spectrometer and detected by a second electron multiplier. The measured mass (mz) corresponds to the molecular mass +1 which may correspond to several compounds. For this specific campaign, a focus was made on selected masses which can be attributed to the following compounds m33 (methanol), m42 (acetonitrile), m45 (acetaldehyde), m59 (acetone) [*de Gouw and Warneke*, 2007].

[23] Measurement conditions during the campaign were 15 to 20 millions of primary ions (H_3O^+), a pressure of 2.24 mbar into the reaction chamber and a drift field maintained at 600V/cm. Air was sampled through a 5-m Teflon line (1/16″ inner diameter) heated at 60°C with a flow rate of about 75 ml/min. Time resolution of the measurements was every 30 s, with an integration time of 1s for each mz (about 30 masses were monitored, but only four were selected for the present study).

[24] The instrumental background was determined by switching incoming air over a catalytic converter Platinum coated wool heated to 350°C during 5 min every 15 min. The background signals obtained for each measured mass were averaged and subtracted from the atmospheric signals. The background levels of the compounds considered here were 62.8 ± 1.9, 0.4 ± 0.2, 16.6 ± 0.3 and 2.8 ± 0.0 normalized counts per second (ncps) for methanol, acetonitrile, acetaldehyde and acetone, respectively.

[25] The primary reagent count varied between 15 to 20 millions counts. After normalization to 1 million primary ions the instrument sensitivity was between 5 (methanol) and 18 ncps/ppbv (acetonitrile and acetone). The instrument was calibrated at the Max Planck Institute for chemistry (Mainz, Germany), using a gas standard bottle (Apel-Riemer Environmental Inc.) containing about 500 ppb of each measured compound and injected at different amounts by dilution with synthetic air. Details about this standard is provided by *Gros et al.* [2011]. As the response of the PTR-MS is directly influenced by the humidity rate of the analyzed sample, calibrations with diverse humidity rates were performed. For the present data, the 80% humidity rate calibration was taken into consideration, as the ambient relative humidity varied in-between 65 and 95% during the campaign.

3. The Aethalometer Model

[26] The source apportionment performed by the aethalometer model [*Sandradewi et al.*, 2008a] is based on the strong spectral dependence of light absorption properties of brown carbon aerosols [*Hoffer et al.*, 2006 and references therein], and the use of a multiwavelength aethalometer to detect the presence of this brown carbon fraction in ambient biomass burning aerosols [e.g., *Jeong et al.*, 2008; *Sandradewi et al.*, 2008b; *Yang et al.*, 2009]. In the present study, the large contribution of brown carbon aerosols on the spectral dependence of light absorption properties could be observed as illustrated in Figure 3 by the temporal variation of the angstrom exponent ($\alpha_{470-950}$) calculated between the 2 wavelengths of the aethalometer (470 and 950 nm). As shown by this Figure, large changes in the spectral dependence of the light absorption were observed with higher contribution of brown carbon aerosols (i.e., higher α values) at night.

[27] Recent studies have shown that information delivered by a multiwavelength aethalometer could be used in a more quantitative way - in conjunction with complementary carbon measurements - to provide a source apportionment of biomass burning aerosols in the context of an atmospheric mixture of carbonaceous aerosols having both modern (biomass burning) and fossil fuel origins [*Sandradewi et al.*, 2008a; *Favez et al.*, 2009, 2010]. This aethalometer model has been applied to our data sets. Details of this model are given below.

[28] Total carbonaceous material (CM_{total}) is primarily considered as the sum of brown-carbon-containing carbonaceous material originating from wood burning (noted as CM_{wb}), non brown-carbon-containing carbonaceous material originating from fossil fuel combustion (noted as CM_{ff}), and non-combustion OA (noted as $OM_{residual}$). Note that the assumption made here that wood burning is the main contributor of UV-absorbing brown carbon during the cold months has been recently verified by *Hecobian et al.* [2010] who have performed a year-round record of light absorption spectra of fine WSOC. Note also that such an assumption is

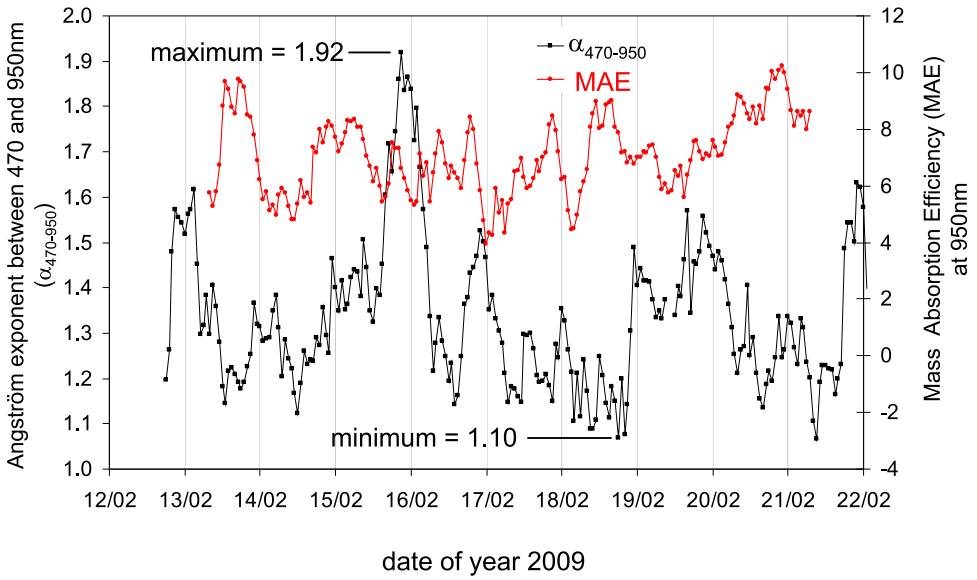

Figure 3. Temporal variations of the angstrom exponent between 470 and 950 nm ($\alpha_{470-950}$) obtained from the 7-λ aethalometer instrument and the Mass Absorption Efficiency (MAE) calculated as the ratio between EC (OCEC Sunset Lab instrument) and b_{abs} at 950 nm (7-λ aethalometer instrument). Minimum and maximum of ($\alpha_{470-950}$) are noted here and stand for the highest contribution to the light absorption properties of fossil fuel and wood burning combustion sources, respectively.

valid only if we assume a weak influence of dust aerosols which have shown to contribute also to the absorbance in the UV range [*Fialho et al.*, 2005].

[29] Non combustion OA ($OM_{residual}$) comprises both primary biogenic organic aerosols (PBOA) (plants, pollen, spores …) and secondary organic aerosols (SOA). Based on the fact most of the particulate mass of primary biogenic aerosols is located in supermicron aerosols [*Bauer et al.*, 2008a, and references therein], it can be reasonably assumed here that biogenic POA do not contribute significantly to $OM_{residual}$ in our fine aerosol fraction. Note that estimates of biogenic POA can be performed here using arabitol and mannitol as tracers of fungal spore emissions (i.e., primary biological aerosol particles [*Bauer et al.*, 2008b]). Non detectable amounts of arabitol and mannitol (<35 ng/m^3) were obtained in the filter samples collected during our study. Using the emission factors of arabitol and mannitol per fungal spore reported by *Bauer et al.* [2008b] and an OC content of 5.2pg/spore proposed by *Bauer et al.* [2002] for PM_{10} samples, a raw estimate of maximum 0.15μgC/m^3 can be calculated here for PBOA. This is about 35 times lower compared to our mean value of 5.36 ± 1.33 μg/m^3 calculated for $OM_{residual}$. For that reason, it can be reasonably assume that our $OM_{residual}$ refers mainly to SOA. This is also supported by recent results obtained by *Gilardoni et al.* [2011] who have shown PBOA concentrations below 0.1μg/m^3 for the entire year in fine aerosols at a European background site.

[30] Based on these different observations, carbonaceous material can then be decomposed as:

$$CM_{total} = CM_{ff} + CM_{wb} + OM_{residual} = C_1 \times b_{abs,ff,950nm} + C_2 \times b_{abs,wb,470nm} + C_3 \quad (3)$$

where $b_{abs,ff,950nm}$ stands for the absorption coefficient of CM_{ff} at 950 nm, $b_{abs,wb,470nm}$ for the absorption coefficient of CM_{wb} at 470 nm, C_1 and C_2 for the light absorption to the particulate mass of both sources, and C_3 corresponds to the amount of non-combustion OA ($OM_{residual}$). It should be noted that fossil fuel carbonaceous material (CM_{ff}) comprises traffic emissions as well as carbonaceous aerosols originating from domestic heating using fuel oil and natural gas combustion. It should also be mentioned that in the aethalometer model, CM_{ff} and CM_{wb} may contain a fraction of secondary material (or oxidized primary organic aerosols) that have been condensed on primary combustion particles of fossil fuel and wood burning origin. For that reason, it may be appropriate to consider $OM_{residual}$ as the fraction of SOA that has not rapidly condensed onto primary combustion CM. Equation (3) can be solved when combined with the following ones:

$$CM_{total} = EC + OM \quad (4)$$

$$b_{abs,\lambda} = b_{abs,ff,\lambda} + b_{abs,wb,\lambda} \quad (5)$$

$$\left(b_{abs,ff,470nm}/b_{abs,ff,950nm}\right) = (470/950)^{-\alpha ff}. \quad (6)$$

$$\left(b_{abs,wb,470nm}/b_{abs,wb,950nm}\right) = (470/950)^{-\alpha wb}. \quad (7)$$

EC and OM data in equation (4) are obtained from the OCEC Sunset field instrument and a conversion factor for OC-OM of 1.80. In equations (6) and (7), α_{ff} and α_{wb} stand for the Angstrom absorption exponents of fossil fuel and

wood burning, respectively. In this study, a α_{ff} value of 1.1 was taken, corresponding to the mean α value obtained for the lowest OC/EC ratios observed during our study (afternoon traffic peak on the 18/02, Figure 3). This value is similar to the ones used in the previous studies using the aethalometer model (see for instance *Favez et al.* [2010]). A α_{wb} value of 2.0 was taken here, based on values previously reported for wood burning aerosols [e.g., *Clarke et al.*, 2007; *Lewis et al.*, 2008] and used by *Favez et al.* [2010]. This value is also close to our highest α value of 1.92 obtained on 15/02 at 22:00 LT (Figure 3).

[31] In order to properly assign the contribution of fossil fuel (CM_{ff}) and wood burning (CM_{wb}) to BC (BC_{ff} and BC_{wb}) and to OM (OM_{ff}, OM_{wb} and $OM_{residual}$), we first calculated BC mass concentrations from absorption measurements provided by the aethalometer instrument using a specific Mass Absorption Efficiency (MAE) calculated from $b_{abs,950nm}$ (aethalometer) and EC loadings measured by the OCEC Sunset field instrument. A mean MAE value of 7.3 ± 0.1 m^2/g was obtained from this linear regression ($r^2 = 0.85$, N = 206) and was used here to estimate BC concentrations every 5 min from the $b_{abs,950nm}$ data set. This MAE value is significantly higher than that recommended by *Bond and Bergstrom* [2006] at this wavelength for fresh soot (~4.3 ± 0.6 m^2/g). This could be attributed to a possible encapsulation of soot particles by organic/inorganic compounds leading to an increase of MAE [*Liousse et al.*, 1993; *Bond and Bergstrom*, 2006; *Lack et al.*, 2008]. Alternatively, the use of the NIOSH protocol in the OCEC Sunset field instrument for biomass burning aerosols may lead to an underestimation of EC concentrations that could explain our high MAE [*Sciare et al.*, 2003].

[32] In order to calculate BC_{ff} and BC_{wb} from BC concentrations, an assumption was made of an equivalent MAE for these 2 sources. In order to test the consistency of this assumption we have reported in Figure 3, together with $\alpha_{470-950}$, the temporal variations of MAE defined as the ratio between $b_{abs,950nm}$ and EC. Although the MAE has shown to vary substantially from 4 to 10 m^2/g, no clear relationship ($r^2 = 0.05$) could be define between MAE and the relative contribution of wood burning depicted here by the angstrom exponent ($\alpha_{470-950}$). The lack of correspondence between these 2 data sets may suggest that other processes (such as encapsulation of soot particle by organic/inorganic compounds) could be responsible for the MAE variability instead of the abundance of one combustion source (fossil fuel, wood burning) relatively to the other. This is consistent with Figure S4 (auxiliary material) which shows that periods with high MAE do coincide most of the time with pollution episodes (elevated $PM_{2.5}$ values) that are favorable to an enhancement of the condensation of organic/inorganic compounds onto soot particles.[1] Based on these observations, we have assumed equivalent MAE for BC_{ff} and BC_{wb}, and calculated these 2 fractions following the equation:

$$BC_{ff} = BC \times \left(b_{abs,ff,950nm}/b_{abs,ff,950nm}\right) \quad (8)$$

[1]Auxiliary materials are available in the HTML. doi:10.1029/2011JD015756.

The details of the calculation of C_1, C_2, C_3 (equation (3)) are presented below. The factor C_1 can be calculated from the following equations:

$$BC_{ff} = b_{abs,ff,950nm}/MAE \quad (9)$$

$$OM_{ff} = f_{OC-OM} \times (OC/EC)_{ff} \times BC_{ff} \quad (10)$$

$$CM_{ff} = BC_{ff} + OM_{ff} \quad (11)$$

where BC_{ff}, OM_{ff}, and MAE, stand for BC, OM, and MAE from fossil fuel respectively; $f_{OC\text{-}OM}$ stands for the OC-OM conversion factor; and $(OC/EC)_{ff}$ stands for a typical OC/EC ratio for fossil fuel emissions. The factor C_1 can then be calculated using these 3 equations and equation (3) as:

$$C_1 = \left[\left(1 + f_{OC-OM} \times (OC/EC)_{ff}\right)/MAE\right]. \quad (12)$$

[33] The MAE of 7.3 m^2/g calculated previously can be used here to calculate BC_{ff} (equation (9)). A value of 1.3 can be proposed here for $f_{OC\text{-}OM}$ assuming that organic aerosols originating from fossil fuel are mainly of primary origin and poorly oxygenated [*Turpin and Lim*, 2001; *Zhang et al.*, 2005]. The choice of $(OC/EC)_{ff}$ may be difficult to obtain from our data set due to the presence of possibly elevated background concentrations of other organic aerosol sources (biomass burning, secondary organics). For that reason, we have taken a ratio of 0.70 obtained from semi-continuous EC and OC measurements we have performed (with the same ECOC Sunset Field instrument) in the city of Paris during springtime [*Sciare et al.*, 2010]. This OC/EC ratio is close to those reported by *Lonati et al.* [2007] and *El Haddad et al.* [2009] for measurements performed in tunnels in Italy and France, respectively. It is also in line with the ratio of 0.7 suggested for the overall fossil fuel consumption in the EU15 area [*Kupiainen and Klimont*, 2007]. Based on these assumptions, a C_1 value of 2.616×10^5 $\mu g/m^2$ was calculated here which is very close to the C_1 values of 2.588×10^5 $\mu g/m^2$ and 2.648×10^5 $\mu g/m^2$ reported by *Sandradewi et al.* [2008a] and *Favez et al.* [2009], respectively.

[34] Hourly measurements obtained by the OCEC Sunset field and aethalometer instruments during the campaign (12–21/06) were used to calculate every hour $b_{abs,ff,950nm}$, $b_{abs,wb,470nm}$, and CM_{total}. This data set (N = 206) was used in equation (3) to derive C_2 and C_3 using a simple linear regression analysis. Values of $5.41 \times 10^5 \pm 0.20 \times 10^5 \mu g/m^2$ and $5.36 \pm 0.17 \mu g/m^3$ are obtained for these 2 coefficients, respectively. Our C_2 value is 14% and 19% lower compared to the ones reported by *Sandradewi et al.* [2008a] and *Favez et al.* [2009], respectively. This discrepancy can be due to different analytical methods used to determine CM concentrations. Our CM data set was based on hourly VOC-denuded semi-continuous EC and OC concentrations, whereas the CM data set used by *Sandradewi et al.* [2008a] was based on AMS measurements and the CM data set used by *Favez et al.* [2009] was based on undenuded 24 h filter-based EC and OC concentrations. Note also that *Favez et al.* [2010] have reported different C_2 values when using either filter-based EC and OC measurements or AMS measurements.

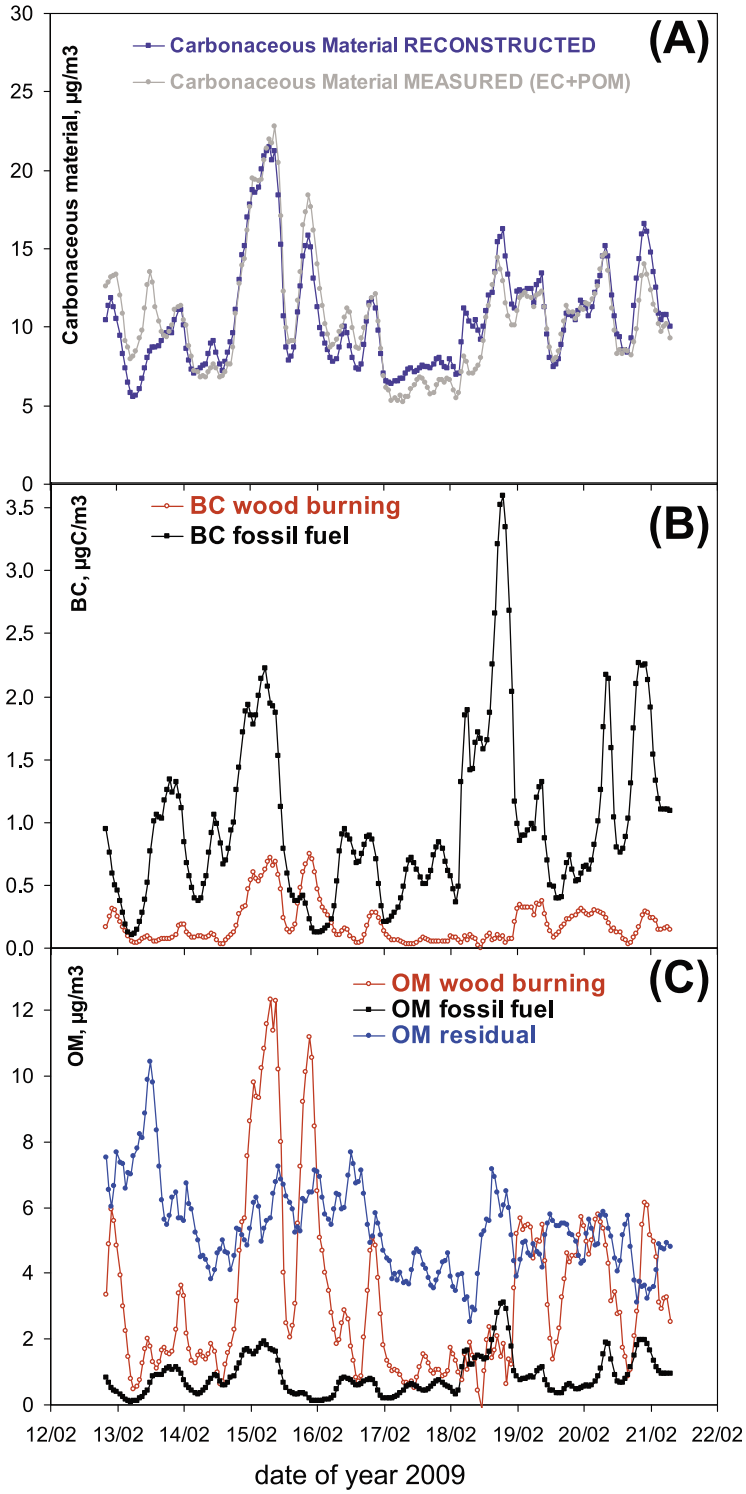

Figure 4. Results of the aethalometer model: (a) Comparison between measured and reconstructed carbonaceous material. (b) Temporal variations of fossil fuel and wood burning black carbon. (c) Temporal variations of fossil fuel, wood burning, and residual (SOA) organic matter.

Finally, the C_2 value may not be necessary identical from one study to another. As illustrated in equation (11) for the calculation of C_1 (fossil fuel), C_2 may depend on various factors such as the MAE for wood burning as well as the OM_{wb}/EC_{wb}, both factors being dependent on parameters such as combustion efficiencies and/or biofuel types.

[35] Results of the aethalometer model are illustrated in Figure 4a which reports the comparison between the

measured and reconstructed carbonaceous matter (CM). This comparison shows a slope close to one (0.99) and a good correlation coefficient ($r^2 = 0.89$; N = 204). This model appears to be consistent with the measurements performed with the OCEC sunset field instrument and well constrained by the large number of EC and OC data points obtained by this instrument.

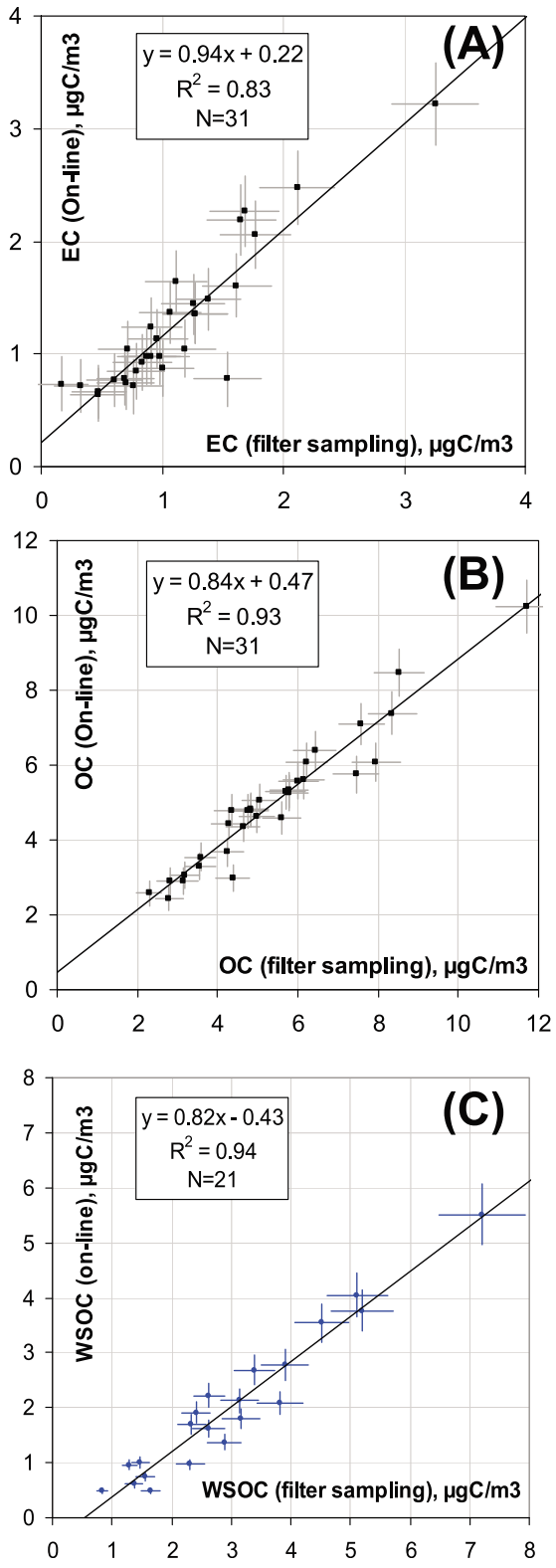

4. Results

4.1. Comparison Between Online and Filter Sampling Measurements of EC, OC, and WSOC

[36] Filter-based measurements of EC and OC were compared with the results obtained by the (online) OCEC Sunset field instrument. Results are reported in Figures 5a and 5b. Error bars reported in Figure 5 stand for the uncertainties in OC and EC concentrations following the recommendation of the manufacturer. Figure 5 shows a high correlation coefficient of $r^2 = 0.83$ and $r^2 = 0.93$ for EC and OC, respectively. The intercepts were close to 0 and slopes close to one (0.94 and 0.84 for EC and OC, respectively). Sample-to-sample comparison has shown similar good agreement with median difference values of 11.6 and 7.4% for EC and OC, respectively.

[37] The same filter samples were compared for their concentrations in WSOC with the PILS-TOC instrument. Results are reported in Figure 5c and show a good agreement between the two techniques ($r^2 = 0.94$, N = 21). Intercept was found close to 0 ($-0.43\mu gC/m^3$) and the slope showed an 18% overestimation from the filter sampling technique. Sample-to-sample comparison between these two techniques shows a median difference value of 38.4% ($\sim 1\mu gC/m^3$) in favor of the filter sampling and confirms the overestimation of WSOC given from the filter sampling.

[38] Filter sampling artifacts may probably be responsible for the almost constant overestimation of about $1\mu gC/m^3$ of WSOC. Although a VOC denuder was placed upstream to the filter sampling, VOCs may still have passed through this denuder and be adsorbed on the active sites of the filter matrix. This artifact is not observed with the PILS-TOC technique which avoids filter media for collecting particles.

[39] Note that online and off-line OC measurements may be affected by similar positive and negative sampling artifacts, since they are based on filter sampling techniques. This is not the case for online and off-line WSOC measurements which may explain why the OC intercomparison appears slightly better than the WSOC intercomparison. Note also that discrepancies between online and filter sampling WSOC (and OC) measurements may also be explained by evaporative losses of (semi-volatile) organic aerosols into the online instruments (OCEC Sunset field and PILS-TOC instruments) when the sample air was drawn from the cold outdoor to the warm indoor environment. In order to reduce such heat up of the sampled air, the length of inlet tubing for the online instruments exposed to room temperature was reduced, being 1 m or below.

Figure 5. Comparison between online (OCEC Sunset Field instrument and PILS-TOC) and off-line (Partisol Plus filter sampling) measurements for (a) Elemental Carbon (EC), (b) Organic Carbon (OC), and (c) water-soluble Organic Carbon (WSOC). Error bars for EC and OC are calculated following the analytical uncertainty given for the Sunset instrument ($0.2\mu g\ C/cm^2 \pm 5\%$). Error bars for WSOC are calculated using the 10% uncertainty estimated for this compound.

Table 1. Atmospheric Concentrations of the Different Carbonaceous Fractions in Fine Aerosols (AD < 2.5μm) for the Period (12–21/02/2009)[a]

Compound	Unit	Range	Mean Concentrations (± 1σ)
BC	μgC/m^3	0.15–3.36	0.97 (± 0.61)
OC	μgC/m^3	2.32–12.05	5.27 (± 1.84)
WSOC	μgC/m^3	0.02–6.18	2.08 (± 1.31)
Levoglucosan	μg/m^3	0.072–0.919	0.28 (± 0.22)
BC_{ff}	μgC/m^3	0.10–3.49	0.96 (± 0.66)
BC_{wb}	μgC/m^3	0.00–0.81	0.22 (± 0.18)
OM_{ff}	μg/m^3	0.09–3.17	0.88 (± 0.60)
OM_{wb}	μg/m^3	0.00–12.33	3.33 (± 2.67)
$OM_{residual}$	μg/m^3	1.33–10.45	5.36 (± 1.33)

[a]Calculations are based on hourly averaged data.

[40] Note that possible evaporative losses of (semi-volatile) organic aerosols into the online instruments may be more important when the temperature gradient is high between outdoor and indoor conditions. Concentrations of OC should be particularly affected by such evaporative losses since the temperature of the filter inside the Sunset Field instrument is typically 20°C during the sampling step. In order to investigate this possibility, we have plotted in auxiliary material (Figure S1) the off-line to online OC ratio as a function of the outdoor temperature. No relationship was observed suggesting that differences observed between the two techniques (off-line and online) could not be explained by temperature gradient (between outdoor and indoor conditions).

4.2. Source Apportionment of Carbonaceous Aerosols Using the Aethalometer Model

[41] Based on the availability of the aethalometer model to properly reproduce temporal variations of CM determined experimentally, we have decided to modify (enhance) this model in order to document hourly concentrations of non-combustion organic aerosols. To do so, $OM_{residual}$ was not set as a constant value any more but was deduced from equation (3) by the difference between CM and (CM_{ff} + CM_{wb}) determined previously. Doing so, SOA concentrations (assumed here to refer to $OM_{residual}$) were then obtained every hour. It is important to note here that the use of a variable concentration of SOA represents the main difference between our (modified) aethalometer model and those previously reported in literature.

[42] Temporal variations of the different carbonaceous fractions (BC, OM) are reported in Figures 4b and 4c. The two combustion sources (fossil fuel and biomass burning) exhibit quite different patterns. High concentrations of wood burning aerosols are observed almost every evening with the highest concentrations during the week-end (14–15/02) which corresponds to the coldest period of our study with hourly mean air temperature minima of −3°C. Note also that the lowering of the planetary boundary layer (PBL) height at night may have also enhanced significantly the nighttime concentrations of wood burning aerosols. A clear double maximum is observed during daytime for BC originating from fossil fuel (the 16, 17, 19 and 21/02) and can be attributed to traffic emissions since these 2 maxima are observed at rush hours (08:00–10:00 LT and 18:00–21:00 LT). The temporal variations of SOA ($OM_{residual}$) are reported in Figure 4c and show significant concentration levels ranging from 1.3 to 10.4μg/m^3 (average 5.38 ± 1.33μg/m^3). These variations are disconnected (and less variable) from those observed for fossil fuel and wood burning and will be discussed in more details in the following.

[43] Atmospheric concentrations of the different carbonaceous fractions are summarized in Table 1. During our study, the relative contribution of BC_{wb} to the total BC was highly variable ranging from 0 to 79% with, however, a rather small mean contribution (25 ± 16%). The wood burning source (CM_{wb}) contributes on average to 61% of the total mass of combustion aerosols (29% to the total mass of CM). Contribution of these wood burning aerosols to $PM_{2.5}$ ranges from 0 to 55% (average of 15 ± 11%).

[44] Our wood burning contribution of 61% (relative to combustion aerosols) is significantly higher compared to the 46% reported by *Favez et al.* [2009] for a background urban site in Paris during winter 2005. Lower traffic emissions combined with larger residential areas (i.e., stronger domestic wood burning emissions) at our suburban site may explain this discrepancy. This discrepancy may also originate from the time period of our study which encompassed school holidays, leading to less traffic and possibly higher domestic heating emissions.

[45] Another comparison can be performed with a recent source apportionment study of carbonaceous aerosols performed in Grenoble (France) during the same period (winter 2009) and using also the aethalometer model [*Favez et al.*, 2010]. These authors found that 83% of BC in Grenoble originated from fossil fuel which is close to our value of 75%. Values of OM_{ff}, OM_{wb}, and $OM_{residual}$ were found to contribute to about 14%, 56%, and 30%, respectively of OM, which are comparable to ours (10%, 31%, and 59%, respectively).

[46] Our large contribution of $OM_{residual}$ (5.38 ± 1.33μg/m^3 on average) strongly suggests that non-combustion OA (i.e., SOA) are playing a major role during wintertime. This concentration is consistent with the 5.9μgC/m^3 reported by *Gilardoni et al.* [2011] for secondary organic carbon at a European rural site during wintertime.

[47] Diurnal variations of the 3 OM sources have been investigated and show consistent temporal variability with a maximum in the evening (21:00–23:00) for the wood burning source corresponding to the domestic heating period (Figure 6a), and a double maximum for the fossil fuel source consistent with the 2 traffic peaks (08:00–10:00 and 18:00–21:00) (Figure 6b). The diurnal variations of $OM_{residual}$ show a double peak, one during midday and another one after the night maximum of wood burning (Figure 6c). This pattern will be discussed later in section 5.

4.3. Sensitivity Study of the Aethalometer Model

[48] The purpose of this section is to test the sensitivity of the Aethalometer model on the few assumptions we have used in this model regarding CM (i.e., $f_{OC\text{-}OM}$), C_1 (i.e., $f_{OC\text{-}OM}$, $(OC/EC)_{ff}$), MAE_{ff}), α_{ff}, and α_{wb}. Uncertainties associated with atmospheric measurements will not be addressed here as they have been discussed previously from the comparison with the filter sampling (section 4.1).

4.3.1. Influence of $f_{OC\text{-}OM}$ on the Results of the Aethalometer Model

[49] Although the aethalometer model reported in previous studies has been used solely to reconstruct CM, this model

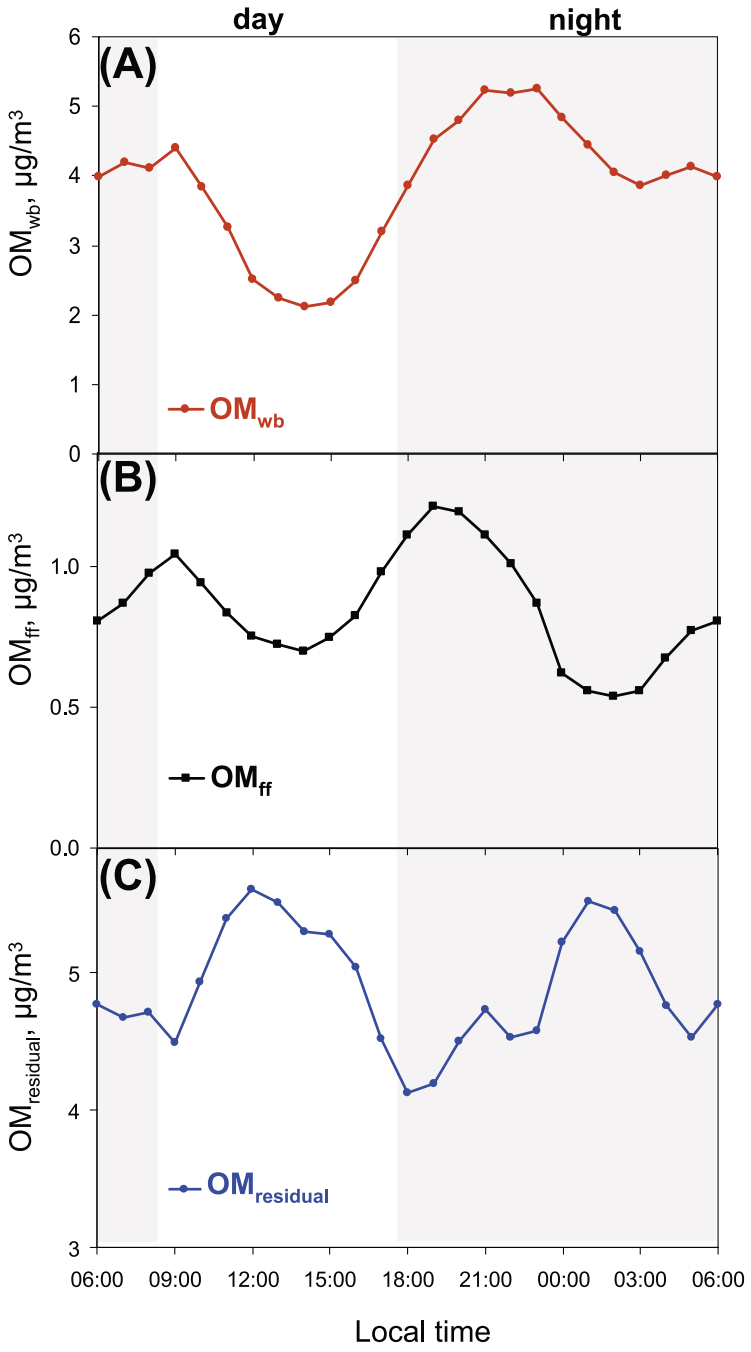

Figure 6. Diurnal variations of (a) OM from the wood burning combustion source (OM_{wb}), (b) OM from fossil fuel combustion source (OM_{ff}), and (c) OM from the residual (secondary) organic source ($OM_{residual}$). The gray zones stand for nighttime.

can also be used to reconstruct total carbon (TC) following exactly the same methodology as for CM (see section 3). The main interest to reconstruct TC from OC measurements is that no assumptions are needed regarding the choice of $f_{OC\text{-}OM}$. These assumptions concern the determination of CM and C_1. Results of the TC reconstruction are reported in the auxiliary material (Figures S2 and S3). Results are very similar as those reported for CM reconstruction. The correlation coefficient (r^2) of 0.77 between measured and reconstructed TC is similar to the one found between measured and reconstructed CM (0.79).

4.3.2. Influence of α_{ff} on the Results of the Aethalometer Model

[50] We have let here α_{ff} range from 0.8 to 1.2 (keeping α_{wb} = 2.0). These values stand for the maximum range of commonly reported α_{ff} in literature [*Kirchstetter et al.*, 2004; *Schnaiter et al.*, 2003, 2005]. Results are summarized in Table 2 and compared with the base case (α_{ff} = 1.1). The α_{ff} value of 1.2 was found to be unrealistic (leading, for some periods, to negative values for BC_{wb} and OM_{wb}). Although scenarios with α_{ff} values of 0.9 and 1.0 cannot be excluded, they lead to lower correlation coefficients

Table 2. Results of the Sensitivity Tests of the Aethalometer Model for Different Scenarios With Variable α_{ff}, α_{wb}, and C_1[a]

Scenario	C1	C2	C3	α_{ff}	α_{wb}	r^{2b}	Percent Difference BC_{ff}[c]	Percent Difference BC_{wb}[c]	Percent Difference OM_{ff}[c]	Percent Difference OM_{wb}[c]	Percent Difference $OM_{residual}$[c]	Remark
α_{ff} = 0.9	0.262	0.421	4.819	0.9	2	0.65	−14%	+42%	−14%	+18%	−11%	
α_{ff} = 1.0	0.262	0.484	4.868	1	2	0.72	−7%	+25%	−7%	+16%	−10%	
α_{ff} = 1.1	**0.262**	**0.541**	**5.363**	**1.1**	**2**	**0.79**	**0%**	**0%**	**0%**	**0%**	**0%**	**base case**
α_{ff} = 1.2	0.262	0.529	6.643	1.2	2	0.76	+9%	−45%	+9%	−52%	+21%	negative BC_{wb} and OM_{wb} values
α_{wb} = 1.8	0.262	0.469	5.363	1.1	1.8	0.81	−9%	+33%	−9%	+3%	0%	negative BC_{ff} and OM_{ff} values
α_{wb} = 1.9	0.262	0.510	5.363	1.1	1.9	0.79	−4%	+16%	−4%	+1%	0%	
α_{wb} = 2.0	**0.262**	**0.541**	**5.363**	**1.1**	**2**	**0.79**	**0%**	**0%**	**0%**	**0%**	**0%**	**base case**
α_{wb} = 2.1	0.262	0.573	5.363	1.1	2.1	0.77	+3%	−14%	+3%	−1%	0%	
α_{wb} = 2.2	0.262	0.603	5.363	1.1	2.2	0.77	+5%	−28%	+5%	−2%	0%	
C1 = 0.1867	0.187	0.552	5.813	1.1	2	0.79	0%	0%	−64%	+2%	+8%	
C1 = 0.2616	**0.262**	**0.541**	**5.363**	**1.1**	**2**	**0.79**	**0%**	**0%**	**0%**	**0%**	**0%**	**base case**
C1 = 0.3730	0.373	0.449	4.443	1.1	2	0.74	0%	0%	+53%	−4%	−13%	

[a]Base case (used in this paper) is reported in bold.
[b]Correlation coefficient between CM measured and CM reconstructed.
[c]Percentage difference calculated from the base case.

between measured and reconstructed CM (r^2 = 0.65 and 0.72 for α_{ff} values of 0.9 and 1.0, respectively) by comparison with the base case (r^2 = 0.79). Our α_{ff} value appears here to lead to the best agreement between measured and reconstructed CM, even though our α_{ff} value of 1.1 was directly deduced from field measurements (when the traffic source contribution was the highest; Figure 3) and was consistent with literature data. As shown in Table 2, the use of α_{ff} values of 0.9 and 1.0 do not lead to significant changes in the BC and OM concentrations from the 3 different sources (except for BC_{wb} concentrations), with slightly lower concentration levels of $OM_{residual}$ (~−10%) These slight changes will not alter the main conclusions of the paper regarding the major contribution of SOA ($OM_{residual}$).

4.3.3. Influence of α_{wb} on the Results of the Aethalometer Model

[51] We have let here α_{wb} range from 1.8 to 2.2 (keeping α_{ff} = 1.1). As shown in Table 2, the choice of α_{wb} appears much less sensitive than α_{ff}. Comparison between measured and reconstructed CM shows a correlation coefficient of r^2 ranging from 0.81 to 0.77 for α_{wb} ranging from 1.8 to 2.2. An α_{wb} value of 1.8 leads, for some periods of the campaign, to negative concentrations of BC_{ff}, and OM_{ff}. The use of α_{wb} values ranging from 1.9 to 2.2 does not lead to significant changes in the BC and OM concentrations from the 3 different sources (except for BC_{wb} concentrations); $OM_{residual}$ concentrations remaining unchanged. For that reason, it can be concluded here that hypotheses related to the choice of a specific α_{wb} value will not alter the main conclusions of the paper regarding the major contribution of SOA ($OM_{residual}$).

4.3.4. Influence of C_1 on the Results of the Aethalometer Model

[52] As defined in equation (11), C_1 is a function of 3 parameters; $f_{OC\text{-}OM}$, $(OC/EC)_{ff}$, and MAE_{ff}, assigned to be 1.3, 0.7, and 7.3 m^2/g, respectively (see section 3). We have let here $f_{OC\text{-}OM}$ range from 1.1 to 1.5, $(OC/EC)_{ff}$ range from 0.5 to 0.9, and MAE_{ff} range from 6.3 to 8.3 m^2/g. These different ranges can be considered as covering the maximum variability of each parameter. Based on these different ranges, one minimum C_1 value of 1.867×10^5 (corresponding to $f_{OC\text{-}OM}$ = 1.1; $(OC/EC)_{ff}$ = 0.5; MAE_{ff} = 8.3 m^2/g) and one maximum C_1 value of 3.730×10^5 (corresponding to $f_{OC\text{-}OM}$ = 1.5; $(OC/EC)_{ff}$ = 0.9; MAE_{ff} = 6.3 m^2/g) were taken here as an input parameter for the aethalometer model. These 2 scenarios were compared in Table 2 with the base case ($C_1 = 2.616 \times 10^5$). Except for OM_{ff} concentrations - which have shown to vary by almost 50% - the use of a large range of C_1 values do not strongly affect our BC and OM results, providing further confidence on our conclusions of an important source of SOA ($OM_{residual}$).

4.4. Comparison of the Aethalometer Model Results With Other Tracers of Fossil Fuel and Wood Burning Combustion

[53] The ability of the aethalometer model to properly derive BC and OM from both fossil fuel and wood burning is a critical issue in the determination of $OM_{residual}$ concentrations (assessed as SOA in the present study). The consistency of this model was tested for that purpose against different real-time measurements of fossil fuel and wood burning tracers performed in parallel during our study. Results of these comparisons are presented here.

4.4.1. Biomass Burning Tracers

4.4.1.1. Water-Soluble Potassium

[54] Water-soluble potassium, mainly emitted in the form of KCl during biomass burning combustion, can be produced in different amounts depending on fuel and combustion types making difficult its use to properly quantify wood burning aerosols [*Puxbaum et al.*, 2007; *Sullivan et al.*, 2008]. At a given location and for a limited period where fuel type and combustion processes are homogeneous, emission of potassium in the atmosphere may remain quite stable allowing its use to follow the concentration of wood burning aerosols. Hence, once emitted in the atmosphere, potassium will not undergo aging like other wood burning tracers such as levoglucosan [*Hennigan et al.*, 2010]. Time-resolved water-soluble potassium measurements were performed during our study every 10 min by the PILS-IC and are reported in Figure 7a together with BC_{wb} for the periods of the campaign when the PILS-IC was operating. Comparison between these 2 data sets shows most of the time a good

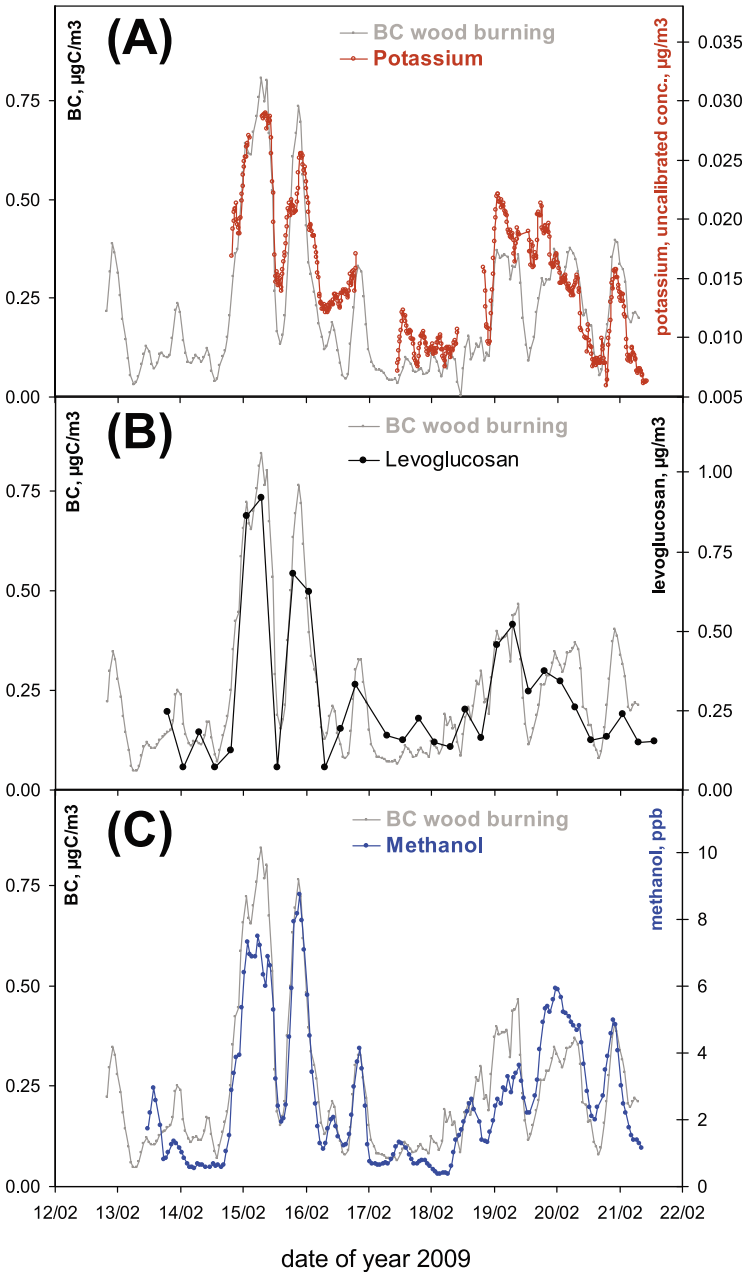

Figure 7. Comparison of black carbon from wood burning (BC_{wb}) obtained with the aethalometer model with: (a) co-located online measurements of water-soluble potassium obtained by PILS-IC, (b) co-located filter-based measurements of levoglucosan, and (c) co-located online measurements of methanol obtained by PTR-MS.

accordance (r^2 = 0.71; N = 129) with concomitant maxima (nights of 15, 16, 19, 20, and 21/02). This good accordance between two compounds of biomass burning aerosols obtained independently brings further confidence on the aethalometer model results and points also to the potential use of a real-time determination of water-soluble potassium by PILS-IC as a useful tracer to follow biomass burning aerosols.

4.4.1.2. Levoglucosan

[55] This compound, produced by the combustion of cellulose, is widely used to derive in a quantitative way the contribution of primary biomass burning smoke to the total organic carbon [*Puxbaum et al.*, 2007; *Sullivan et al.*, 2008; *Sandradewi et al.*, 2008b; *Szidat et al.*, 2009]. During our study, levoglucosan concentrations obtained from filter sampling were ranging from 0.072 to 0.919μg/m^3 with a mean concentration of 0.28 ± 0.22μg/m^3 (Table 1). This concentration falls in the medium range of those reported for European urban areas during wintertime [*Szidat et al.*, 2009]. Comparison between hourly concentrations of BC_{wb} and 6-h integrated levoglucosan concentrations is reported in Figure 7b. Correlation between OM_{wb} and levoglucosan

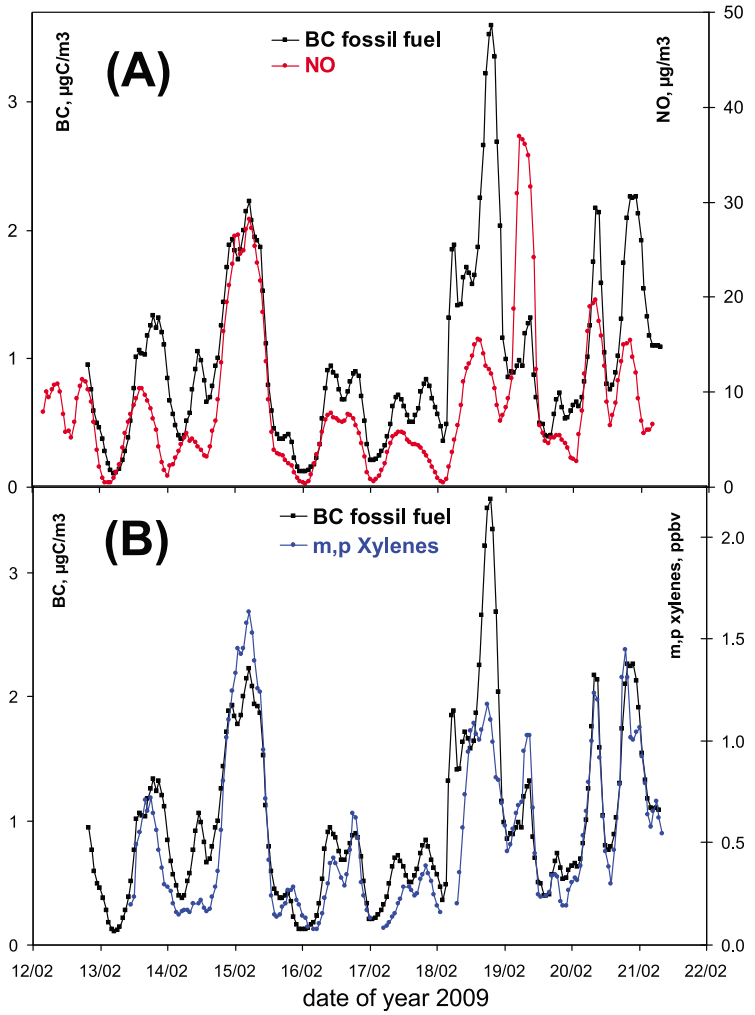

Figure 8. Comparison of black carbon from fossil fuel (BC_{ff}) obtained with the aethalometer model with: (a) nitric oxide (NO) obtained from the local air quality network at 20km distance from our station, and (b) co-located online measurements of m,p-xylenes obtained by GC-FID.

is satisfactory (r^2 = 0.66) and leads to a slope of about 10.3μg/μg, which is close to the OM_{wb}/levoglucosan ratio of 10.8 reported by *Favez et al.* [2010] for the city of Grenoble (France). This ratio corresponds to an OC_{wb}/levoglucosan ratio of 6.2μgC/μg, when using an OC-OM conversion factor of 1.7 for OM_{wb} [*Puxbaum et al.*, 2007, and references therein]. This ratio is in the range of the values of 6–7 reported by *Puxbaum et al.* [2007] which should be representative for domestic heating in European countries.

4.4.1.3. Methanol

[56] This oxygenated VOC is one of the most significant organic compounds in the atmosphere and has been reported as a major primary product of biomass burning [*Holzinger et al.*, 2005; *de Gouw et al.*, 2006; *Gaeggeler et al.*, 2008], with secondary production in aged biomass burning playing a minor role [*Karl et al.*, 2007]. A methanol-to-acetonitrile average ratio of 13.6 ± 7.6 (ppbv/ppbv) obtained during our study falls in the range of those reported for biomass burning conditions [*Holzinger et al.*, 2005; *Karl et al.*, 2007]. Comparison of hourly mean concentrations of methanol and BC_{wb} is reported in Figure 7c and exhibits very similar temporal variations (r^2 = 0.77; N = 183) with, however, some differences in terms of maxima that could be partly explained by changes in background concentrations of methanol governed by air mass origin. Similar good agreement with BC_{wb} can be found with acetonitrile another VOC emitted in large quantity by biomass burning (data not shown here).

4.4.2. Fossil Fuel Tracers

4.4.2.1. Nitric Oxide (NO)

[57] This compound is a well-known tracer of primary fossil fuel combustion which is often used in literature to support the role of traffic emissions on BC concentrations [see, e.g., *Jiang et al.*, 2005, and references therein]. Such measurements were available from two stations of the local air quality network (AIRPARIF) located respectively at 20km north and south of our measurement site. Averaged NO concentrations from these 2 stations are reported in Figure 8a together with BC_{ff}. Although very local traffic emissions may significantly alter NO measurements performed at 20km distance from our station, a relatively good agreement is observed with BC_{ff} (r^2 = 0.56; N = 199).

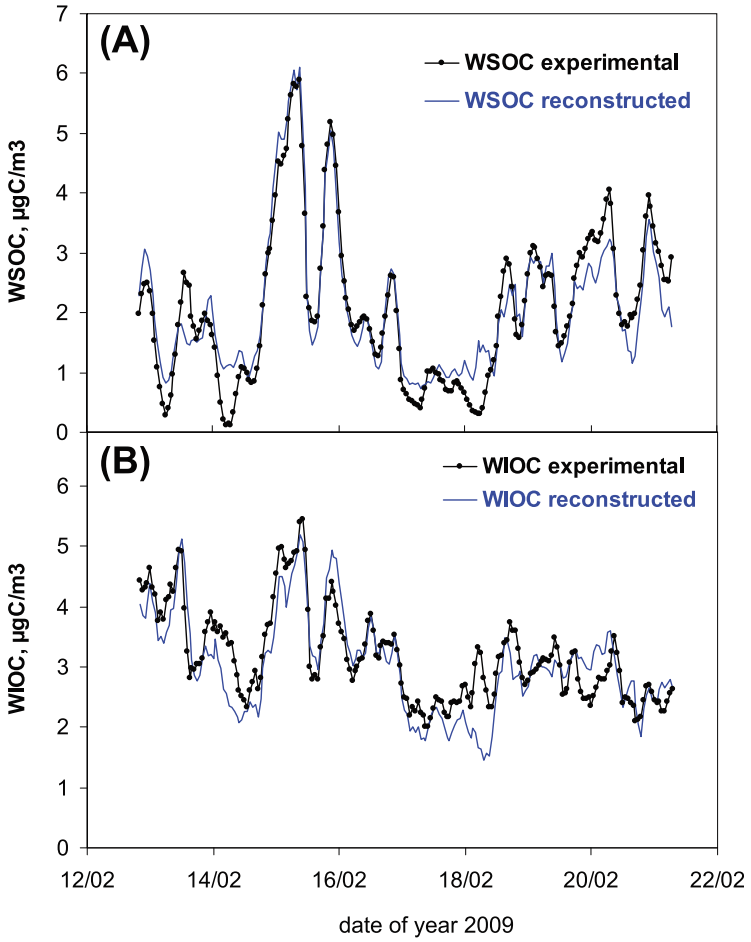

Figure 9. Comparison between experimentally determined (OCEC Sunset Field and PILS-TOC instruments) and reconstructed (aethalometer model) concentrations of (a) WSOC and (b) WIOC.

4.4.2.2. The m,p-xylenes

[58] Hourly concentrations of this compound measured by the automatic GC-FID instrument are reported in Figure 8b together with BC_{ff}. This compound was used here to trace the fossil fuel source as reported by *Gaimoz et al.* [2011] from a VOC source apportionment study in Paris. A very good agreement was found between m,p-xylenes and BC_{ff} ($r^2 = 0.74$; N = 174) bringing further evidence of the ability of the aethalometer model to determine the fossil fuel source.

4.5. Comparison of the Aethalometer Model Results With WSOC and WIOC Data Sets

[59] In order to better document the water-soluble properties of SOA, a source apportionment of WSOC can be performed using a multilinear regression analysis and the 3 OA sources (wood burning, fossil fuel, residual) which have been determined previously by the aethalometer model. Results can be expressed as:

$$[\mathrm{WSOC}]_{\mathrm{reconstructed}} = [\mathrm{WSOC}]_{\mathrm{ff}} + [\mathrm{WSOC}]_{\mathrm{wb}} + [\mathrm{WSOC}]_{\mathrm{residual}} = (0.005 \pm 0.043) \times [\mathrm{OM}_{\mathrm{ff}}] + (0.439 \pm 0.014) \times [\mathrm{OM}_{\mathrm{wb}}] + (0.079 \pm 0.010) \times [\mathrm{OM}_{\mathrm{residual}}] \quad (13)$$

Similarly a source apportionment of WIOC can be performed following the same methodology:

$$[\mathrm{WIOC}]_{\mathrm{reconstructed}} = [\mathrm{WIOC}]_{\mathrm{ff}} + [\mathrm{WIOC}]_{\mathrm{wb}} + [\mathrm{WIOC}]_{\mathrm{residual}} = (0.227 \pm 0.045) \times [\mathrm{OM}_{\mathrm{ff}}] + (0.139 \pm 0.011) \times [\mathrm{OM}_{\mathrm{wb}}] + (0.464 \pm 0.009) \times [\mathrm{OM}_{\mathrm{residual}}] \quad (14)$$

Table 3. Source Apportionment Results for WSOC and WIOC From the Three OA Sources (Wood Burning, Fossil Fuel, Residual) Estimated by the Aethalometer Model[a]

Compound	Wood Burning	Fossil Fuel	Residual
WSOC ($\mu gC/m^3$)	1.72 ± 1.14 (0.24–5.62)	0.005 ± 0.003 (0.001–0.018)	0.39 ± 0.12 (0.12–0.79)
WIOC ($\mu gC/m^3$)	0.54 ± 0.36 (0.07–1.78)	0.23 ± 0.16 (0.02–0.84)	2.26 ± 0.72 (0.70–4.63)

[a]Results are expressed as mean concentrations ± 1 standard deviation (σ); ranges are reported in brackets.

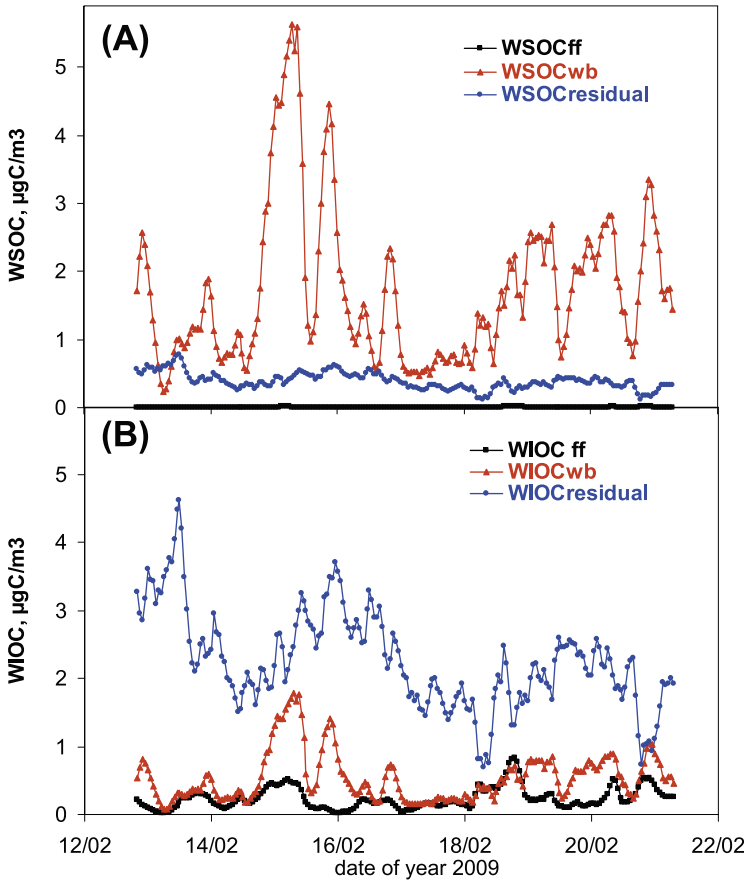

Figure 10. Temporal variation of (a) water-soluble and (b) water-insoluble organic aerosol concentrations from the 3 sources (fossil fuel, wood burning, and SOA) determined by the aethalometer model.

Temporal variations of measured and reconstructed WSOC and WIOC are reported in Figures 9a and 9b, respectively. Comparison between measured and reconstructed data sets shows significant correlation with $r^2 = 0.87$ and $r^2 = 0.73$ for WSOC and WIOC, respectively. Therefore, it can be assumed that the 3 OA sources obtained with the aethalometer model are sufficient to explain most of the temporal variability of both WSOC and WIOC. Results of this source apportionment are summarized in Table 3 and show that 77% of our WSOC was originating from wood burning; the rest (23% of WSOC) was assigned as residual (secondary). Negligible concentrations of WSOC from fossil fuel was found here, which is consistent with literature data on OA emissions from fossil fuel which are composed of poorly oxidized, therefore poorly water-soluble OA [*Weber et al.*, 2007]. WIOC was found to be composed of fossil fuel (8%), wood burning (17%) and residual (75%). Hourly concentrations of WSOC and WIOC from the 3 OA sources are reported in Figures 10a and 10b, respectively. Figure 10 clearly shows that WIOC and WSOC have very different contributions for each of the 3 sources. Therefore, there is a clear interest to better understand the water-soluble properties of OA as they may bring new insights in particular on the origin of SOA.

[60] We have also performed the source apportionment of WSOC and WIOC using the aethalometer model with the reconstruction of TC (see section 4.3). Results are reported in the auxiliary material in Figure S3 and lead to very similar results compared to those obtained using CM reconstruction. Some discrepancies are observed for the water-insoluble fossil fuel source (mean concentration of 0.78μgC/m3 for the TC reconstruction instead of 0.51μgC/m3 for the CM reconstruction). The other sources are almost identical. In conclusion, the use of TC (instead of CM) leads to very similar results in the source apportionment of WSOC and WIOC made here with the 3 OA sources. The water-soluble properties of the 3 OA sources (fossil fuel, biomass burning, and SOA) are presented and discussed below in more details.

5. Discussion

5.1. Water-Soluble Properties of Biomass Burning Organic Aerosols (OM_{wb})

[61] Based on equations (13) and (14), 82 ± 5% of OC_{wb} can be assigned as water-soluble in agreement with literature data [*Mayol-Bracero et al.*, 2002; *Sullivan and Weber*, 2006a; *Yang et al.*, 2009]. This is consistent with the close relationship observed between OM_{wb} and WSOC ($r^2 = 0.87$; N = 204). It is interesting to note that the low dispersion (5%) around the average value of 82% suggest a relatively constant contribution of WSOC to OA from wood burning during this study, independently of combustion processes (flaming/smoldering).

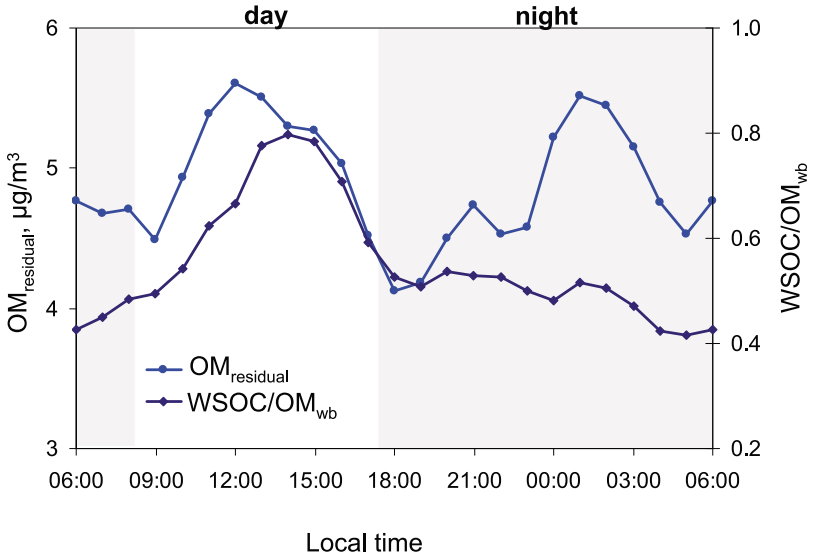

Figure 11. Diurnal variations of residual organic matter ($OM_{residual}$, i.e., SOA) and the ($WSOC/OM_{wb}$) ratio. The gray zones stand for nighttime.

5.2. Water-Soluble Properties of Fossil Fuel Organic Aerosols (OM_{ff})

[62] Results reported in Table 3 show that our fossil fuel emissions are almost exclusively composed of WIOC. This result is in agreement with those reported in Tokyo by *Miyazaki et al.* [2006] and *Kondo et al.* [2007] who have noticed a strong correlation between WIOC and motor vehicle emission tracers (EC, CO). A strong connection between WIOC and hydrogen-like organic aerosols (HOA) derived by AMS measurements was also observed in Tokyo in which HOA can refer to POA from fossil fuel emissions [*Zhang et al.*, 2005; *Lanz et al.*, 2007].

5.3. Water-Soluble Properties of SOA ($OM_{residual}$)

5.3.1. Contribution of WSOC to SOA

[63] Although wood burning has shown to be a major contributor of WSOC, other sources may have contributed to the levels of WSOC, in particular secondary organic formation. A 23% (0.39 ± 0.12 $\mu gC/m^3$) contribution of the residual (secondary) organic source is assigned here as water-soluble. In order to support this result showing that there must be secondary production of WSOC and it is likely from the residual source, we have reported in Figure 11 the diurnal variations of the ratio between WSOC (directly measured by the PILS-TOC instrument) and OM_{wb} (derived from the aethalometer model). Any increase of this $WSOC/OM_{wb}$ ratio should be interpreted as a secondary production of WSOC. The diurnal variation of this $WSOC/OM_{wb}$ ratio shows rather stable ratios close to 0.5 which are observed during the evening peak of domestic heating and during the rest of the night (18:00–08:00 LT). This suggests that WSOC is mainly originating from wood burning during this period. However, a significant increase in this ratio is observed during daytime with maximum values in the afternoon, with ratio values 75% higher compared to those observed during the wood burning period. An extra (residual) water-soluble OA source is needed to explain such increase which may be attributed to secondary (photochemical) production of WSOC during daytime. Note that this daytime maximum is fully consistent with the one calculated independently from the diurnal variation of our residual OA source (Figure 11).

[64] Several sources can be proposed to explain this secondary production of WSOC during daytime. Source dilution experiments have shown that a large fraction of primary OM_{wb} is semi-volatile [*Lipsky and Robinson*, 2006; *Shrivastava et al.*, 2006]; more than half of primary OM_{wb} being evaporated at 50°C [*Grieshop et al.*, 2009b]. Such dilution could occur during daytime and originate from the combining of reduction of wood burning emissions, PBL development, and/or changes in thermodynamic equilibrium during daytime. This may induce a change in the partitioning between water-soluble and water-insoluble OA fractions in wood burning, resulting in higher $WSOC/OM_{wb}$ ratios during the day (Figure 11). Alternatively, photochemical oxidation of wood burning gas precursors can also be proposed since recent laboratory studies (performed on wood burning emissions under plume-like conditions) could produce substantial new OA, increasing OM_{wb} concentrations by a factor of 1.5 to 2.8 after several hours of exposure to typical summertime hydroxyl radical (OH) concentrations [*Grieshop et al.*, 2009a].

[65] Anthropogenic water-soluble SOA could also be formed here and explain the daytime maximum observed in the $WSOC/OM_{wb}$ ratio. Several studies have noted correlations between OOA determined by AMS and other aerosol species attributed to secondary sources, notably sulfate and nitrate. This would indicate a similarity in the (anthropogenic) emissions of precursors and (photochemical) formation of such species [*Lanz et al.*, 2007, 2008; *Zhang et al.*, 2007]. Comparison has been performed for that purpose using ammonium (PILS-IC) as an indicator of the abundance of sulfate and nitrate, and the difference ($WSOM\text{-}OM_{wb}$) as an estimate of water-soluble SOA. No clear relationship was observed here in these 2 data sets (data not shown), suggesting different emissions and/or formations.

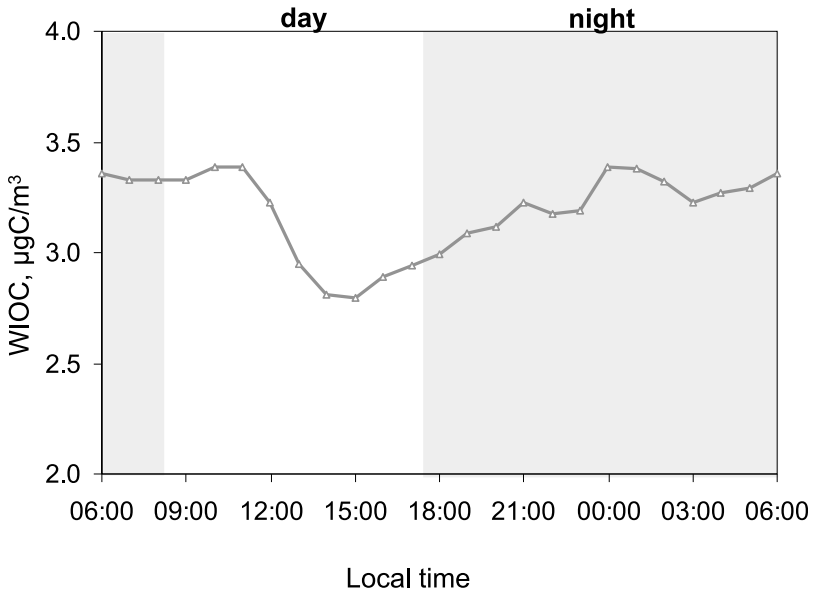

Figure 12. Diurnal variations of water-insoluble organic carbon (WIOC). The gray zones stand for nighttime.

[66] Although biogenic emissions are considerably reduced during wintertime, they still can contribute to SOA formation. Based on ^{14}C analyses and source apportionment of primary (wood burning and fossil fuel) organic sources in Sweden, *Szidat et al.* [2009] have reported the existence of a biogenic source of SOA during wintertime, with concentration levels ranging from 0.46 to 0.91 $\mu gC/m^3$, the highest concentrations being observed over a period characterized by continental air masses. These results, together with the assumption that biogenic SOA are mainly water-soluble [*Weber et al.*, 2007, and references therein] can be proposed to explain our increase of WSOC (relative to OM_{wb}) during the afternoon.

5.3.2. Contribution of WIOC to SOA

[67] Our results indicate that as much as ~85% of $OM_{residual}$ was water-insoluble. As reported previously, PBOA (which can be considered mainly as water-insoluble) are likely to play a negligible role here in $OM_{residual}$. For that reason, it can reasonably be assumed that most of our water-insoluble $OM_{residual}$ is of secondary origin. These water-insoluble SOA can be formed through gas-to-particle conversion processes involving products of reactive organic gases although heterogeneous (aqueous phase) reactions leading to less water-soluble oligomers cannot be ruled out [*Altieri et al.*, 2008]. Secondary formation of water-insoluble SOA could be the result of weak photochemical activity occurring during winter; leading to less oxidized (i.e., less water-soluble) SOA.

[68] By contrast with water-soluble SOA which shows a clear maximum during daytime, the diurnal pattern of WIOC reported in Figure 12 is weakly pronounced and shows only a slight decrease during daytime probably due to PBL development. Such poor temporal variability could suggest a long range transport origin rather than a local pattern for WIOC. Back-trajectory analysis was performed for that purpose and results are reported in Figure 13 together with water-insoluble SOA variations. Periods with higher water-insoluble SOA concentrations are characterized by continental air masses, whereas lower concentrations are more related to marine air masses. Marine contribution may poorly contribute to the WIOC levels during the winter period [*O'Dowd et al.*, 2004, *Sciare et al.*, 2009]. Therefore, our results are consistent with a major continental origin for water-insoluble SOA.

[69] In order to better characterize the secondary origin of our residual WIOC, we have investigated the relationship between this fraction and specific oxygenated VOCs measured by PTR-MS that were not significantly affected by biomass burning and could be used to trace photochemical processes. A general good agreement was found between residual WIOC and acetone (Figure 13), with most of time concomitant maxima and minima. Based on a detailed source apportionment performed in Paris during springtime, *Gaimoz et al.* [2011] have found that acetone was associated with a photochemically processed industrialized source originated from Central and Eastern Europe. This result is consistent with those reported in Figure 13 which shows high values of acetone for continental air masses. They are also consistent with those reported by the literature which has shown important anthropogenic sources of acetone in the northern hemisphere [*Jacob et al.*, 2005; *Filella and Penuelas.*, 2006] originating from a secondary production by the oxidation of NMHC [*Holzinger et al.*, 2005; *Legreid et al.*, 2007]. All these results are in line

Figure 13. Temporal variation of residual WIOC (i.e., water-insoluble SOA) and acetone. Periods noted 1, 3, and 5 (in red) are characterized by continental air masses as shown by the red back trajectory plots reported in the 3 maps above the figure. Periods noted 2 and 4 (in blue) are characterized by marine air masses as shown by the blue back trajectory plots in the 2 maps below the figure.

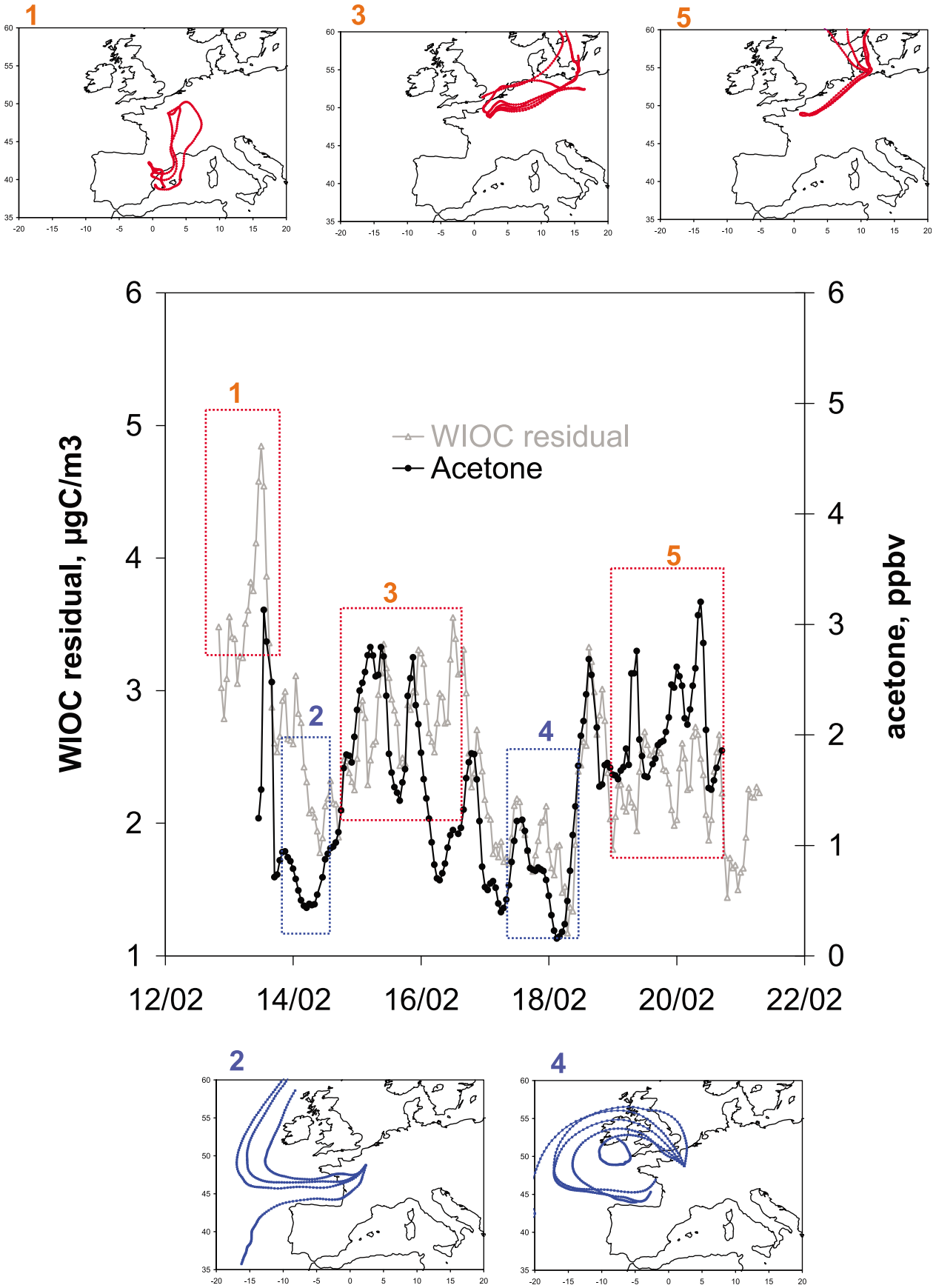
1
3
5
2
4
WIOC residual
Acetone
WIOC residual, µgC/m3
acetone, ppbv
12/02
14/02
16/02
18/02
20/02
22/02

Figure 13

with our assumption that residual WIOC is mainly composed of water-insoluble SOA. However, the origin of this secondary fraction still remains uncertain. Condensation of biomass burning semi-volatile species can be proposed here since the concentration levels of this source are particularly important during our study. Our results can also be compared with those reported by *Robinson et al.* [2007] who proposed that a substantial amount of SOA may originate from the condensation of aged semi-volatile anthropogenic POA composed of long chains of hydrocarbons which can be assumed as mainly water-insoluble. Such an assumption is supported by a number of recent studies which clearly show that anthropogenic VOCs lead to much more SOA than expected [*de Gouw et al.*, 2005; *Volkamer et al.*, 2006] suggesting unknown production pathways. Photochemical formation of water-insoluble SOA have already been reported in literature by *Favez et al.* [2008] in a semi-arid urban environment poorly affected by biogenic emissions, suggesting a possible anthropogenic contribution for SOA. Water-insoluble SOA have also been reported by *Kondo et al.* [2007] who showed that a small fraction of OOA (derived from AMS measurements) could be water-insoluble in Tokyo (Japan). Finally, it is worth noting here that significantly high levels of anthropogenic secondary organic carbon have recently been reported by *Gilardoni et al.* [2011] at a European rural site located in Northern Italy during the winter period (2.2μgC/m^3) supporting our observations of a significant source of SOA mainly being water-insoluble.

[70] Although the role of biogenic emissions cannot be excluded, primary sources (wood burning and anthropogenic emissions) appear to be good candidates to explain our large concentrations of water-insoluble SOA since their emissions are particularly high during winter. This result indicates that the oxidation of intermediate volatility organic compounds co-emitted with primary organics is a significant source of SOA, as suggested by AMS measurements in anthropogenically influenced Northern Hemisphere areas [*Zhang et al.*, 2007]. As a whole, these results bring a new light on SOA which have been generally assigned as water-soluble.

6. Conclusions

[71] A large set of near real-time instruments have been deployed at a suburban site in the region of Paris (France) during wintertime in order to characterize fine carbonaceous aerosols (A.D. < 2.5μm) and volatile organic compounds (VOC). Comparisons of EC, OC, and WSOC between online instruments (OCEC Sunset Field and PILS-TOC instruments) and VOC-denuded filter-based measurements were very satisfactory, pointing out the ability of our online instruments to provide reliable information on fast changes in ambient OA concentrations.

[72] A modified aethalometer model [*Sandradewi et al.*, 2008a] applied to semi-continuous measurements of EC and OC was used to derive 3 sources of OA (fossil fuel, wood burning, and secondary). This source apportionment was tested for primary OA (fossil fuel, wood burning) against real-time measurements of tracers commonly used for these combustion sources (levoglucosan, water-soluble potassium, and methanol for wood burning; nitrogen oxide and m,p-xylenes for fossil fuel). A good agreement was obtained from these comparisons, giving further confidence on the results of the aethalometer model to properly determine primary OA. Residual OA (i.e., SOA) showed significant concentration levels during our study, ranging from 1.3 to 10.4μg/m^3 (average 5.38 ± 1.33μg/m^3) and represented the most abundant OA species during our study.

[73] Hourly measurements of WSOC and WIOC were obtained during our study using the PILS-TOC and OCEC Sunset Field instruments. A source apportionment of these 2 fractions was performed using the 3 OA sources obtained with the aethalometer model providing useful information on the water-soluble properties of these different OA sources. A very large fraction (82 ± 5%) of OC originating from wood burning could be assigned as water-soluble in agreement with literature data. A negligible amount of fossil fuel OA (<1%) was identified as water-soluble, which is also consistent with primary OA from fossil fuel emissions being poorly oxidized and thus mainly water-insoluble. About 23% of WSOC was found to be of secondary origin, with a clear diurnal pattern showing a maximum during daytime linked to local photochemical production.

[74] Less expected is the large fraction of secondary organic carbon (~85%) identified as water-insoluble. This fraction did not show an important diurnal variation suggesting a weak local (photochemical) production, and pointing to a more regional (long range transport) origin. This is consistent with back trajectory analysis which revealed that the highest water-insoluble SOA concentrations were observed for continental air masses. The poor contribution of biogenic SOA during wintertime and its water-soluble properties suggest that our water-insoluble SOA may originate from semi-volatile primary combustion emissions (fossil fuel, wood burning). Modern versus fossil fuel source apportionment of carbonaceous aerosols would aid the conclusions presented here. An independent estimate of SOA - and its oxygen content - using an AMS may also considerably contribute to better depicting wintertime SOA levels and oxidation state.

[75] These results bring new light on the commonly accepted idea that SOA is mainly water-soluble. They have been obtained at a typical suburban site of France and may be then representative of a larger European area. They also have important implications for the SOA lifetime which is partly controlled by removal processes in which the water-soluble properties play an important role.

[76] **Acknowledgments.** This work is a contribution to the ANR-AEROCOV program. It was funded by ANR, ADEME, CEA, and CNRS. J. Williams, T. Custer and T. Kluepfel from the Max Planck Institute (Mainz, Germany) are gratefully thanked for their help with the PTR-MS calibration. AIRPARIF is thanked here for their contribution in NO measurements.

References

Altieri, K. E., S. P. Seitzinger, A. G. Carlton, B. J. Turpin, G. C. Klein, and A. G. Marshall (2008), Oligomers formed through in-cloud methylglyoxal reactions: Chemical composition, properties, and mechanisms investigated by ultra-high resolution FT-ICR mass spectrometry, *Atmos. Environ.*, *42*, 1476–1490, doi:10.1016/j.atmosenv.2007.11.015.

Bae, M.-S., J. J. Schauer, J. T. DeMinter, J. R. Turner, D. Smith, and R. A. Cary (2004), Validation of a semi-continuous instrument for elemental, carbon and organic carbon using a thermal-optical method, *Atmos. Environ.*, *38*, 2885–2893, doi:10.1016/j.atmosenv.2004.02.027.

Bauer, H., A. Kasper-Giebl, F. Zibuschka, R. Hitzenberger, G. Kraus, and H. Puxbaum (2002), Determination of the carbon content of airborne fungal spores, *Anal. Chem.*, *74*, 91–95, doi:10.1021/ac010331+.

Bauer, H., E. Schueller, G. Weinke, A. Berger, R. Hitzenberger, I. L. Marr, and H. Puxbaum (2008a), Significant contributions of fungal spores to the organic carbon and to the aerosol mass balance of the urban atmospheric aerosol, *Atmos. Environ.*, *42*, 5542–5549, doi:10.1016/j.atmosenv.2008.03.019.

Bauer, H., M. Claeys, R. Vermeylen, E. Schueller, G. Weinke, A. Berger, and H. Puxbaum (2008b), Arabitol and mannitol as tracers for the quantification of airborne fungal spores, *Atmos. Environ.*, *42*, 588–593, doi:10.1016/j.atmosenv.2007.10.013.

Birch, M. E., and R. A. Cary (1996), Elemental carbon-based method for monitoring occupational exposures to particulate diesel exhaust, *Aerosol Sci. Technol.*, *25*, 221–241, doi:10.1080/02786829608965393.

Blake, R. S., P. S. Monks, and A. M. Ellis (2009), Proton-Transfer Reaction Mass Spectrometry, *Chem. Rev.*, *109*, 861–896, doi:10.1021/cr800364q.

Bond, T. C., and R. W. Bergstrom (2006), Light absorption by carbonaceous particles: An investigative review, *Aerosol Sci. Technol.*, *40*, 27–67, doi:10.1080/02786820500421521.

Bonsang, B., B. Al Aarbaoui, and J. Sciare (2008), Diurnal variation of non methane hydrocarbons in the subantarctic atmosphere, *Environ. Chem.*, *5*, 16–23, doi:10.1071/EN07018.

Clarke, A., et al. (2007), Biomass burning and pollution aerosol over North America: Organic components and their influence on spectral optical properties and humidification response, *J. Geophys. Res.*, *112*, D12S18, doi:10.1029/2006JD007777.

Collaud Coen, M., et al. (2010), Minimizing light absorption measurement artifacts of the aethalometer: Evaluation of five correction algorithms, *Atmos. Meas. Tech.*, *3*, 457–474, doi:10.5194/amt-3-457-2010.

Decesari, S., M. C. Facchini, E. Matta, F. Lettini, M. Mircea, S. Fuzzi, E. Tagliavini, and J.-P. Putaud (2001), Chemical features and seasonal variation of fine aerosol water-soluble organic compounds in the Po Valley, Italy, *Atmos. Environ.*, *35*, 3691–3699, doi:10.1016/S1352-2310(00)00509-4.

de Gouw, J., and C. Warneke (2007), Measurements of volatile organic compounds in the earths atmosphere using proton-transfer-reaction mass spectrometry, *Mass Spectrom. Rev.*, *26*, 223–257, doi:10.1002/mas.20119.

de Gouw, J. A., et al. (2005), The budget of organic carbon in a polluted atmosphere: Results from the New England Air Quality Study in 2002, *J. Geophys. Res.*, *110*, D16305, doi:10.1029/2004JD005623.

de Gouw, J. A., et al. (2006), Volatile organic compounds composition of merged and aged forest fire plumes from Alaska and western Canada, *J. Geophys. Res.*, *111*, D10303, doi:10.1029/2005JD006175.

Eatough, D. J., A. Wadsworth, D. A. Eatough, J. W. Crawford, L. D. Hansen, and E. A. Lewis (1993), A multiple system, multi-channel diffusion denuder sampler for the determination of fine-particulate organic material in the atmosphere, *Atmos. Environ. Part A*, *27*, 1213–1219, doi:10.1016/0960-1686(93)90247-V.

El Haddad, I., et al. (2009), Comprehensive primary particulate organic characterization of vehicular exhaust emissions in France, *Atmos. Environ.*, *43*(39), 6190–6198, doi:10.1016/j.atmosenv.2009.09.001.

Favez, O., H. Cachier, J. Sciare, and Y. Le Moullec (2007), Semi-volatile aerosols in Paris (France): Characterization and contribution to $PM_{2.5}$, *Atmos. Environ.*, *41*, 7969–7976, doi:10.1016/j.atmosenv.2007.09.031.

Favez, O., J. Sciare, H. Cachier, S. C. Alfaro, and M. M. Abdelwahab (2008), Significant formation of water-insoluble secondary organic aerosols in semi-arid urban environment, *Geophys. Res. Lett.*, *35*, L15801, doi:10.1029/2008GL034446.

Favez, O., H. Cachier, J. Sciare, R. Sarda-Estève, and L. Martinon (2009), Evidence for a significant contribution of wood burning aerosols to $PM_{2.5}$ during the winter season in Paris, France, *Atmos. Environ.*, *43*, 3640–3644, doi:10.1016/j.atmosenv.2009.04.035.

Favez, O., et al. (2010), Inter-comparison of source apportionment models for the estimation of wood burning aerosols during wintertime in an Alpine city (Grenoble, France), *Atmos. Chem. Phys.*, *10*, 5295–5314., doi:10.5194/acp-10-5295-2010.

Fialho, P., A. D. A. Hansen, and R. E. Honrath (2005), Absorption coefficients by aerosols in remote areas: A new approach to decouple dust and black carbon absorption coefficients using seven-wavelength aethalometer data, *J. Aerosp. Sci.*, *36*(2), 267–282, doi:10.1016/j.jaerosci.2004.09.004.

Filella, I., and J. Penuelas (2006), Daily, weekly, and seasonal time courses of VOC concentrations in a semi-urban area near Barcelona, *Atmos. Environ.*, *40*, 7752–7769, doi:10.1016/j.atmosenv.2006.08.002.

Gaeggeler, K., A. S. H. Prévôt, J. Dommen, G. Legreid, S. Reimann, and U. Baltensperger (2008), Residential wood burning in an Alpine valley as a source for oxygenated volatile organic compounds, hydrocarbons and organic acids, *Atmos. Environ.*, *42*, 8278–8287, doi:10.1016/j.atmosenv.2008.07.038.

Gaimoz, C., et al. (2011), Volatile organic compounds sources in Paris in spring 2007. Part II: Source apportionment using positive matrix factorization, *Environ. Chem.*, *8*, 91–103, doi:10.1071/EN10067.

Gelencsér, A., B. May, D. Simpson, A. Sánchez-Ochao, A. Kasper-Giebl, H. Puxbaum, A. Caseiro, C. Pio, and M. Legrand (2007), Source apportionment of $PM_{2.5}$ organic aerosol over Europe: Primary/secondary, natural/anthropogenic, fossil/biogenic origin, *J. Geophys. Res.*, *112*, D23S04, doi:10.1029/2006JD008094.

Gilardoni, S., E. Vignati, F. Cavalli, J. P. Putaud, B. R. Larsen, M. Karl, K. Stenström, J. Genberg, S. Henne, and F. Dentener (2011), Better constraints on sources of carbonaceous aerosols using a combined 14C–macro tracer analysis in a European rural background site, *Atmos. Chem. Phys. Discuss.*, *11*, 2503–2547, doi:10.5194/acpd-11-2503-2011.

Grieshop, A. P., N. M. Donahue, and A. L. Robinson (2009a), Laboratory investigation of photochemical oxidation of organic aerosol from wood fires 2: Analysis of aerosol mass spectrometer data, *Atmos. Chem. Phys.*, *9*, 2227–2240, doi:10.5194/acp-9-2227-2009.

Grieshop, A. P., J. M. Logue, N. M. Donahue, and A. L. Robinson (2009b), Laboratory investigation of photochemical oxidation of organic aerosol from wood fires 1: Measurement and simulation of organic aerosol evolution, *Atmos. Chem. Phys.*, *9*, 1263–1277, doi:10.5194/acp-9-1263-2009.

Gros, V., et al. (2011), Volatile organic compounds sources in Paris in spring 2007. Part I: Qualitative analysis, *Environ. Chem.*, *8*, 74–90, doi:10.1071/EN10068.

Grover, B. D., M. Kleinmain, N. L. Eathough, D. J. Eatough, P. K. Hopke, R. W. Long, W. E. Wilson, M. B. Meyer, and J. L. Ambs (2005), Measurement of total $PM_{2.5}$ mass (non volatile plus semivolatile) with the Filter Dynamic Measurement System tapered element oscillating microbalance monitor, *J. Geophys. Res.*, *110*, D07S03, doi:10.1029/2004JD004995.

Heald, C. L., et al. (2006), Concentrations and sources of organic carbon aerosols in the free troposphere over North America, *J. Geophys. Res.*, *111*, D23S47, doi:10.1029/2006JD007705.

Hecobian, A., X. Zhang, M. Zheng, N. Frank, E. S. Edgerton, and R. J. Weber (2010), Water-Soluble Organic Aerosol material and the light-absorption characteristics of aqueous extracts measured over the Southeastern United States, *Atmos. Chem. Phys.*, *10*, 5965–5977, doi:10.5194/acp-10-5965-2010.

Hennigan, C. J., M. H. Bergin, J. E. Dibb, and R. J. Weber (2008a), Enhanced secondary organic aerosol formation due to water uptake by fine particles, *Geophys. Res. Lett.*, *35*, L18801, doi:10.1029/2008GL035046.

Hennigan, C. J., et al. (2008b), On the volatility and production mechanisms of newly formed nitrate and water-soluble organic aerosol in Mexico City, *Atmos. Chem. Phys.*, *8*, 3761–3768, doi:10.5194/acp-8-3761-2008.

Hennigan, C. J., A. P. Sullivan, J. L. Collett Jr., and A. L. Robinson (2010), Levoglucosan stability in biomass burning particles exposed to hydroxyl radicals, *Geophys. Res. Lett.*, *37*, L09806, doi:10.1029/2010GL043088.

Hoffer, A., A. Gelencsér, P. Guyon, G. Kiss, O. Schmid, G. P. Frank, P. Artaxo, and M. O. Andreae (2006), Optical properties of humic-like substances (HULIS) in biomass burning aerosol, *Atmos. Chem. Phys.*, *6*, 3563–3570, doi:10.5194/acp-6-3563-2006.

Holzinger, R., J. Williams, G. Salisbury, T. Klüpfel, M. de Reus, M. Traub, P. J. Crutzen, and J. Lelieveld (2005), Oxygenated compounds in aged biomass burning plumes over the Eastern Mediterranean: Evidence for strong secondary production of methanol and acetone, *Atmos. Chem. Phys.*, *5*, 39–46, doi:10.5194/acp-5-39-2005.

Iinuma, Y., G. Engling, H. Puxbaum, and H. Herrmann (2009), A highly resolved anion-exchange chromatographic method for determination of saccharidic tracers for biomass combustion and primary bio-particles in atmospheric aerosol, *Atmos. Environ.*, *43*, 1367–1371, doi:10.1016/j.atmosenv.2008.11.020.

Jacob, D. J., B. D. Field, Q. B. Li, D. R. Blake, J. de Gouw, C. Warneke, A. Hansel, A. Whisthaler, H. B. Singh, and A. Guenther (2005), Global budget of methanol: Constraints from atmospheric observations, *J. Geophys. Res.*, *110*, D08303, doi:10.1029/2004JD005172.

Jeong, C.-H., et al. (2008), Influence of biomass burning on wintertime fine particulate matter: Source contribution at a valley site in rural British Columbia, *Atmos. Environ.*, *42*, 3684–3699, doi:10.1016/j.atmosenv.2008.01.006.

Jiang, M., et al. (2005), Vehicle fleet emissions of black carbon, polycyclic aromatic hydrocarbons, and other pollutants measured by a mobile laboratory in Mexico City, *Atmos. Chem. Phys.*, *5*, 3377–3387, doi:10.5194/acp-5-3377-2005.

Karl, T. G., T. J. Christian, R. J. Yokelson, P. Artaxo, W. M. Hao, and A. Guenther (2007), The Tropical Forest and Fire Emissions Experiment: Method evaluation of volatile organic compound emissions measured by

PTR-MS, FTIR, and GC from tropical biomass burning, *Atmos. Chem. Phys.*, *7*, 5883–5897, doi:10.5194/acp-7-5883-2007.

Kirchstetter, T. W., T. Novakok, and P. V. Hobbs (2004), Evidence that the spectral dependence of light absorption by aerosols is affected by organic carbon, *J. Geophys. Res.*, *109*, D21208, doi:10.1029/2004JD004999.

Kiss, G., B. Varga, I. Galambos, and I. Ganszky (2002), Characterization of water-soluble organic matter isolated from atmospheric fine aerosol, *J. Geophys. Res.*, *107*(D21), 8339, doi:10.1029/2001JD000603.

Kondo, Y., Y. Miyazaki, N. Takegawa, T. Miyakawa, R. J. Weber, J. L. Jimenez, Q. Zhang, and D. R. Worsnop (2007), Oxygenated and water-soluble organic aerosols in Tokyo, *J. Geophys. Res.*, *112*, D01203, doi:10.1029/2006JD007056.

Kupiainen, K., and Z. Klimont (2007), Primary emissions of fine carbonaceous particles in Europe, *Atmos. Environ.*, *41*, 2156–2170, doi:10.1016/j.atmosenv.2006.10.066.

Lack, D., et al. (2008), Bias in filter-based aerosol light absorption measurements due to organic aerosol loading: Evidence from ambient measurements, *Aerosol Sci. Technol.*, *42*, 1033–1041, doi:10.1080/02786820802389277.

Lanz, V. A., M. R. Alfarra, U. Baltensperger, B. Buchmann, C. Hueglin, and A. S. H. Prévôt (2007), Source apportionment of submicron organic aerosols at an urban site by factor analytical modelling of aerosol mass spectra, *Atmos. Chem. Phys.*, *7*, 1503–1522, doi:10.5194/acp-7-1503-2007.

Lanz, V. A., et al. (2008), Source attribution of submicron organic aerosols during wintertime inversions by advanced factor analysis of aerosol mass spectra, *Environ. Sci. Technol.*, *42*, 214–220, doi:10.1021/es0707207.

Lanz, V. A., et al. (2010), Characterization of aerosol chemical composition with aerosol mass spectrometry in Central Europe: An overview, *Atmos. Chem. Phys.*, *10*, 10,453–10,471, doi:10.5194/acp-10-10453-2010.

Legreid, G., J. B. Lööv, J. Staehelin, C. Hueglin, M. Hill, B. Buchmann, A. S. H. Prévôt, and S. Reimann (2007), Oxygenated volatile organic compounds (OVOCs) at an urban background site in Zürich (Europe): Seasonal, variation and source allocation, *Atmos. Environ.*, *41*, 8409–8423, doi:10.1016/j.atmosenv.2007.07.026.

Lewis, K., W. P. Arnott, H. Moosmüller, and C. E. Wold (2008), Strong spectral variation of biomass smoke light absorption and single scattering albedo observed with a novel dual-wavelength photoacoustic instrument, *J. Geophys. Res.*, *113*, D16203, doi:10.1029/2007JD009699.

Lindinger, W., A. Hansel, and A. Jordan (1998), On-line monitoring of volatile organic compounds at pptv levels by means of proton-transfer-reaction mass spectrometry (PTR-MS)—Medical applications, food control and environmental research, *Int. J. Mass Spectrom.*, *173*, 191–241, doi:10.1016/S0168-1176(97)00281-4.

Liousse, C., H. Cachier, and S. G. Jennings (1993), Optical and thermal measurements of black carbon aerosol content in different environments–variation of the specific attenuation cross section, sigma (σ), *Atmos. Environ.*, *27A*, 1203–1211.

Lipsky, E. M., and A. L. Robinson (2006), Effects of dilution on fine particle mass and partitioning of semivolatile organics in diesel exhaust and wood smoke, *Environ. Sci. Technol.*, *40*(1), 155–162, doi:10.1021/es050319p.

Lonati, G., S. Ozgen, and M. Giugliano (2007), Primary and secondary carbonaceous species in $PM_{2.5}$ samples in Milan (Italy), *Atmos. Environ.*, *41*, 4599–4610, doi:10.1016/j.atmosenv.2007.03.046.

Lukács, H., et al. (2007), Seasonal trends and possible sources of brown carbon based on 2-year aerosol measurements at six sites in Europe, *J. Geophys. Res.*, *112*, D23S18, doi:10.1029/2006JD008151.

Mayol-Bracero, O. L., P. Guyon, B. Graham, G. Roberts, M. O. Andreae, S. Decesari, M. C. Facchini, S. Fuzzi, and P. Artaxo (2002), Water-soluble organic compounds in biomass burning aerosols over Amazonia: 2. Apportionment of the chemical composition and importance of the polyacidic fraction, *J. Geophys. Res.*, *107*(D20), 8091, doi:10.1029/2001JD000522.

Miyazaki, Y., Y. Kondo, N. Takegawa, Y. Komazaki, K. Kawamura, M. Mochida, K. Okuzawa, and R. J. Weber (2006), Time-resolved measurements of water-soluble organic carbon in Tokyo, *J. Geophys. Res.*, *111*, D23206, doi:10.1029/2006JD007125.

Nel, A. (2005), Air pollution-related illness: Effects of particles, *Science*, *308*, 804–806, doi:10.1126/science.1108752.

O'Dowd, C. D., M. C. Facchini, F. Cavalli, D. Ceburnis, M. Mircea, S. Decesari, S. Fuzzi, Y. J. Yoon, and J.-P. Putaud (2004), Biogenically driven organic contribution to marine aerosol, *Nature*, *431*, 676–680, doi:10.1038/nature02959.

Orsini, D. A., Y. Ma, A. Sullivan, B. Sierau, K. Baumann, and R. J. Weber (2003), Refinements to the particle-into-liquid sampler (PILS) for ground and airborne measurements of water-soluble aerosol composition, *Atmos. Environ.*, *37*, 1243–1259, doi:10.1016/S1352-2310(02)01015-4.

Peltier, R. E., R. J. Weber, and A. P. Sullivan (2007), Investigating a liquid-based method for online organic carbon detection in atmospheric particles, *Aerosol Sci. Technol.*, *41*, 1117–1127, doi:10.1080/02786820701777465.

Puxbaum, H., A. Caseiro, A. Sánchez-Ochoa, A. Kasper-Giebl, M. Claeys, A. Gelencsér, M. Legrand, S. Preunkert, and C. Pio (2007), Levoglucosan levels at background sites in Europe for assessing the impact of biomass combustion on the European aerosol background, *J. Geophys. Res.*, *112*, D23S05, doi:10.1029/2006JD008114.

Ramanathan, V., et al. (2007), Atmospheric brown clouds: Hemispherical and regional variations in long range transport, absorption, and radiative forcing, *J. Geophys. Res.*, *112*, D22S21, doi:10.1029/2006JD008124.

Robinson, A. L., N. M. Donahue, M. K. Shrivastava, E. A. Weitkamp, A. M. Sage, A. P. Grieshop, T. E. Lane, J. R. Pierce, and S. N. Pandis (2007), Rethinking organic aerosols: Semivolatile emissions and photochemical aging, *Science*, *315*(5816), 1259–1262, doi:10.1126/science.1133061.

Sandradewi, J., A. S. H. Prévôt, S. Szidat, N. Perron, M. R. Alfarra, V. A. Lanz, E. Weingartner, and U. Baltensperger (2008a), Using aerosol light absorption measurements for the quantitative determination of wood burning and traffic emission contributions to particulate matter, *Environ. Sci. Technol.*, *42*, 3316–3323, doi:10.1021/es702253m.

Sandradewi, J., A. S. H. Prévôt, E. Weingartner, R. Schmidhauser, M. Gysel, and U. Baltensperger (2008b), A study of wood burning and traffic aerosols in an Alpine valley using a multi-wavelength aethalometer, *Atmos. Environ.*, *42*, 101–112, doi:10.1016/j.atmosenv.2007.09.034.

Schnaiter, M., H. Horvath, O. Möhler, K. H. Naumann, and H. W. Saathoff (2003), UV-VIS-NIR spectral optical properties of soot and soot containing aerosols, *J. Aerosol Sci.*, *34*, 1421–1444, doi:10.1016/S0021-8502(03)00361-6.

Schnaiter, M., et al. (2005), Measurement of wavelength-resolved light absorption by aerosols utilizing a UV-VIS extinction cell, *Aerosp. Sci. Technol.*, *39*, 249–260, doi:10.1080/027868290925958.

Sciare, J., H. Cachier, K. Oikonomou, P. Ausset, R. Sarda-Estève, and N. Mihalopoulos (2003), Characterization of carbonaceous aerosols during the MINOS campaign in Crete, July August 2001: A multi-analytical approach, *Atmos. Chem. Phys.*, *3*, 1743–1757, doi:10.5194/acp-3-1743-2003.

Sciare, J., H. Cachier, R. Sarda-Estève, T. Yu, and X. Wang (2007), Semivolatile aerosols in Beijing (R.P. China): Characterization and influence on various $PM_{2.5}$ measurements, *J. Geophys. Res.*, *112*, D18202, doi:10.1029/2006JD007448.

Sciare, J., O. Favez, K. Oikonomou, R. Sarda-Estève, H. Cachier, and V. Kazan (2009), Long-term observation of carbonaceous aerosols in the Austral Ocean: Evidence of a marine biogenic origin, *J. Geophys. Res.*, *114*, D15302, doi:10.1029/2009JD011998.

Sciare, J., O. d'Argouges, Q. Zhang, R. Sarda-Estève, C. Gaimoz, V. Gros, M. Beekmann, and O. Sanchez (2010), Comparison between simulated and observed chemical composition of fine aerosols in Paris (France) during springtime: Contribution of regional versus continental emissions, *Atmos. Chem. Phys.*, *10*, 11,987–12,004, doi:10.5194/acp-10-11987-2010.

Shrivastava, M. K., E. M. Lipsky, C. O. Stanier, and A. L. Robinson (2006), Modeling semivolatile organic aerosol mass emissions from combustion systems, *Environ. Sci. Technol.*, *40*(8), 2671–2677, doi:10.1021/es0522231.

Sorooshian, A., F. Brechtel, Y. Ma, R. Weber, A. Corless, R. Flagan, and J. Seinfeld (2006), Modeling and Characterization of a Particle-into-Liquid Sampler (PILS), *Aerosol Sci. Technol.*, *40*(6), 396–409.

Sullivan, A. P., and R. J. Weber (2006a), Chemical characterization of the ambient organic aerosol soluble in water: 1. Isolation of hydrophobic and hydrophilic fractions with a XAD-8 resin, *J. Geophys. Res.*, *111*, D05314, doi:10.1029/2005JD006485.

Sullivan, A. P., and R. J. Weber (2006b), Chemical characterization of the ambient organic aerosol soluble in water: 2. Isolation of acid, neutral, and basic fractions by modified size-exclusion chromatography, *J. Geophys. Res.*, *111*, D05315, doi:10.1029/2005JD006486.

Sullivan, A. P., R. J. Weber, A. L. Clements, J. R. Turner, M. S. Bae, and J. J. Schauer (2004), A method for on-line measurement of water-soluble organic carbon in ambient aerosol particles: Results from an urban site, *Geophys. Res. Lett.*, *31*, L13105, doi:10.1029/2004GL019681.

Sullivan, A. P., R. E. Peltier, C. A. Brock, J. A. de Gouw, J. S. Holloway, C. Warneke, A. G. Wollny, and R. J. Weber (2006), Airborne measurements of carbonaceous aerosol soluble in water over north-eastern United States: Method development and an investigation into water-soluble organic carbon sources, *J. Geophys. Res.*, *111*, D23S46, doi:10.1029/2006JD007072.

Sullivan, A. P., A. S. Holden, L. A. Patterson, G. R. McMeeking, S. M. Kreidenweis, W. C. Malm, W. M. Hao, C. E. Wold, and J. L. Collett Jr. (2008), A method for smoke marker measurements and its potential

application for determining the contribution of biomass burning from wildfires and prescribed fires to ambient $PM_{2.5}$ organic carbon, *J. Geophys. Res.*, *113*, D22302, doi:10.1029/2008JD010216.

Szidat, S., M. Ruff, N. Perron, L. Wacker, H.-A. Synal, M. Hallquist, A. S. Shannigrahi, K. E. Yttri, C. Dye, and D. Simpson (2009), Fossil and non-fossil sources of organic carbon (OC) and elemental carbon (EC) in Göteborg, Sweden, *Atmos. Chem. Phys.*, *9*, 1521–1535, doi:10.5194/acp-9-1521-2009.

Turpin, B. J., and H. J. Lim (2001), Species contribution to $PM_{2.5}$ mass concentrations: Revisiting common assumptions for estimating organic mass, *Aerosol Sci. Technol.*, *35*, 602–610.

Volkamer, R., J. L. Jimenez, F. S. Martini, K. Dzepina, Q. Zhang, D. Salcedo, L. T. Molina, D. R. Worsnop, and M. J. Molina (2006), Secondary organic aerosol formation from anthropogenic air pollution: Rapid and higher than expected, *Geophys. Res. Lett.*, *33*, L17811, doi:10.1029/2006GL026899.

Weber, R. J., et al. (2007), A study of secondary organic aerosol formation in the anthropogenic influenced southeastern United States, *J. Geophys. Res.*, *112*, D13302, doi:10.1029/2007JD008408.

Weingartner, E., H. Saathoff, M. Schnaiter, N. Streit, B. Bitnar, and U. Baltensperger (2003), Absorption of light by soot particles: Determination of the absorption coefficient by means of aethalometers, *J. Aerosol Sci.*, *34*, 1445–1463, doi:10.1016/S0021-8502(03)00359-8.

Yang, M., S. G. Howell, J. Zhuang, and B. J. Huebert (2009), Attribution of aerosol light absorption to black carbon, brown carbon, and dust in China—Interpretations of atmospheric measurements during EAST-AIRE, *Atmos. Chem. Phys.*, *9*, 2035–2050, doi:10.5194/acp-9-2035-2009.

Zhang, Q., M. R. Alfarra, D. R. Worsnop, J. D. Allan, H. Coe, M. R. Canagaratna, and J. L. Jimenez (2005), Deconvolution and quantification of hydrocarbon-like and oxygenated organic aerosols based on aerosol mass spectrometry, *Environ. Sci. Technol.*, *39*, 4938–4952, doi:10.1021/es048568l.

Zhang, Q., J. L. Jimenez, M. R. Canagaratna, et al. (2007), Ubiquity and dominance of oxygenated species in organic aerosols in anthropogenically influenced Northern Hemisphere mid-latitudes, *Geophys. Res. Lett.*, *34*, L13801, doi:10.1029/2007GL029979.

N. Bonnaire, B. Bonsang, O. d'Argouges, C. Dolgorouky, C. Gaimoz, V. Gros, R. Sarda-Estève, and J. Sciare, Laboratoire des Sciences du Climat et de l'Environnement, CNRS-CEA-UVSQ, Orme des Merisiers, Bat. 701, F-91191 Gif-sur-Yvette, France. (jean.sciare@lsce.ipsl.fr)

O. Favez, Institut National de l'Environnement Industriel et des Risques, Parc Technologique Alata, F-60550 Verneuil-en-Halatte, France.